P2RX7: a double-edged sword in tumor immunotherapy

A DISSERTATION
SUBMITTED TO THE FACULTY OF THE
UNIVERSITY OF MINNESOTA
BY

Kelsey Marie Wanhainen

IN PARTIAL FULFILLMENT OF THE REQUIREMENTS
FOR THE DEGREE OF
DOCTOR OF PHILOSOPHY

Advisor: Stephen C. Jameson

August 2022

Acknowledgements

I am immensely grateful for the support and guidance I have had throughout my life and my experience during my PhD has been no exception. I first want to thank my parents, George and Joyce Wanhainen. They have both always encouraged me and supported me pursuing my goals in life, whether that was playing tennis in college, moving to DC for my postbac at the NIH, or entering the MSTP at University of Minnesota. I appreciate them always being someone that I can go to for advice or when I am stressed. They always give me great perspective and I feel much better once we hang up the phone. I also want to thank my older brother George. His visits to Minneapolis over the past few years have been a highlight for me. We always have a blast together and I consider myself very lucky to have such a strong relationship with him. I am also very grateful for my Minnesota family. My boyfriend Travis adds balance to my life and immediately cheers me up after a long day in lab. He listens to me when I need to vent about an experiment that went wrong, even if he has no idea what I am talking about (I think he is familiar with P2RX7 at this point, though). And of course, I must thank by bunny Dumbo and my cat Hank. Their emotional support (and cuddles) have been so important for my mental health and wellbeing over the years. The great friends I have made in Minnesota over these years have helped me maintain work-life balance and provided me with many great stories and memories. I look forward to celebrating this chapter with you all!

I'd also like to thank the members of the Center for Immunology (CFI), MICaB graduate program and the MSTP. Thank you, Yoji Shimizu for giving me the opportunity to join the MSTP and for your continued support each year of the program. The CFI is such a collaborative and engaging environment for research. My project has benefitted greatly from Stub and Herbs happy hours or teatime discussions with my colleagues. I feel very lucky to have completed my PhD here. Thank you to the members of my thesis committee, Drs. Bryce

Binstadt, Dave Masopust, Dan Mueller, Chris Pennell, and Ingunn Stromnes. I appreciate all our insightful discussions over the years and your valuable input on my project.

To the members of the Jamequist lab (past and present), thank you all for creating such a fantastic work environment. The past four years have been so enjoyable, and I am lucky to work with such interesting, intelligent and engaging people. I greatly appreciate all your insight and constructive criticism that has helped my project move forward. In particular, I'd like to thank Henrique Borges da Silva for his mentorship throughout my PhD. In addition to teaching me different techniques upon joining the lab, he also provided guidance on graduate school course work, my qualifying exam and writing my F30 grant application. Even after leaving the University of Minnesota to start his own lab at Mayo, he still so generous with his time and has been a huge help with the resubmission process for my manuscript. I will greatly miss working with everyone in the lab.

Lastly, I'd like to thank my advisor and mentor, Steve Jameson. Not only are you an incredible scientist but you are also a very nice and thoughtful person. I consider myself very lucky to have had the opportunity to work with you for my PhD. Thank you for taking my clinical interests in oncology/tumor immunotherapy into account while we were discussing projects when I first joined the lab. Your sincere support for me as an individual has always been evident. Thank you for engaging weekly meetings – your sense of humor and scientific insight made the meetings both productive and enjoyable. Your guidance over the past four years has made me a better scientist, writer and overall communicator. Lastly, thank you for fostering such a healthy and collaborative work environment. I have had a great experience, and I look forward to continuing to work with you over the next two years and hopefully in the future as well!

Abstract

Expression of the purinergic receptor P2RX7 by $CD8^+$ T cells promotes generation of memory populations following acute infections, but recent studies have indicated that P2RX7 may limit the efficacy of anti-tumor responses. We show that P2RX7 is beneficial for optimal melanoma control in a mouse $CD8^+$ T cell adoptive transfer model. Tumor specific *P2rx7*$^{-/-}$ $CD8^+$ T cells exhibited impaired mitochondrial maintenance and function but did not display signs of overt exhaustion early in the anti-tumor response. However, as the tumor burden increased, the relative frequency of P2RX7 deficient $CD8^+$ T cells declined within the tumor, correlating with reduced proliferation, increased apoptosis and mitochondrial dysfunction. Extending these studies, we found that transient in vitro stimulation of P2RX7 using the ATP analog BzATP led to enhanced B16 tumor control by $CD8^+$ T cells which was dependent on sustained P2RX7 signaling within the tumor.

We also demonstrate that $P2RX7^+$ $CD8^+$ T cells are vulnerable to NAD^+- induced cell death (NICD) by ADP-ribosylation of P2RX7. Tumor cells express the ADP-ribosyltransferase ART1 which induces NICD in $P2RX7^+$ $CD8^+$ T cells. We found that ART1 deficient B16 tumors were more susceptible to $CD8^+$ T cell adoptive cell therapy. Furthermore, we found that loss of ART1 on B16 tumors allowed for $P2RX7^+$ $CD8^+$ T cells to persist within the tumor microenvironment. These findings are consistent with the concept that extracellular ATP (eATP) sensing by P2RX7 on $CD8^+$ T cells is required for their ability to efficiently eliminate tumors by promoting mitochondrial fitness and highlights the potential for P2RX7 stimulation, potentially combined with ART1 blockade, as a novel therapeutic treatment to enhance tumor immunotherapy.

Table of Contents

List of Figures

Chapter 1

Introduction

1.1 The evolution of the vertebrate immune system

The immune system is composed of diverse populations of cells and factors have an essential role in protecting organisms against pathogens while maintaining tissue homeostasis. Vertebrate immune systems have two branches, innate and adaptive immunity, each with important independent and complementary functions. The innate immune system is thought to have evolved first and serves as an initial line of defense against pathogens or malignancy. Innate immune cells recognize general, nonspecific signs of infection or tissue damage and respond quickly (*1, 2*). However, these cells are not capable of discriminating between different pathogens and therefore cannot 'remember' a specific encounter. Vertebrates then evolved a more complex aspect of immunity, the adaptive branch, which allows for precise recognition and potent recall responses to invading pathogens (*3*).

The adaptive immune system is primarily made up of two cell types, B and T cells, and T cells can be further subdivided into subsets based on coreceptor expression (e.g., CD4 and CD8). Both B and T cells have randomly rearranged surface receptors (BCRs and TCRs, respectively) that recognize a specific antigen. The repertoire of randomly rearranged BCRs and TCRs have the capacity to recognize seemingly infinite number of potential pathogens and self-derived mutated proteins. Receptors that are reactive to normal host proteins are mostly deleted during B or T cell development (*4-6*). B and T cells initially exist in a resting or naïve state and are unable to elicit an immune response until recognizing its cognate antigen with appropriate costimulatory and cytokine signals. This mechanism protects the host against inappropriate inflammatory responses, but also makes the adaptive immune response slower to begin. However, once B and T cells become activated, they proliferate to high numbers, and a subpopulation of daughter cells become long-lived memory cells. These

memory cells can more rapidly and specifically respond when re-exposed to their cognate antigen, resulting in long-term immunity.

1.2 CD8$^+$ T cells in adaptive immunity

1.2.1 Overview

In general, T cells express TCRs with alpha and beta chains that undergo random rearrangement within the thymus during development. Non-self-reactive T cells undergo positive selection, allowing them to enter the periphery as mature naïve T cells (*6*). T cells are broadly subdivided by expression of CD4 or CD8 co-receptors. CD4$^+$ T cells are characterized as 'helper T cells' and produce cytokines to induce and skew an appropriate cytotoxic or humoral immune response. CD8$^+$ T cells are known as 'cytotoxic T cells' (CTL) and are capable of directly killing host cells that display signs of intracellular infection or malignant transformation, in a tightly regulated manner (*7*).

1.2.2 CD8$^+$ T cell activation

CD8$^+$ T cells recognize peptide presented in association with Class I major histocompatibility complex molecules (MHC I). In general, MHC I present proteasomal degraded peptide fragments derived from intracellular proteins. Notably, some antigen presenting cells (APCs) are also capable of presenting peptides from exogenous proteins on MHC I through a cross-presentation pathway (*8*). MHC I are expressed on all nucleated cells in the body, so CD8$^+$ T cells have an important role in circulating through the body and surveying the host cells for their infection- or malignancy-derived peptides. For a CD8$^+$ T cell to become activated, it must first encounter its cognate antigen presented by a professional APC, such as a dendritic cell (DC), usually within the lymph node draining from an infected or malignant site (*9*). It also requires sufficient co-stimulation, typically through interactions between CD28 on the T cell and

CD80/86 on the surface of the APC, as well as exposure to cytokines (e.g., IL-12) (*10*). Upon activation, $CD8^+$ T cells clonally expand and give rise to cells with effector function (*11, 12*).

Effector $CD8^+$ T cells enter circulation and traffic to the site of infection or malignancy based on recognition of regionally produced chemokines and cytokines. Once a $CD8^+$ T cell recognizes its cognate antigen, it can kill the target cell through either direct or indirect mechanisms. Cytolytic killing requires direct cell-cell contact and involves $CD8^+$ T cell release of perforin and granzyme proteins resulting in target cell lysis. $CD8^+$ T cells can also directly kill interactions between Fas ligand on the $CD8^+$ T cell and Fas receptor on the target cell triggering the caspase pathway. $CD8^+$ T cells kill indirectly by secreting cytokines such as IFNγ and TNFα. The majority of $CD8^+$ effector T cells are short-lived (SLECs) and act to clear the ongoing infection or malignancy. However, there is a smaller subset of the clonally expanded $CD8^+$ T cells differentiate into memory precursor effector cells (MPECs) which give rise to the memory $CD8^+$ T cell compartment (*12*).

1.2.3 $CD8^+$ T cell memory

Memory $CD8^+$ T cells differentiate from MPECs following the contraction phase of an immune response where most clonally expanded SLECs undergo apoptotic death. Memory $CD8^+$ T cells do not require the same threshold for activation as naïve $CD8^+$ T cells and are therefore able to respond more robustly and rapidly to re-exposure to their cognate antigens. In general, $CD8^+$ memory T cells are characterized into central memory (T_{CM}), effector memory (T_{EM}), and resident memory (T_{RM}) subsets.

T_{CM} and T_{EM} subsets are known as the circulating memory T cell populations, whereas T_{RM} are kept within tissue and do not recirculate. T_{CM} traffic through

lymphoid tissue where they await antigen re-encounter within lymph nodes. They are characterized by lymphoid homing markers CD62L, CCR7, and S1PR1. T_{EM}, on the other hand, also circulate through blood/lymphatics but also survey non-lymphoid tissues (NLT) and are generally characterized as lacking CD62L/CCR7 expression. T_{RM} are retained within NLT or lymphoid tissues and are uniquely positioned to immediately recognize a re-infection at barrier sites. They are generally characterized by markers that promote tissue retention, such as CD69 and CD103, but there is heterogeneity depending on NLT type (*13*).

1.2.4 $CD8^+$ T cell metabolism

$CD8^+$ T cell differentiation throughout an immune response can also be characterized by changes in metabolism. Naïve $CD8^+$ T are metabolically quiescent and primarily undergo oxidative phosphorylation (OXPHOS) to make ATP. As T cells become activated, they become more dependent on aerobic glycolysis to support anabolic growth (*14*). While inefficient in terms of ATP generation, aerobic glycolysis allows for synthesis of metabolic intermediates to be used to produce cellular components needed for proliferation (e.g., lipids, nucleic acids, etc.) (*15*). Memory $CD8^+$ T cells primarily utilize OXPHOS and engage in increased fatty acid oxidation (FAO) to support metabolic requirements (*16*). They are characterized by increased mitochondrial mass and spare respiratory capacity (SRC), which is the maximal respiratory capacity of a cell particularly in times of stress. Increased mitochondrial mass and function allow for memory T cells to rapidly and efficiently produce ATP upon re-exposure to their antigen. These mitochondrial changes are driven in part by IL-15 signaling (*17*). Metabolic alterations also can promote memory T cell differentiation, such as the negative modulation of mammalian target of rapamycin (mTOR) signaling pathway and activation of the adenosine monophosphate activated protein kinase (AMPK) pathway (*18, 19*). Reduced reliance on glycolysis also allows $CD8^+$ T_{RM} to survive in environments where glucose concentrations are low (e.g.,

epithelial tissues or tumors). Notably, skin T_{RM} express fatty acid transporters FABP4/5 to fuel OXPHOS and for synthesis of biomolecules (*20*).

1.3 CD8$^+$ T cell response to cancer

1.3.1 Immune surveillance of tumors

The hypothesis that the immune system could control cancer initially arose in the early 1900s, but it wasn't until the 1950s where there was considerable interest in the antigenic potential of tumor cells. Investigators Burnet and Thomas hypothesized that transformation of tumor cells during progression would create new antigens that would be recognized and eliminated by the adaptive immune system (*21*). These hypotheses were met with criticism as others felt that the immune system would be tolerant of tumors since they were self-derived. Overtime, observations that tumors grew more rapidly in immunocompromised mouse models and characterization of tumor neoantigens provided strong evidence that the immune system was able to recognize and kill cancer cells (*22-25*). These studies laid the foundation for identifying ways to harness anti-tumor immune responses to better control cancer.

1.3.2 Induction of CD8$^+$ T cell anti-tumor responses

CD8$^+$ T cells are critical for effective tumor recognition and control. CD8$^+$ T cells require cross-presentation of tumor antigens within the tumor draining-LN (dLN) by Batf3$^+$ CD103$^+$ conventional type I DCs (cDC1s). cDC1s migrate into tumors by interactions between chemokine receptors CCR5 and XCR1 and their ligands CCL4/5 and XCL1, respectively (*26-28*). cDC1s sensing of cytosolic DNA within the tumor activates the GMP-AMP-synthase-stimulator of interferon genes (cGAS-STING) pathway, resulting in cDC1 activation, more efficient antigen processing/presentation and type I IFN production (*29*). cDC1s transport the tumor antigens into the tumor dLN where present to naïve CD8$^+$ T cells waiting to

encounter their cognate antigen. The importance of cDC1s in initiating the $CD8^+$ T cell anti-tumor response has been demonstrated in mouse models in which the cDC1 transcription factor Batf3 is deleted resulting in poor $CD8^+$ T cell responses to tumors (*30*). Furthermore, cDC1s within the tumor produce chemokines CXCL9/10 to drive $CD8^+$ T cell recruitment (*31*), act to restimulate and expand tumor-specific $CD8^+$ T cells within the tumor (*32*), and are essential for effective responses to immune checkpoint blockade (ICB) (*33*).

Once activated, $CD8^+$ T cells traffic to the tumor microenvironment via interactions between CXCR3 and its ligands CXCL9/10 as well as other tissue-specific chemokines depending on tumor location (*34*). Once within the tumor, $CD8^+$ T cells must recognize their cognate antigen presented on MHC I expressed directly by tumor cell or cross-presented by an APC within the tumor. Tumors frequently downregulate MHC I expression in order to evade $CD8^+$ T cell detection (*35*). Tumors also generate an immunosuppressive environment by increasing expression of immune-checkpoint ligands such as PD-L1/2 and by producing immunosuppressive cytokines and factors such as TGFβ and adenosine.

1.3.3 $CD8^+$ T_{RM} and anti-tumor immunity

The position of $CD8^+$ T_{RM} within barrier tissues make them uniquely poised to detect tumors as they begin or recur. This is particularly relevant for epithelial tumors where circulating $CD8^+$ T cells are generally excluded in the absence of inflammation (*36*). There is considerable evidence that $CD8^+$ T_{RM} have an important role in tumor surveillance. In humans, increased frequencies of $CD103^+$ tumor infiltrating $CD8^+$ T cells correlate with improved prognosis and longer disease-free survival in patients with many different types of cancer including breast, lung, endometrial, cervical, etc. (*37-40*). Murine melanoma models have also demonstrated the ability of $CD8^+$ T_{RM} to prevent tumor

outgrowth (*41-44*). Intratumoral CD103$^+$ CD8$^+$ T cells are often characterized by expression of several inhibitory receptors including PD1, Lag3, and CD39. Despite expression of these receptors, CD8$^+$ T_{RM} maintain proliferative and effector functions (*45*).

Given that CD8$^+$ T_{RM} are associated with favorable prognosis in patients in many tumor types, there is considerable interest incorporating them in immunotherapy regimens. CD8$^+$ T_{RM} have been shown to expand well in response to immune checkpoint blockade in human melanoma (*46, 47*). There is also interest in other strategies that preferentially expand T_{RM} cells within tumors such as DC vaccination or using cytokine nanogels to directly deliver cytokines such as IL-15 into the tumor microenvironment (TME) (*7, 48*). Overexpression of transcription factors such as Bhlhe40 or Runx3 on tumor infiltrating lymphocytes (TILs) may also promote T_{RM} differentiation in adoptive cell therapy regimens (*44, 49*). Despite evidence that CD8$^+$ T cells can evoke potent anti-tumor immunity, there are still many individuals that do not have a complete response to immunotherapy or do not respond at all, particularly in solid tumors. Therefore, there is a need to better understand T cell biology within the TME to further optimize anti-tumor responses.

1.3.4 CD8$^+$ T cell dysfunction within the TME

CD8$^+$ T cells within the tumor are often rendered dysfunctional due to a combination of interrelated factors including immunosuppression, chronic antigen stimulation and impaired metabolic function. Tumor infiltrating immune cells are often outcompeted by cancer cells for essential nutrients to support energy production. Tumor cells undergo high levels of aerobic glycolysis, which depletes the tumor microenvironment of nutrients such as glucose and glutamine and increases acidity due to lactic acid build-up (*15*). Furthermore, tumors rapidly outgrow their blood supply leaving many areas of the tumor extremely hypoxic.

The metabolic stressors of the TME have functional consequences on $CD8^+$ T cells which suppresses antitumor immunity.

$CD8^+$ T cells require metabolic plasticity in order to effective respond to tumors. Effector $CD8^+$ T cells primarily rely on aerobic glycolysis to generate sufficient substrates to produce factors necessary for rapid proliferation (e.g., lipids, amino acids, nucleic acid, etc.) and effector molecules. Tumor depletion of glucose stores compromises effector $CD8^+$ T cell glycolytic capacity, but there are also reduced levels of glycolysis metabolites that are important for T cell activation. For example, phosphoenolpyruvate (PEP), a byproduct of glycolysis, is important for sustaining Ca^{2+}-NFAT signaling during T cell activation (*50*). TCR signaling in the TME is also dampened by hypoxia-induced overactivity of HIF1α, which drives overexpression of genes that reduce intracellular Ca^{2+} stores in T cells as well as directly stimulating PD-L1 expression in cancer cells (*51, 52*).

While $CD8^+$ effector T cells play an important role in tumor control, long-term persistence of $CD8^+$ T cells is also needed to sustain the response. Long-term survival of $CD8^+$ T cells is dependent on efficient OXPHOS and fatty acid oxidation. Mitochondrial homeostasis is maintained through biogenesis and fusion of mitochondria in times of energy demand followed by degradation of damaged or non-functional mitochondria (*53*). Both mechanisms are impaired in $CD8^+$ T cells within tumors, particularly T cells with an exhausted phenotype. T cell exhaustion occurs due to chronic TCR stimulation and is characterized by expression of multiple inhibitory receptors, reduced proliferative capacity and loss of effector function. Chronic TCR stimulation in the setting of hypoxia has been shown to repress expression of the mitochondrial biogenesis promotor PPAR-gamma coactivator 1α (PGC1α) (*54, 55*). Defects in mitophagy cause damaged/depolarized mitochondria to accumulate in TILs. In addition to this leading to poor mitochondrial quality, impaired mitophagy was also associated

with epigenetic modifications that promote an exhaustion phenotype (*56*). Restoring mitochondrial quality control mechanisms has been shown to improve $CD8^+$ T cell effector function both in the setting of chronic infections and tumors (*54, 56-58*). These studies demonstrate that impairing T cell metabolism is a mechanism of immunosuppression for tumors, and strategies that increase $CD8^+$ T cell metabolic fitness may also improve function and longevity.

1.4 Purinergic signaling receptor P2RX7

1.4.1 Overview

ATP is the quintessential cell fuel, driving virtually all cell functions that require energy. Typically, intracellular ATP concentrations vary between 3 and 10mM (*59*). Conversely, the concentration of extracellular ATP (eATP) at steady-state is very low, in the nanomolar range (*60*). However, in response to infections or tissue damage, passive or active release of ATP into the extracellular microenvironment increases eATP concentrations into the hundred micromolar range (*61, 62*). In mammals, extracellular nucleotides are recognized by purinergic receptors. These receptors can be roughly divided into adenosine-recognizing G-protein coupled P1 receptors, and P2 receptors which bind to eATP, eADP or other nucleotides (*63*). P2 receptors can be further subdivided into P2Y or P2X receptors (P2YRs, P2XRs). P2YRs are G-protein coupled receptors with mixed nucleotide selectivity, while P2X receptors are ligand-gated ion channels that specifically respond to ATP. The P2XR subfamily includes 7 members (P2RX1-7) and all can induce cation exchange (including Ca^{2+} influx) following eATP engagement (*64*). P2RX7 is unique among all P2XRs and is the primary focus of this dissertation.

P2RX7 has a low affinity for eATP relative to other P2XRs. Its activation only occurs in the presence of ~100μM eATP (*64*). P2RX7 is a trimer with three ATP

binding pockets. Consistent with P2RX7 having low sensitivity to eATP relative to other P2XRs, binding of a single ATP to one pocket subsequently reduces the affinity of the receptor for ATP binding the other two pockets. Binding of eATP to all three pockets results in rotation of each monomer and opening of an ion channel within the plasma membrane of the cell (*65*).

Upon activation, P2RX7 drives rapid influx of Ca^{2+} and Na^{+} and efflux of K^{+} (*64*). Mechanistically, P2RX7 stimulation engages an array of intracellular signaling and metabolic pathways, which control proliferation and activation in various cell types. However, sustained or intense activation of P2RX7 by high concentrations of eATP (or through ADP-ribosylation by the nicotinamide adenine dinucleotide (NAD^{+})-activated enzyme ARTC2.2, in murine cells) can lead to non-specific pore formation and subsequent cell death (*66*). While the precise mechanism of P2RX7 pore formation is unknown, P2RX7 uniquely carries a long C-terminal region which is essential for this process (*64, 67*). A human splice variant of P2RX7 (P2RX7B) is shortened at the C-terminal end and lacks the ability to form the macropore but still retains some ion channel activity (*68*).

P2RX7 and P2RX4 are adjacent to one another in the human and mouse genomes and are thought to be derived from a gene duplication event. Their proximity to each other in the mouse genome has led to mouse background-specific P2RX7 passenger mutations to persist in P2RX4 knock-out mouse models, regardless of backcrossing (*69*). P2RX4 is not as well-studied as P2RX7, but both receptors are often co-expressed on immune cells, and there is some evidence that they may form heteromeric receptors (*70, 71*). They both have been shown to play essential roles in Ca^{2+} influx during T cell activation where P2RX4 is activated first followed by P2RX7 (*72*). While P2RX4 is not the focus on this dissertation, it is important to acknowledge it may have a complementary role to P2RX7 particularly in T cell function.

1.4.2 Role of P2RX7 in the Immune Response

P2RX7 is likely best known for its role in promoting maturation of the NLRP3 inflammasome. eATP binding to P2RX7 on myeloid cells causes K^+ efflux, allowing for NLRP3 inflammasome components to assemble and promote IL-1β and IL-18 release (*64*). The pore-opening function of P2RX7 allows for massive release of intracellular ATP which acts to amplify the signal. P2RX7-macropore formation also has an important role in inducing pyroptosis in mononuclear cells infected with intracellular bacteria (*73*). In T cells, together with TCR stimulation and co-stimulation, eATP sensing play important roles in initial effector responses such as CD27 or CD62L shedding (*74, 75*), IL-2 and IFNγ production (*76*), and cell proliferation (*77, 78*). Whether P2RX7 drives lymphocyte proliferation versus cell death is dependent on P2RX7 expression levels among T cell subsets and ligand concentrations.

Indeed, during *in vivo* immune responses, P2RX7 has been found to play either a negative or a positive role in cell function and homeostasis depending on the T cell subset studied. For example, in very high P2RX7 expressing CD4 follicular helper and regulatory T cell (T_{reg}) populations, P2RX7 stimulation predominately leads to pore-induced cell death (*79, 80*). Conversely, P2RX7 can promote generation of T-helper 1 (Th1) and Th17 cells (*81-83*). Recent works from our group and others show high expression of this receptor by $CD8^+$ T_{RM} renders them susceptible to cell death induced by sterile damage and subsequent release of high eATP and especially NAD^+ (*84-86*). Importantly, however, our group has also shown that in response to acute viral infections, eATP sensing through P2RX7 promotes the generation, homeostasis and function of $CD8^+$ T_{CM} and T_{RM} (*87, 88*).

1.4.3 P2RX7 in CD8⁺ T cell memory

Our group has identified an important role for P2RX7 in promoting long-lived memory CD8⁺ T cell populations. Early in the effector response, there is heterogenous expression of P2RX7 among MPECs, and those with the highest levels of expression preferentially become T_{CM} and T_{RM} (*89*). P2RX7 deficiency causes loss of mitochondrial mass and function in memory precursor and long-lived memory CD8⁺ T cells (*87, 88*). The role of P2RX7 in promoting mitochondrial maintenance in CD8⁺ T cells is consistent with previous studies showing that transfection of cell lines with P2RX7 increased their mitochondrial health (*90*), and that P2RX7 expression is required for mitochondrial maintenance in microglia (*91*). There are also reports that strong stimulation of P2RX7 led to mitochondrial Ca^{2+} overload, ultimately resulting in fragmentation of the mitochondrial network and cell death (*90, 92*). These results highlight the notion that P2RX7 is a double-edged sword, promoting mitochondrial health and cell growth or causing mitochondrial damage and cell death, depending on the intensity of the eATP encounter (Fig 1.1).

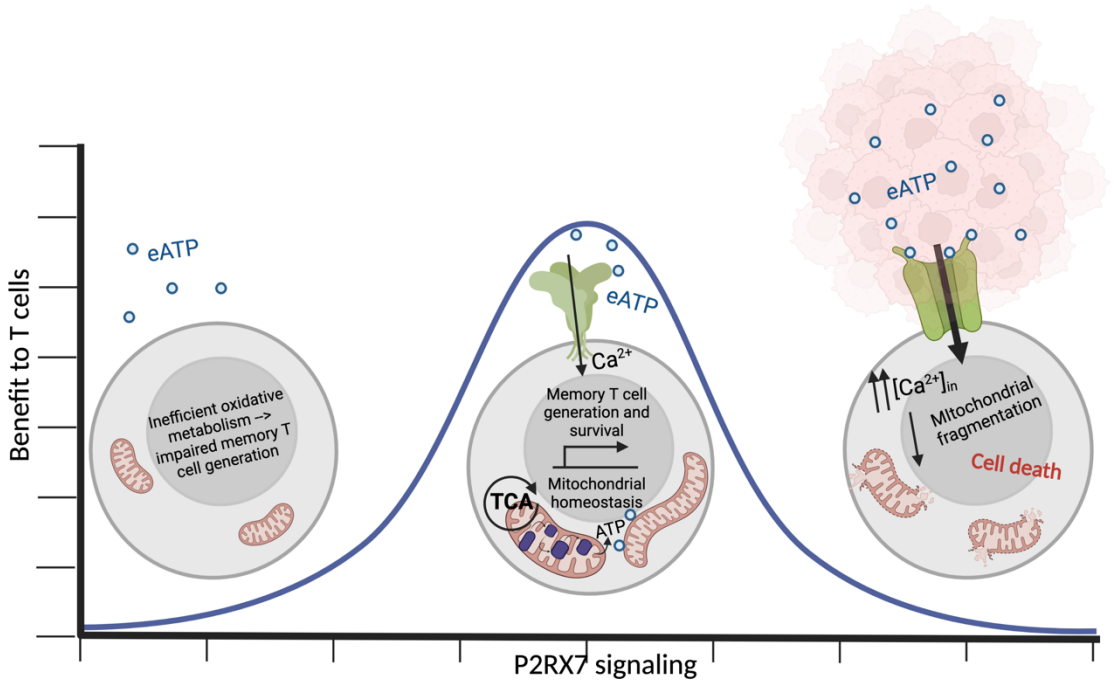

Figure 1.1: Intermediate level of P2RX7 signaling is optimal for CD8⁺ T cell homeostasis.

CD8⁺ T cells require low-level tonic signaling through P2RX7 to promote Ca^{2+} influx, resulting in mitochondrial homeostasis and differentiation into long-lived memory CD8⁺ T cells. Without P2RX7 (left), CD8⁺ T cells are not able to form fused mitochondrial networks in response to memory promoting cytokines and OXPHOS is less efficient. These defects impair differentiation and maintenance of long-lived central and resident memory T cells. On the other hand, P2RX7 overstimulation in context of high expression of P2RX7 or elevated ligand concentrations, P2RX7 becomes a macropore. Macropore formation results in massive Ca^{2+} influx which is toxic to mitochondria and ultimately results in induction of T cell apoptosis. Elevated eATP concentrations within the TME may have the capacity to induce P2RX7-pore formation.

Made with BioRender

P2RX7 signaling must also be sustained for the long-term survival of memory T cells (*87, 88*). In the context of acute infections, sufficient eATP is released by inflamed and/or dying cells from the surrounding microenvironment to engage P2RX7 on effector and memory precursor cells. However, after the acute infection is resolved and inflammation recedes, paracrine sources of eATP diminish. Sustained P2RX7 signaling is likely mediated through cell-intrinsic ATP sources. Pannexin I (Panx1) is part of the pannexin hemichannel family and is broadly expressed by immune and epithelial cells. Panx1 has a well-defined role of exporting ATP from cells during apoptotic pathways or transiently during normal homeostasis (*93-95*). It has been shown that Panx1 releases a wave of ATP in response to TCR stimulation and Ca^{2+}-mediated ATP production by mitochondria. This wave of ATP can activate P2RX7 (and other eATP receptors) in an autocrine feedback loop (*72, 96, 97*). Indeed, it has been shown *in vitro* that Panx1 increases pericellular eATP concentrations in the micromolar range, while concentrations further from the cell membrane are considerably lower (*98*). This mechanism allows for controlled, local production of eATP to sustain low-level, tonic P2RX7 signaling, even in the absence of extrinsic sources of eATP (Fig 1.2). In this setting, CD8⁺ T cells can benefit from P2RX7 signaling driving metabolic fitness and proliferation without causes overstimulation and cell death. However, the dominant pathway of ATP release into the extracellular space occurs passively as a result of tissue damage. In these settings, it may be reasonable to expect that P2RX7 may become a liability and the cell-death causing pathway would predominate (Fig 1.1).

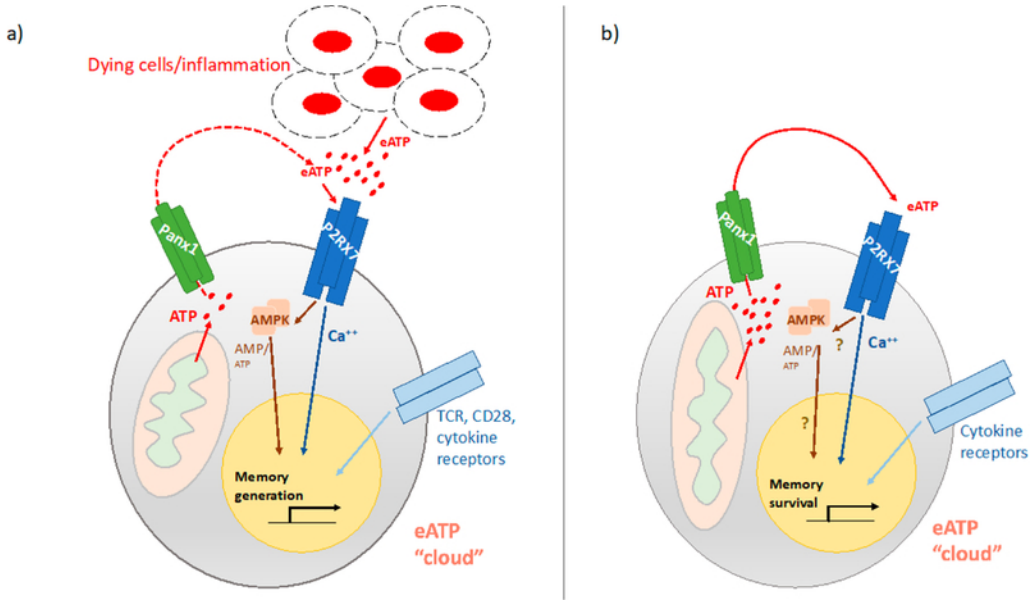

Figure 1.2: Role of the Panx1-P2RX7 signaling axis for memory CD8⁺ T cell homeostasis.

a) During effector immune responses or during contraction, CD8⁺ memory precursors express P2RX7, which senses eATP and induces activation of the AMPK pathway. Together with TCR, costimulatory and cytokine signals, this promotes generation of memory CD8⁺ T cells. Panx1 is expression by these cells and exports ATP, but eATP coming from inflamed/dying cells (due to ongoing infection) is likely dominant. **b)** After infection and inflammation is controlled, circulating memory CD8⁺ T cells still rely on P2RX7 for their long-term survival. Cell-extrinsic sources of eATP, however, are expected to be scarce. Panx1-mediated eATP release is likely crucial to provide eATP in an autocrine way, thereby guaranteeing the maintenance of a pericellular eATP 'cloud.' Periodic and/or sustained activation of P2RX7 in memory CD8⁺ T cells could maintain memory CD8⁺ T cell metabolic homeostasis. Simultaneously, ATP export itself maintain the AMP/ATP ratios optimal for AMPK activation, which reinforeces the metabolic fitness of memory CD8⁺ T cells through negative regulation of mTOR. Overall, the Panx1-P2RX7 circuit maintains metabolic homeostasis of memory CD8⁺ T cells to ensure ability to rapidly respond to secondary antigen encounter.

1.4.4 P2RX7 and tumor immunity

The role of P2RX7 in tumor immunity is complicated. This is in part because P2RX7 is expressed by both tumor cells and infiltrating immune cells. Furthermore, P2RX7-expressing immune cells within the tumor can be driving an anti-tumor immune response or acting to suppress it (*99*). The TME contains extremely high levels of eATP due to ongoing cell death/damage as the tumor grows (*62*). While eATP generally promotes an inflammatory response, tumors express high levels of ectonucleotidases CD39 and CD73 that rapidly degrade eATP into immunosuppressive adenosine (*100*). Regardless of whether P2RX7

has a beneficial or detrimental role, purinergic signaling pathways are prevalent within the TME and are attractive targets for cancer therapy.

P2RX7 expression on cancer cells is generally beneficial for the tumor. P2RX7 signaling drives tumor cell proliferation and accelerated growth (*101, 102*). Furthermore, extracellular nucleotide signaling increases them motility and metastatic potential of tumor cell lines (*103, 104*). Tumors often export ATP into the extracellular space to sustain P2RX7 signaling in an autocrine fashion (*99*). In order to avoid P2RX7 overstimulation and cell death, many types of tumors have evolved to use P2RX7 variants. A poorly defined variant of P2RX7 (nfP2RX7) is expressed by many different types of human tumors and has functional ion channel activity but is unable to form the macropore (*105*). Similarly, some murine tumor cell lines express a splice variant of P2RX7 (*P2RX7-a)* that is less sensitive to P2RX7-pore formation by ADP-ribosylation relative to the variant predominately expressed by T cells (*P2RX7-k*) (*106, 107*). Some human tumors release matrix metalloproteinases in response to sustained P2RX7 activation which cleaves the receptor to avoid formation of the macropore (*108*). While inhibiting P2RX7 on tumor cells has been shown to reduce tumor growth *in vitro* and *in vivo,* it is likely that P2RX7 inhibitors have off-target effects on other P2RX7-expressing immune cells within the tumor which could compromise tumor immunity (*109, 110*).

For the host immune response, P2RX7 deficiency results in accelerated tumor progression characterized by reduced inflammatory infiltrate (*109, 111, 112*). The high levels of eATP in the TME triggers the NLRP3 inflammasome in macrophages and DCs, resulting in inflammatory cytokine production and increased effector T cell infiltration (*113, 114*). P2RX7 can also induce immunogenic cell death (ICD), promoting DC maturation and ability to present tumor antigens to T cells (*115*). Consistent with these findings, a small molecule

P2RX7 agonist enhances DC cytokine production, resulting in improved antitumor immunity and enhanced responses to ICB in lung cancer (*116*).

The role of P2RX7 in $CD8^+$ T cell anti-tumor immune responses is complex. Our group has shown that P2RX7 deficient CD8 are unable to control chronic LCMV clone 13 infection characterized by a marked reduction in *P2rx7*$^{-/-}$ $CD8^+$ T cells, particularly in the $TCF1^+$ $CXCR5^+$ 'stem-like' subset of T cells (*87*), which have been shown to sustain $CD8^+$ T cell responses to both tumors and chronic infections (*117, 118*). A recent report demonstrated that P2RX7 expression on $CD8^+$ and $CD4^+$ T cells impaired tumor control in a B16 melanoma model. The reduced tumor control was associated with impaired ability of P2RX7-expressing T cells to seed the tumor (*119*). However, in this study the $CD8^+$ T cells transferred into tumor bearing mice were not activated using IL-12 as a tertiary signal, which has been shown to be essential for $CD8^+$ T cell control of B16 melanoma tumors (*120*). Furthermore, the impact of P2RX7 deficiency on $CD4^+$ T cell anti-tumor responses was much more striking (*119*). Consistent with this, systemic administration of a P2RX7 antagonist was found to increase effector $CD4^+$ T cells within the tumor while $CD8^+$ T cell populations were not affected (*109*). This suggests that $CD4^+$ T cells may be more sensitive to the P2RX7 overstimulation/cell death in the eATP-rich TME, particularly since many $CD4^+$ T cell subsets express high levels of P2RX7 (*79*). The focus of this dissertation is to understand the $CD8^+$ T cell-intrinsic role of P2RX7 in immune responses against tumors and whether this pathway can be modulated therapeutically.

1.5 Publications

Chapter modified with permission from the following published article:

Wanhainen K.M., Jameson S.C. and Borges da Silva H. Self-regulation of CD8 T cell metabolism through extracellular ATP signaling. *Immunometabolism.* 2019; 1(1):e1900009. PMID: 31428464

Chapter 2

Role of P2RX7 in $CD8^+$ T cells anti-tumor immunity.

2.1 Introduction

The purinergic receptor P2RX7 is a ligand-gated ion channel that recognizes extracellular ATP (eATP) (*64*). P2RX7 stimulation induces Ca^{2+} influx and K^{+} efflux, but prolonged exposure to very high eATP concentrations results in the formation of a macropore that ultimately induces cell death (*64, 66*). Elevated concentrations of eATP can act as a "danger signal" during infection or acute tissue damage, but eATP also accumulates in many solid tumors and contributes to the tumor microenvironment (TME) (*62*). In myeloid cells, P2RX7 stimulation leads to assembly of the NLPR3 inflammasome and promotes immunogenic cell death, innate immune activation and enhanced tumor antigen presentation (*115, 116*). Accordingly, previous studies have shown that host deficiency of P2RX7 leads to accelerated growth of B16 melanoma tumors reduced lymphocyte infiltration and decreased intratumoral inflammatory cytokines (*109, 111*). From these studies, P2RX7 was thought to promote antitumor immune responses. However, some tumors express conformationally altered forms of P2RX7 that may promote their survival in the eATP-rich TME, while P2RX7 expressed by tumor-infiltrating immune cells makes them vulnerable to macropore formation and death (*105*). Hence the impact of P2RX7 on tumor growth and control is complex.

P2RX7 is also expressed by numerous T cell populations and is important for metabolic fitness and durability of memory $CD8^{+}$ T cells following acute and chronic infections (*87, 88*). Parallels between $CD8^{+}$ T cell responses in chronic infections and tumors suggests that P2RX7 may have a similarly beneficial role in $CD8^{+}$ T cell-mediated anti-tumor immunity. On the other hand, it has been proposed that the abnormally high eATP concentrations in the TME could instead result in P2RX7-mediated T cell death instead (*62*). Indeed, using an adoptive cell therapy (ACT) approach, recent studies suggested that P2RX7 expression

by mouse CD8+ T cells limited their ability to control B16 melanoma (*119*). However, those studies employed CD8+ T cells that were expanded with IL-2 alone, and it is known that inclusion of IL-12 during CD8+ T cell stimulation substantially improves tumor control in B16 melanoma models, mediated through increased production of CD8+ effector cytokines and decreased induction of inhibitory receptors associated of T cell exhaustion (*120, 121*). Hence, it is unclear whether P2RX7 limits or enhances the immunotherapeutic potential of ACT using optimally activated CD8+ T cells.

T cell-based immunotherapies have already led to impressive outcomes in the clinic for patients with a variety of malignancies (*122-124*). However, there are still barriers hindering these therapies from reaching their full potential, and a pressing need to better understand how the TME impairs T cell accumulation, function and survival. Determining whether expression and stimulation of P2RX7 on tumor specific CD8+ T cells is an asset or detriment for tumor immunotherapy is important to inform strategies that could enhance the efficacy and durability of T cell adoptive cell therapies. In recent years it has become clear that mitochondrial function is compromised in tumor-infiltrating T cells, and that strategies that enhance the levels of functional mitochondria improve ACT by CD8+ T cells (*54-56, 58*). Our previous work has shown that P2RX7 signaling in long-lived memory CD8+ T cell subsets is essential for normal mitochondrial homeostasis and function, with P2RX7-deficiency leading to impaired mitochondrial maintenance, function and ultrastructure, dysregulated OXPHOS, and altered levels of intracellular ATP and AMP (*87, 88*). However, there is evidence that the different levels of P2RX7 stimulation may enhance or inhibit mitochondrial maintenance (*64, 125*), so it is currently unclear how the presence of P2RX7 impacts mitochondrial function and T cell survival in the eATP-rich solid tumor environment (*62*).

In this study, we demonstrate a $CD8^+$ T cell-intrinsic role for P2RX7 in promoting anti-tumor immune responses, using the B16 melanoma model. This effect was observed for $CD8^+$ T cells activated in the presence of IL-12, which substantially enhances tumor control in WT $CD8^+$ and simultaneously leads to increased P2RX7 expression. P2RX7-deficiency resulted in impaired mitochondrial homeostasis of transferred $CD8^+$ T cells in keeping with previous studies (*87, 88*). Furthermore, *P2rx7*$^{-/-}$ $CD8^+$ T cells displayed elevated expression of certain exhaustion markers, increased apoptosis, reduced proliferation and selective loss as the tumor burden increased. These results lend further support to other studies that have identified links between mitochondrial function and $CD8^+$ T cell dysfunction in settings of chronic antigen stimulation (*55, 56*). Additionally, these results demonstrate the requirement for P2RX7 in $CD8^+$ T cell control of tumors in adoptive cell therapy (ACT), which has clinical relevance as P2RX7 loss-of-function variants are relatively common in the human population (*126*).

2.2 Results

2.2.1 P2RX7 deficiency compromises optimal CD8⁺ T cell adoptive cell therapy in melanoma.

Previous studies suggested that P2RX7 expression is necessary for the host to elicit an effective anti-tumor immune response (*109, 111*). In striking contrast, however, a recent report indicated that P2RX7-deficient CD8⁺ T cells exhibit enhanced tumor control (*119*). In order to investigate this further, we adoptively transferred either wild-type (WT) or *P2rx7*$^{-/-}$ tumor-specific transgenic CD8⁺ T cells into mice with B16 melanoma tumors (the model used by Romagnani *et al.* (*119*)). Briefly, B16 melanoma cells expressing gp33 (B16.gp33), the epitope recognized by P14 CD8⁺ T cells, were injected subcutaneously (s.c.) into WT hosts. Once tumors became palpable, either WT or *P2rx7*$^{-/-}$ P14 CD8⁺ T cells were transferred intravenously (i.v.) after 72 hours of in vitro activation (Fig. 2.1a). WT and *P2rx7*$^{-/-}$ P14 were activated with IL-12 as a tertiary signal (in addition to anti-CD3/-CD28 and IL2) to optimize anti-tumor immune responses, as previously described (*120, 121*). Survival of tumor-bearing mice was significantly improved by adoptive transfer of WT P14 cells, compared to transfer of *P2rx7*$^{-/-}$ P14 cells (Fig. 2.1b). Tumor burden was also substantially reduced in mice that received WT P14 cells, with some mice having fully controlled tumors for >40 days (lines indicated by # in Fig. 2.1b-c, Fig. S2.1a). In contrast, tumor control was markedly impaired in mice transferred with *P2rx7*$^{-/-}$ P14 cells (Fig. 2.1b-c). The effect of P2RX7 deficiency was also confirmed using OT-I CD8⁺ T cells, which were transferred into mice with B16 tumors that express ovalbumin (B16.OVA) (Fig. S1b), paralleling the system used by Romagnani *et al.* (*119*).

Despite these differences in tumor control between WT and P2rx7-/- P14 cells, there was no difference in the ability of the in vitro activated populations to produce interferon-gamma (IFN-γ) (Fig. 2.2a) or kill B16 target cell lines (Fig.

2.2b), in keeping with previous studies indicating that *P2rx7*$^{-/-}$ CD8^{+} T cells differentiate normally into effector cells (*87, 88*).

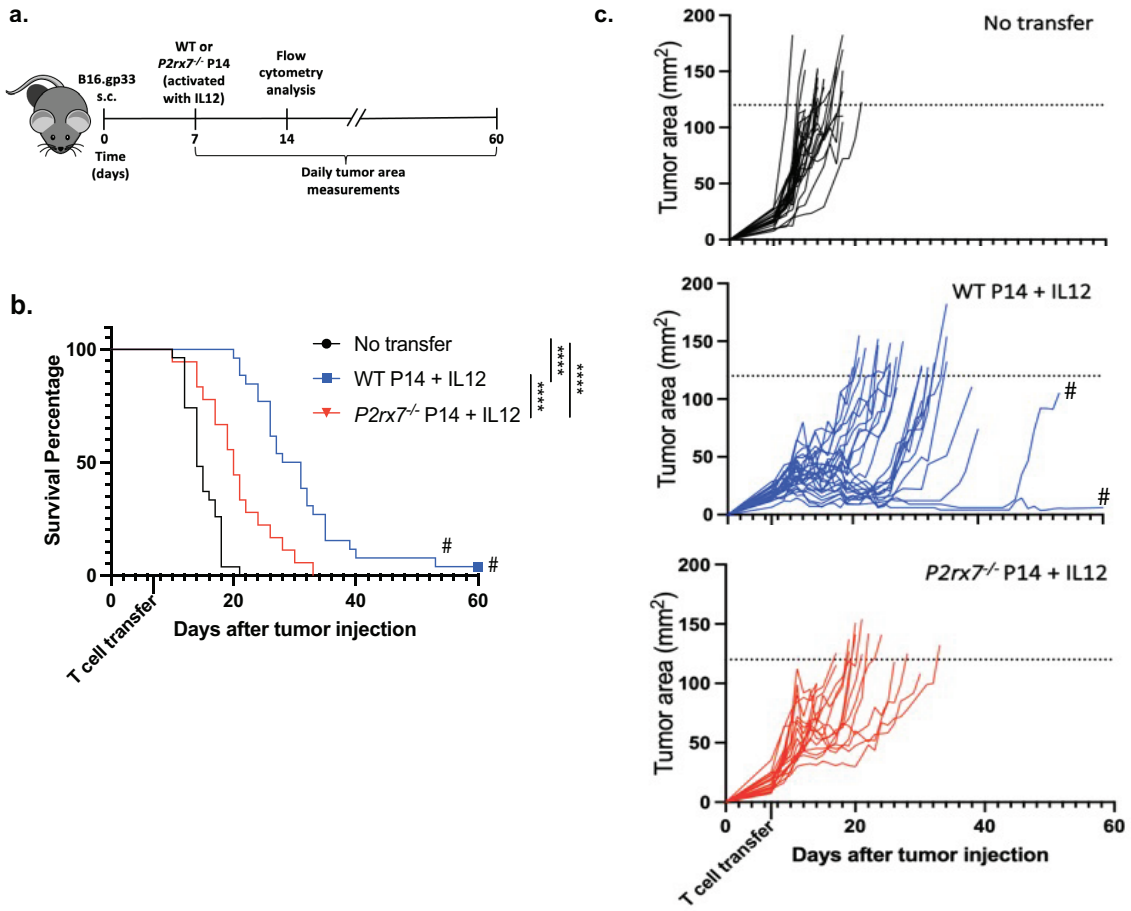

Figure 2.1 P2RX7 is required for IL-12 primed CD8^{+} T cells to control tumors.

a) B6 mice were injected with 3x10^{5} B16.gp33 melanoma cells s.c. and once tumors became palpable (~7 days post-injection) 5x10^{5} WT or *P2rx7*$^{-/-}$ P14 cells were transferred i.v. after 72 hours activation with anti-CD3/-CD28 and 2.5 IU/mL IL-2, with 5 ng/mL IL-12. **b)** Survival curve and **c)** tumor growth curves for individual tumor-bearing mice that received no cell transfer (n=27), WT P14 cells (n=23), or *P2rx7*$^{-/-}$ P14 cells (n=18) with IL-12 priming. Endpoint criteria for survival experiments were tumor ulceration or an area of 120mm^{2} (indicated by dashed line). Data are from 2-3 independent experiments. *, P ⩽ 0.05; **, P ⩽ 0.01; ***, P ⩽ 0.001; ****, P ⩽ 0.0001. Statistical significance for b, d determined by a log-rank Mantel-Cox test.

2.2.2 Without IL-12 priming, WT and P2rx7$^{-/-}$ *CD8*$^{+}$ *T cells provide similar control of tumors.*

A potentially important difference between our studies and those of Romagnani *et al.* (*119*) was their omission of IL-12 in the CD8^{+} T cell activation protocol. Indeed, in parallel studies we found that the advantage we observed for WT P14

cells in controlling tumors (Fig. 2.1b,c) was lost if IL-12 was not included during CD8⁺ T cell stimulation, with transfer of either WT or *P2rx7*$^{-/-}$ P14 cells only modestly improving survival of tumor-bearing mice compared to mice that received no CD8⁺ T cell transfer (Fig. 2.3a-b). Similar outcomes were observed in the OT-I/B16-OVA model (Fig. S2.1c) Consistent with Romagnani *et al*. (*119*), *P2rx7*$^{-/-}$ P14 cells stimulated without IL-12 conferred slightly improved survival relative to WT P14 cells (Fig. 2.3a), although this was not statistically significant in our hands. IL-12 exposure was reported to increase P2RX7 expression on CD8⁺ T cells (*86*), and and we confirmed this on P14 cells assessed at the end of in vitro activation (Fig. 2.3c). Similarly, P2RX7 gene expression by human CD8+ T cells was enhanced by culture with IL-12 (Fig. 2.3d). This is consistent with the hypothesis that the P2RX7-mediated contribution to tumor control may be amplified by IL-12 induced expression of P2RX7.

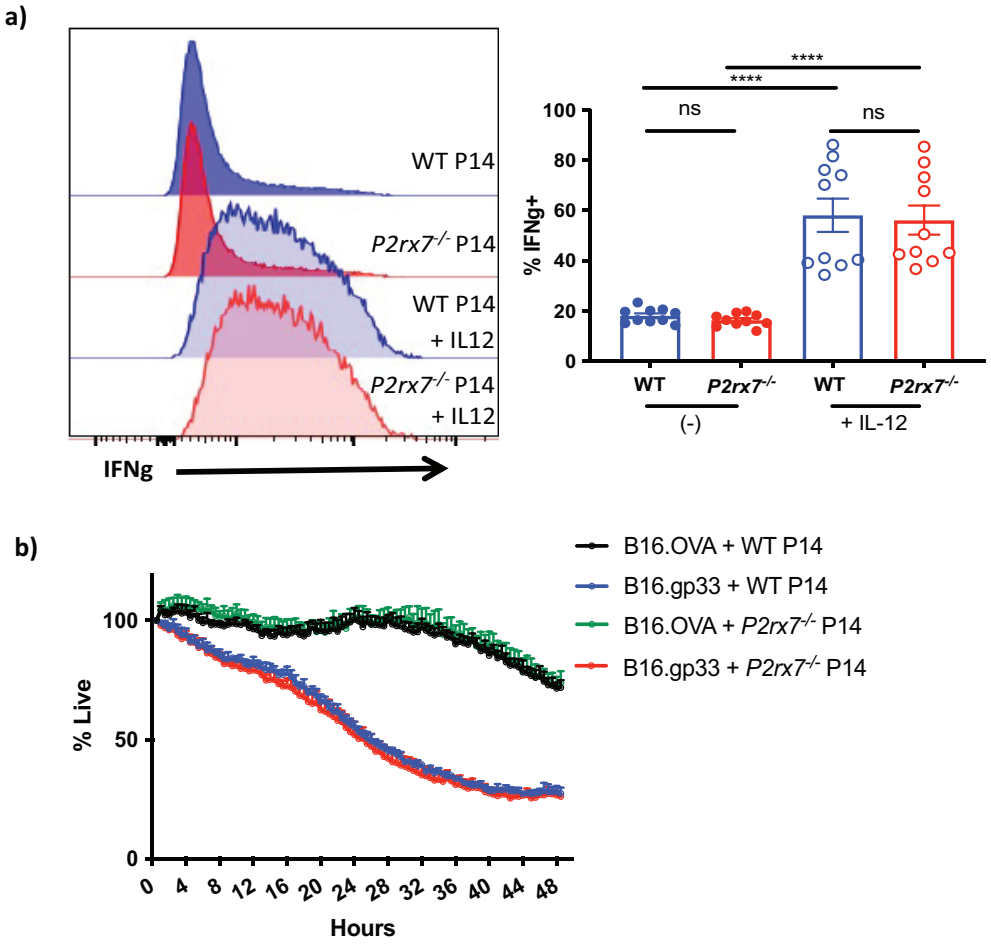

Figure 2.2: Defect in P2rx7$^{-/-}$ CD8^{+} T cell tumor control occurs in vivo.

a-b) WT and *P2rx7*$^{-/-}$ P14 cells were activated with anti-CD3, -CD28, IL2, and +/- IL-12 (5 ng/mL) *in vitro* for 72 hours. After 72 hour activation, CD8^{+} T cells were evaluated for IFN-γ production and cytotoxicity against B16 melanoma cell lines. **a)** Representative flow plot of IFN-γ gMFI (left) and frequency IFN-γ + P14 (right). **b)** Activated WT and P2rx7$^{-/-}$ P14 cells were co-cultured with antigen-specific (B16.gp33) or antigen-nonspecific (B16.OVA) target cells at an effector to target ratio of 3:1. Target cell killing was determined by Caspase 3/7 uptake. Data from 2-4 independent experiments. Graphical data shown as mean with error bars indicating SEM. *, P ≤ 0.05; **, P ≤ 0.01; ***, P ≤ 0.001. Statistical significance for **a** determined by One-way ANOVA

2.2.3 P2rx7$^{-/-}$ CD8^{+} T cells exhibit numeric and phenotypic differences compared to WT CD8^{+} T cells.

In order to determine how P2RX7 deficiency impacts donor CD8^{+} T cells transferred into tumor-bearing mice, we harvested B16.gp33 tumors, tumor-draining lymph nodes (dLN), and spleens from mice 7 days post-transfer of IL-12-activated WT or *P2rx7*$^{-/-}$ P14 cells. At this time point, tumor burden is only slightly greater in mice that received *P2rx7*$^{-/-}$ P14 cells as compared to recipients of WT P14 cells (Fig. 2.4a), providing an opportunity to identify phenotypic differences between WT and *P2rx7*$^{-/-}$ P14 cells, which may correspond with the failure of *P2rx7*$^{-/-}$ P14 cells to effectively control tumors. This analysis revealed fewer *P2rx7*$^{-/-}$ P14 cells per gram of tumor and in the tumor dLN and spleen, compared with WT P14 cells (Fig. 2.4b). Although tumor control by *P2rx7*$^{-/-}$ CD8^{+} T cells was impaired, WT and *P2rx7*$^{-/-}$ P14 cells did not differ significantly in the expression of exhaustion markers Tim3 and PD-1 within the tumor. However, in the dLN, the frequency of Tim3 expressing cells and PD-1 expression levels were elevated on the *P2rx7*$^{-/-}$ P14 population relative to WT P14 cells (Fig 2.4c-d). This finding is significant in light of recent studies showing that cells in the dLN may constitute a reservoir for sustaining the population of antigen specific CD8^{+} TIL (*127-129*). These findings may suggest recent antigen encounter or, perhaps, approaching T cell dysfunction/exhaustion. *P2rx7*$^{-/-}$ P14 cells within the dLN exhibit effector T cell qualities, as evidenced by an increased frequency expressing granzyme B (GzmB), despite no difference in GzmB expression among the groups within the tumor (Fig. 2.4e). Moreover, tumor-infiltrating *P2rx7*$^{-}$

$^{-/-}$ P14 cells were functional, efficiently producing IFN-γ after ex vivo restimulation with PMA/Ionomycin (Fig. 2.4f). Together, these data suggest that the *P2rx7*$^{-/-}$ P14 cells within the tumor are slightly reduced in number but do not show overt signs of exhaustion. However, *P2rx7*$^{-/-}$ P14 cells within the dLN, which presumably continue to seed the tumor over time, exhibit effector-like characteristics but are beginning to increase expression of markers associated with T cell dysfunction, which may ultimately compromise the ability of *P2rx7*$^{-/-}$ P14 cells to sustain an effective anti-tumor response.

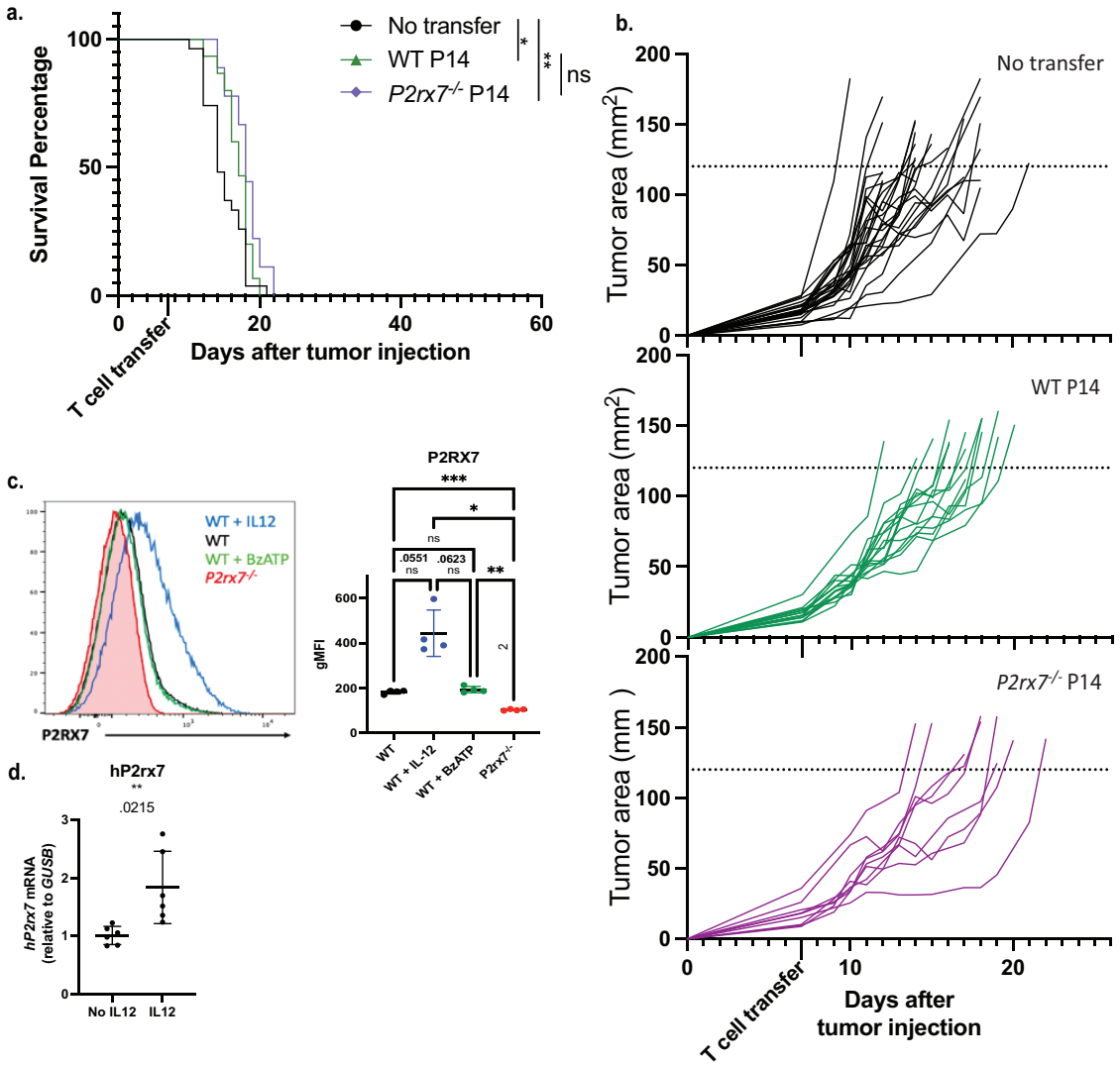

Figure 2.3: Without IL-12 induced P2RX7 expression, WT and *P2rx7*$^{-/-}$ CD8^{+} T cells exhibit similar tumor control

a-b) B6 mice were injected with 3x10^{5} B16.gp33 melanoma cells s.c. and once tumors became palpable (~7 days post-injection) 5x10^{5} WT or *P2rx7*$^{-/-}$ P14 cells were transferred i.v. after 72 hours activation with anti-CD3/-CD28 and 2.5 IU/mL IL-2. **a)** Survival curve and **b)** tumor area for tumor-bearing mice that received WT (n=15) or *P2rx7*$^{-/-}$ (n=9) P14 cells activated without IL12. Endpoint criteria for survival experiments were tumor ulceration or an area of 120mm^{2} (indicated by dashed line). **c)** P2RX7 expression on WT P14 cells after 72-hour in vitro activation with anti-CD3/-CD28, 2.5 IU/mL IL-2, +/- 5 ng/mL IL-12 or +/- the P2RX7 agonist BzATP. **d)** Human CD8+ T cells were activated in vitro with anti-CD3/CD28 for 72 hours with IL-2 +/- IL-12. They were then cultured for an additional 72 hours with indicated cytokines. At the end of cell culture, mRNA levels of hP2rx7 were evaluated by qPCR. Fold change normalized to GUSB control gene. Data are from 2-3 independent experiments. Bars show mean ± SEM. *, P ⩽ 0.05; **, P ⩽ 0.01; ***, P ⩽ 0.001; ****, P ⩽ 0.0001. Statistical significance for **a** determined by a log-rank Mantel-Cox test. Statistical significance for **c** determined by One-way ANOVA. Statistical significance for **d** determined by two-tailed, unpaired t-test.

2.2.4 Tumor infiltrating P2rx7$^{-/-}$ *CD8*$^{+}$ *T cells show signs of mitochondrial dysfunction.*

We have previously shown that *P2rx7*$^{-/-}$ CD8+ T cells have dysregulated metabolism in an acute infection model (*87*). Given the correlation between T cell metabolic fitness and efficacy of anti-tumor responses (*130*), we were interested in whether *P2rx7*$^{-/-}$ P14 cells have altered mitochondrial dynamics in response to metabolic stressors in the tumor microenvironment (TME). We measured mitochondrial mass and membrane potential of WT and *P2rx7*$^{-/-}$ P14 cells from spleens, dLNs and tumors of B16.gp33 engrafted mice by staining for MitoTracker Green (MTG) and Tetramethylrhodamine ethyl ester (TMRE), respectively. Both tumor-infiltrating WT and *P2rx7*$^{-/-}$ P14 cells have increased mitochondrial mass and membrane potential relative to P14 cells within the dLN and spleen (Fig. 2.5a-b). Interestingly, the TMRE/MTG ratio, indicating mitochondrial activity efficiency, was decreased in *P2rx7*$^{-/-}$ P14 cells within the tumor and dLN (Fig. 2.5c). This suggests that, despite both WT and *P2rx7*$^{-/-}$ P14 cells increasing mitochondrial mass in response to cues in the TME, the mitochondria in tumor-infiltrating WT P14 cells are more functional.

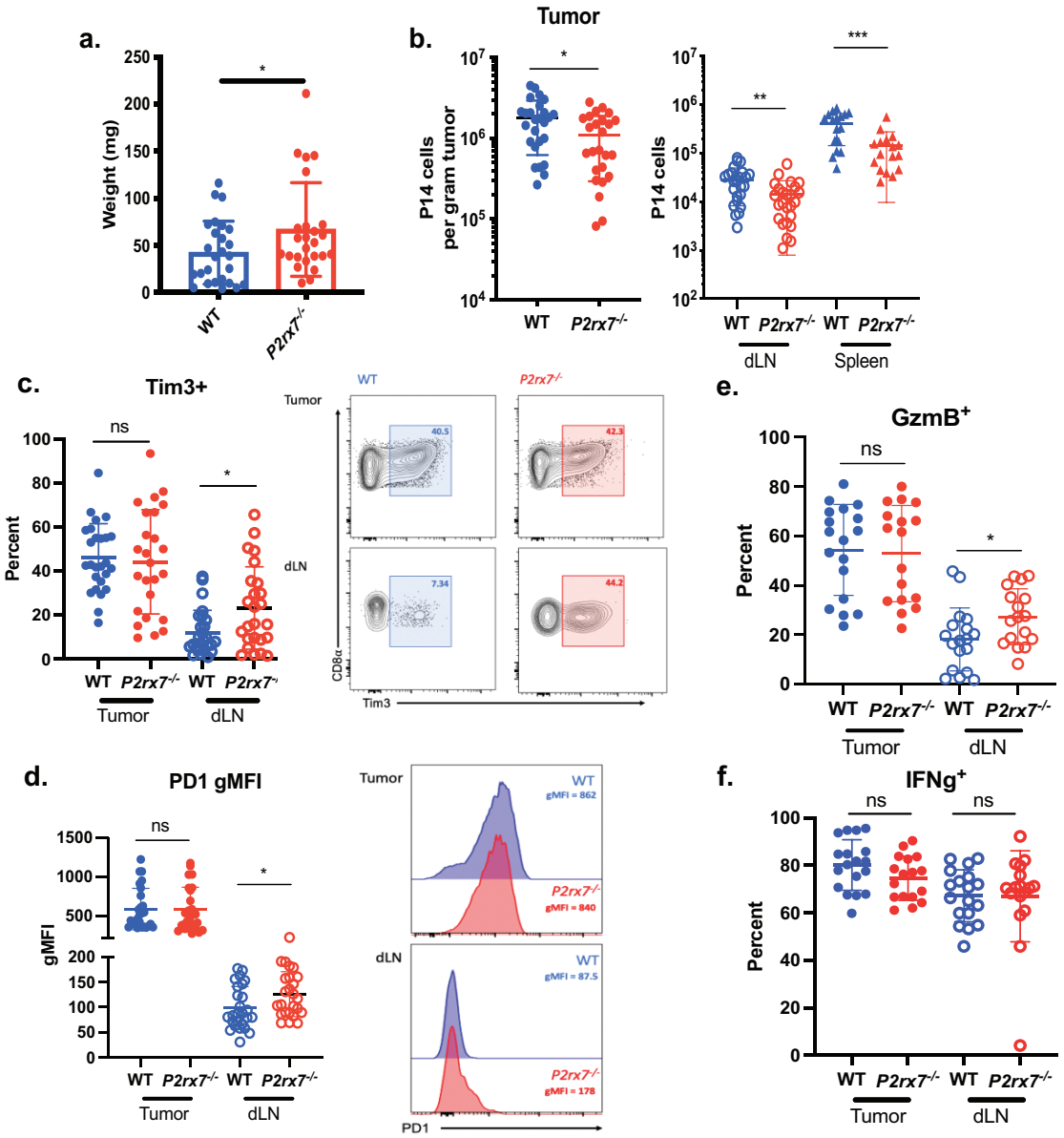

Figure 2.4 Tumor specific *P2rx7*$^{-/-}$ CD8^{+} T cells within dLN have increased expression of exhaustion markers

Activated WT or *P2rx7*$^{-/-}$ P14 cells (with IL-12) were transferred into mice with palpable B16.gp33 tumors. Tumors, tumor dLNs and spleens were harvested from recipient mice 7 days post-T cell transfer. **a)** Weight of tumors from B16.gp33-engrafted mice 7 days post-T cell transfer. **b)** Number of live P14 within tissues. **c)** Percentage of Tim3^{+} P14 cells within tumor (left) and dLN (right). **d)** PD1 gMFI of P14 cells within tumor (left) and dLN (right). **e)** Percentage of GzmB^{+} and **f)** IFNg^{+} P14 cells post-ex vivo restimulation with PMA/Ionomycin. Data are from 3-4 independent experiments. Graphical data shown as means with error bars indicating SEM. *, P $\leqslant$ 0.05; **, P $\leqslant$ 0.01; ***, P $\leqslant$ 0.001. Statistical significance determined by a two-tailed, unpaired t-test

Additionally, we observed a population of P14 cells that had increased mitochondrial mass (MTG^{hi}) but very low mitochondrial membrane potential (TMRE^{lo}). This population (MTG^{hi} TMRE^{lo}) likely represents cells that accumulate 'depolarized' and nonfunctional mitochondria, and this is known to occur at a higher frequency among CD8^{+} T cells within the TME [19]. Consistent with this, we found that both WT and *P2rx7*$^{-/-}$ P14 cells from tumors of some B16.gp33 engrafted mice had a higher percentage of MTGhi TMRElo cells compared to P14 cells from the dLNs and spleens. Despite high variability among samples, this trended higher for tumor-infiltrating *P2rx7*$^{-/-}$ P14 cells compared to WT (Fig. 2.5d). Together, these results suggest that tumor infiltrating P14 cells that lack P2RX7 have dysfunctional mitochondria which has been linked to impaired CD8^{+} T cell anti-tumor responses.

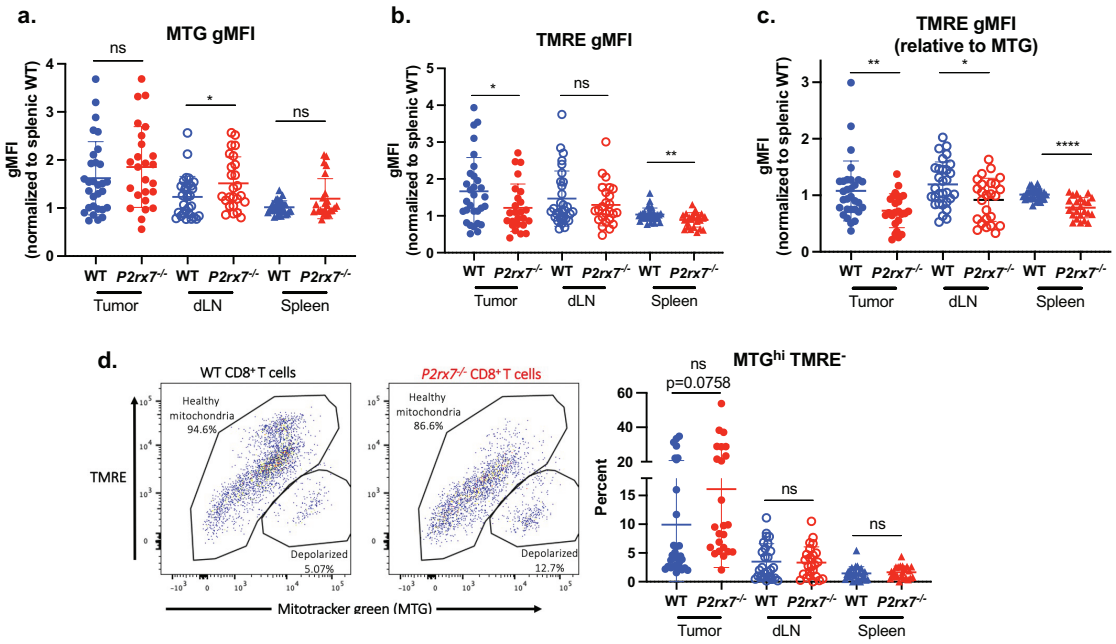

Figure 2.5: *P2rx7*$^{-/-}$ CD8+ T cells show signs of mitochondrial dysfunction.

Activated WT or P2rx7-/- P14 cells were cultured with IL-12 then transferred into mice bearing palpable B16.gp33 tumors. Tumors, tumor dLNs and spleens were harvested from recipient mice 7 days post-T cell transfer. Mitochondrial mass and membrane potential was measured in WT and P2rx7-/- P14 cells within tumors of B16.gp33-engrafted mice by MTG and TMRE gMFI, respectively. Fold changes of a) MTG gMFI, b) TMRE gMFI, c) relative TMRE gMFI (normalized to MTG gMFI). (a-c) For each independent experiment, fold change in gMFI for the indicated molecular probe was calculated relative to average gMFI of donor WT P14 cells within the spleen. d) Frequency of P14 cells with depolarized (MTG^{hi} TMRE^{lo}) mitochondria. Data are from 3 independent experiments. Graphical data shown as means with error bars indicating SEM. *, P ≤ 0.05; **, P ≤ 0.01; ***, P ≤ 0.001; ****, P ≤ 0.0001. Statistical significance determined by a two-tailed, unpaired t-test.

2.2.5 P2rx7$^{-/-}$ CD8^{+} T cells exhibit cell-intrinsic defects during the response to tumor.

Differences in initial tumor control by WT and *P2rx7*$^{-/-}$ CD8^{+} T cells could potentially affect the phenotype or function of these cells even at early time points, due to an altered TME. Hence, we next investigated whether differences seen for WT and *P2rx7*$^{-/-}$ CD8^{+} T cells would be recapitulated when both populations were present in the same tumor environment. Equal numbers of WT and *P2rx7*$^{-/-}$ OT-I cells were co-transferred into mice with palpable B16.OVA tumors. This approach permits evaluation of cell-intrinsic effects of P2RX7-deficiency, while the co-transferred WT cells are expected to limit tumor growth, allowing for evaluation at later time points after ACT. Seven and 18 days later, the ratio and phenotype of cells infiltrating the tumor, dLN and spleens of B16.OVA engrafted mice was analyzed. Between these time points, the tumor size increased considerably, as expected (Fig. 2.6a). At day 7, WT and *P2rx7*$^{-/-}$ OT-I cells were present at equal frequencies within the tumors and SLO (Fig 2.6b). However, by day 18, we observed a preferential loss of *P2rx7*$^{-/-}$ OT-I cells within the tumor, dLN, and spleen (Fig 2.6b). Furthermore, while the frequency of cells expressing exhaustion markers was, surprisingly, greater among the WT donor population at day 7, by d18 we observed increased expression of PD-1 and Lag3 by the *P2rx7*$^{-/-}$ OT-I population (Fig. 2.6c) and the *P2rx7*$^{-/-}$ populations showed impaired *ex vivo* production of IFN-γ (Fig. 2.6d). The frequency of the TCF1^{+} 'stem-like' population within the tumor initially favored the *P2rx7*$^{-/-}$ population, but this advantage was lost by d18 (Fig. S2.2a). Consistent with previous reports, IL-12 priming during T cell activation reduces expression of markers characteristic of T cell exhaustion (*121*), and neither WT or *P2rx7*$^{-/-}$ donor cells express a substantial TOX^{+} population as compared to endogenous CD8^{+} T cells (Fig S2.2b).

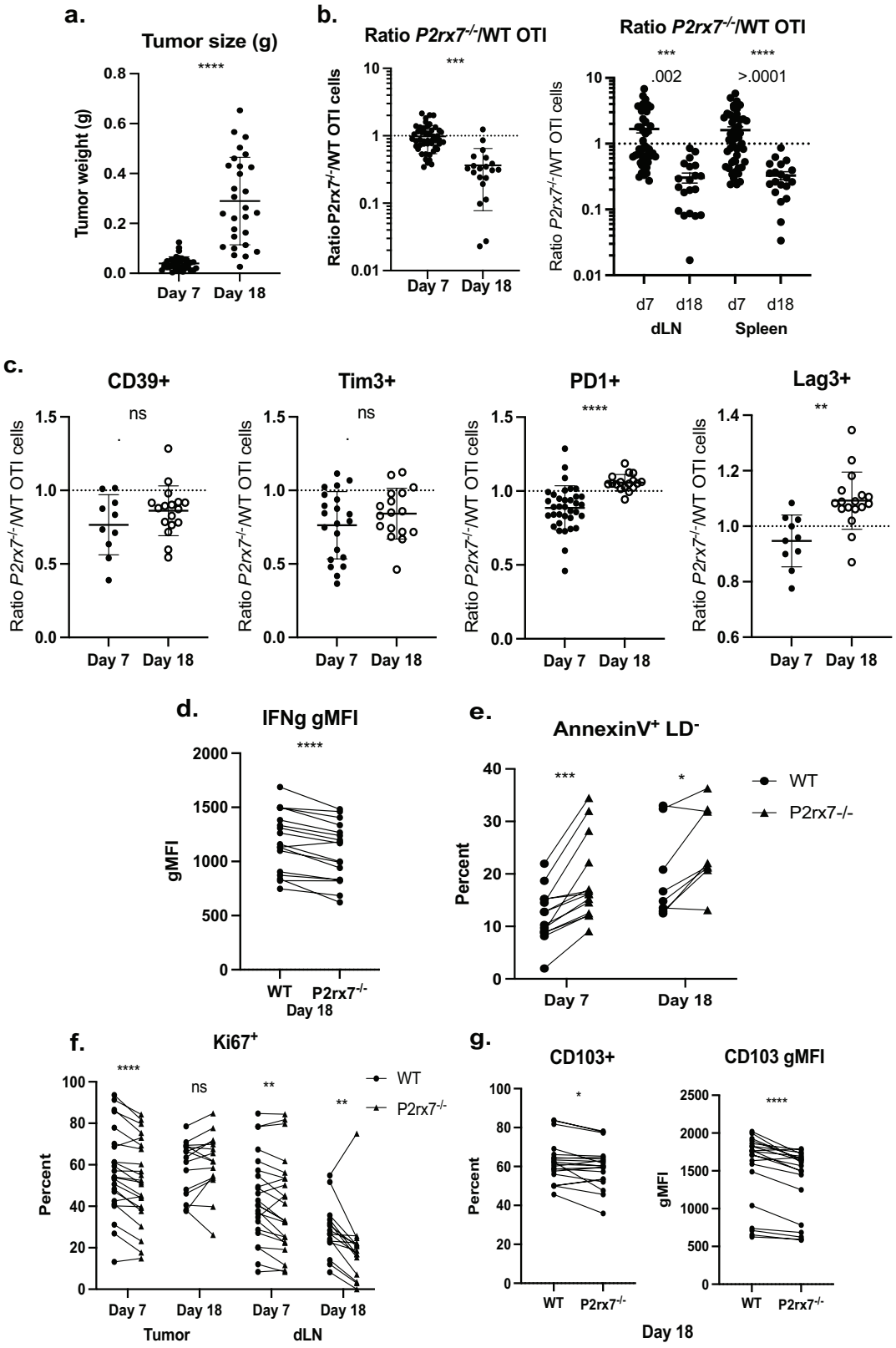
a.
Tumor size (g)
Tumor weight (g)
Day 7
Day 18
b.
Ratio P2rx7-/-/WT OTI
Ratio P2rx7-/-/WT OTI cells
.002
>.0001
d7
d18
dLN
Spleen
c.
CD39+
Tim3+
PD1+
Lag3+
ns
d.
IFNg gMFI
gMFI
WT
P2rx7-/-
e.
AnnexinV+ LD-
Percent
f.
Ki67+
Tumor
dLN
g.
CD103+
CD103 gMFI

Figure 2.6: Cell-intrinsic defects in *P2rx7*$^{-/-}$ CD8+ T cells responding to tumor growth.

Equal numbers of activated WT and *P2rx7*$^{-/-}$ OT-I cells (with IL-12) were co-transferred into mice with palpable B16.OVA tumors. Tumors, tumor dLNs, and spleens were harvested from recipient mice 7- and 18-days post-T cell transfer. **a)** Weight of tumors from B16.OVA engrafted mice at indicated time of harvest. **b)** Ratio *P2rx7*$^{-/-}$ / WT OT-I donor cells within tumor, dLN and spleen at days 7 and 18 after T cell transfer. **c)** Frequency of donor WT or *P2rx7*$^{-/-}$ OT-I cells that express (from left) CD39, Tim3, PD1, and Lag3 at each time point was determined and the ratio *P2rx7*$^{-/-}$ / WT OT-I cells within each population was calculated to indicate change in expression of each marker at day 7 versus day 18. **d)** *Ex vivo* expression of IFN-γ in WT versus *P2rx7*$^{-/-}$ OT-I cells from tumors of mice harvested at day 18. **e)** Frequency of apoptotic donor OT-I cells based on Annexin V+ and propidium iodide- (PI) and LiveDead- (LD). **f)** Frequency of proliferating (Ki67+) donor cells within tumor and dLN. **g)** Frequency of OT-I donor cells within the tumors of mice harvested at day 18 that express CD103 (left) and expression levels (right). Fold changes were calculated by normalizing the average gMFI of the indicated molecular probe in splenic T cells. Data are from 2-4 independent experiments. *, $P \leq 0.05$; **, $P \leq 0.01$; ***, $P \leq 0.001$; ****, $P \leq 0.0001$. Statistical significance determined by a two-tailed, paired t-test.

Notably, at both time points we observed significantly increased frequencies of Annexin V+ (LiveDead/PI-) cells among the *P2rx7*$^{-/-}$ OT-I cells within the tumor (Fig 2.6e), suggesting these cells are preferentially undergoing apoptotic death, potentially contributing to the loss of *P2rx7*$^{-/-}$ cells by d18. *P2rx7*$^{-/-}$ OT-I in the tumor and dLN showed reduced proliferation (measured by Ki67 staining) at d7, and this defect was sustained in the dLN at d18 (Fig 4f). Finally, *P2rx7*$^{-/-}$ TIL displayed reduced expression of the "residency marker" CD103 within the tumor (Fig 4g), which may suggest impaired tumor residency. Taken together, these data suggest a progressive loss in function and maintenance among *P2rx7*$^{-/-}$ CD8+ T cells as time and the tumor burden increase, resulting in increased cell death and reduced representation of *P2rx7*$^{-/-}$ CD8+ TIL.

We also assessed the mitochondrial fitness of co-transferred WT and *P2rx7*$^{-/-}$ OT-I cells at both time points. At day 18, we observed a significant increase in frequency of *P2rx7*$^{-/-}$ OT-I cells with depolarized mitochondria within the tumor (Fig 2.7a). TILs that accumulate depolarized mitochondria are reported to have phenotypic and functional characteristics of terminal exhaustion relative to cells with 'healthy' mitochondria (*56*). Interestingly, IL-12 priming during activation also seems to rescue this population of cells from acquiring exhaustion characteristics when compared to endogenous cells within the same tumor (Fig S2.3a-b). Additionally, consistent with our findings from the single-transfer model, we

observed that WT OT-I cells within the tumor and dLN had higher mitochondrial mass and improved membrane potential and activity per mitochondrion regardless at both time points (Fig. 2.7b-d), suggesting the impaired mitochondrial fitness observed for *P2rx7*$^{-/-}$ CD8^{+} T cells was cell-intrinsic. Additionally, *P2rx7*$^{-/-}$ CD8^{+} T cells within the tumor at d18 had significantly lower levels of mitochondrial reactive oxygen species (ROS), consistent with mitochondrial function being reduced (Fig 2.7e). We also evaluated expression of the mitochondria biogenesis promotor PGC1α, which is reported to be lost overtime in TILs and results in mitochondrial dysfunction (*54*). We did not observe differences in expression of PGC1α between WT and *P2rx7*$^{-/-}$ CD8^{+} T cells (Fig S2.4a-b), suggesting that the defect in *P2rx7*$^{-/-}$ CD8^{+} T cells is more related to mitochondrial function, rather than biogenesis. Taken together, these results demonstrate that the *P2rx7*$^{-/-}$ CD8^{+} T cell population is susceptible to varied mitochondrial defects even when the TME is normalized using a co-transfer approach, signifying that this dysfunction is cell-intrinsic.

2.2.6 Metabolic differences between WT and P2rx7$^{-/-}$ *CD8*$^{+}$ *T cells arise during in vitro activation.*

It was unclear whether the mitochondrial defects observed in tumor-infiltrating *P2rx7*$^{-/-}$ CD8^{+} T cells were already established during in vitro activation or were a result of cells encountering antigen in the hypoxic, nutrient depleted TME. Furthermore, the impact of IL-12 on metabolic activity of cultured CD8^{+} T cells has not been clearly defined. We initially assessed oxidative phosphorylation and glycolysis in WT and *P2rx7*$^{-/-}$ P14 cells at 72h of stimulation, using extracellular flux 'Seahorse' assays. IL-12 culture significantly increased the baseline and maximum oxygen consumption rate (OCR) of WT P14 cells, but not *P2rx7*$^{-/-}$ P14 cells (Fig 2.8a-c) and showed a trend toward increased spare respiratory capacity (SRC) (Fig. 2.8d). Consistent with the metabolic defects in *P2rx7*$^{-/-}$ CD8^{+} T cells being primarily related to mitochondrial function, we observed no

differences in glycolytic capacity of WT and *P2rx7*$^{-/-}$ CD8^{+} T cells, as measured by extracellular acidification rate (Fig. S2.5a-b).

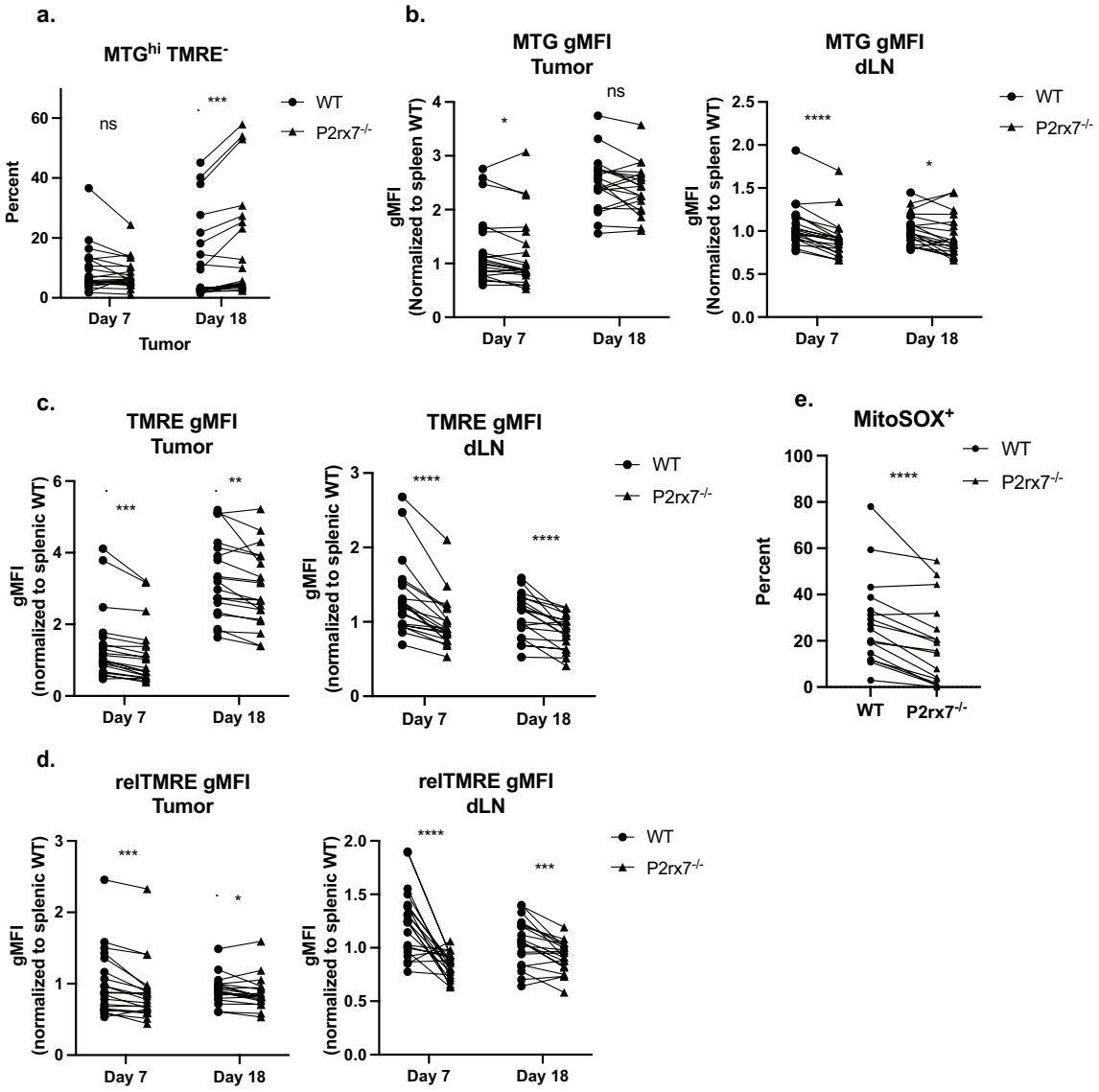

Figure 2.7: Impaired mitochondrial fitness of *P2rx7*$^{-/-}$ CD8+ T cells is cell-intrinsic.

Equal numbers of WT and *P2rx7*$^{-/-}$ OT-I CD8^{+} T cells were activated in the presence of IL-12 and equal numbers of cells were co-transferred into mice with palpable B16.OVA tumors. Tumors, tumor dLNs, and spleens were harvested from recipient mice 7- and 18-days post-T cell transfer. **a)** Frequency of OT-I donor cells with depolarized (MTG^{hi} TMRE^{lo}) mitochondria within the tumors of mice harvested at days 7 or 18. Fold changes of **b)** MTG gMFI, **c)** TMRE gMFI, **d)** relative TMRE gMFI (normalized to MTG gMFI) in OT-I donor cells from tumors and dLN of mice at indicated time points. **(b-d)** For each independent experiment, fold change in gMFI of indicated molecular probe was calculated relative to average gMFI of donor WT P14 cells within the spleen. **e)** Frequency of OT-I donor cells producing mitochondrial reactive oxygen species (ROS), as indicated by MitoSOX+, within tumors of mice harvested at day 18. Data are from 3-4 independent experiments. *, $P \leq 0.05$; **, $P \leq 0.01$; ***, $P \leq 0.001$; ****, $P \leq 0.0001$. Statistical significance determined by a two-tailed, paired t-test.

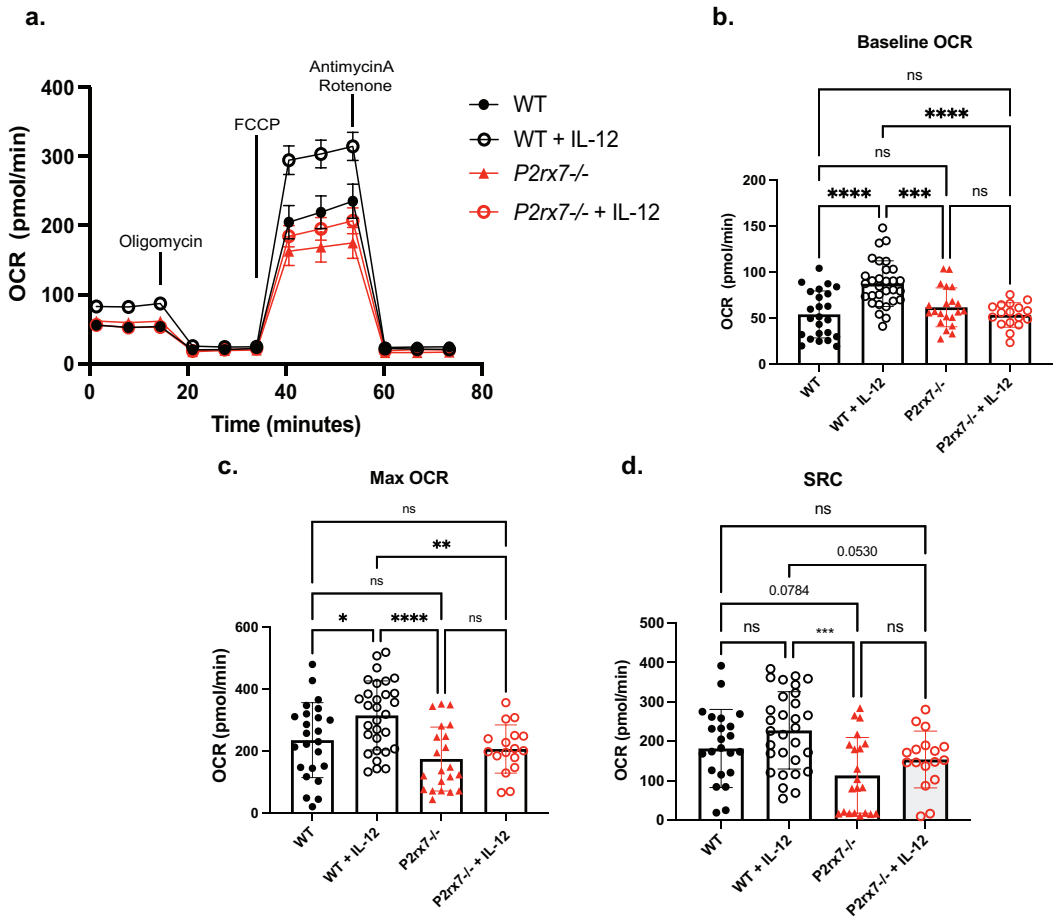

Figure 2.8: Metabolic defects in *P2rx7*$^{-/-}$ CD8+ T cells arise during in vitro activation.

WT and *P2rx7*$^{-/-}$ P14 cells were activated for 72 hours in vitro with anti-CD3, -CD28, IL2, and +/- IL12. **(a-d)** Oxygen consumption rate (OCR) of indicated groups after 72-hour activation was evaluated using Seahorse Extracellular Flux assay. **a)** Oxygen consumption rates (OCRs) were determined for the indicated groups after sequential addition of the listed inhibitors. **b)** Baseline OCR of indicated groups (determined prior to Oligomycin addition). **c)** Maximum OCR of indicated groups (determined after FCCP addition). **d)** Spare respiratory capacity of indicated groups (calculated based on difference between Max OCR and baseline OCR). Data are from 3 independent experiments. Graphical data shown as means with error bars indicating SEM. *, P ⩽ 0.05; **, P ⩽ 0.01; ***, P ⩽ 0.001; ****, P ⩽ 0.0001. Statistical significance determined by One-way ANOVA.

We next determined how this related to mitochondrial homeostasis of in vitro cultured WT and *P2rx7*$^{-/-}$ P14 cells. IL-12 increased mitochondrial mass in both populations, yet mitochondrial membrane population was not elevated proportionally, such that IL-12 exaggerated the differences in relative membrane potential (TMRE/MTG ratio) between WT and *P2rx7*$^{-/-}$ T cells (Fig 2.9a-c). Ultrastructure evaluation of mitochondria from *in vitro* activated WT and *P2rx7*$^{-/-}$ T cells also did not reveal substantial differences in mitochondrial size (Fig 2.9d). In

previous work, we showed that *P2rx7*$^{-/-}$ P14 cells display defective mitochondrial fusion when differentiated into a memory-like population through extended culture in the presence of IL-15 (*87*). Whether prolonged culture with IL-12 would induce similar effects is currently unclear, but our current data indicate that defective relative membrane potential can occur without ultrastructural changes in IL-12 cultured *P2rx7*$^{-/-}$ CD8^{+} T cells. These results illustrate the ability of IL-12 to boost the levels of functional mitochondria in WT CD8+ T cells but not to the same extent in *P2rx7*$^{-/-}$ cells. These results mirror mitochondrial defects observed in vivo and suggest that *P2rx7*$^{-/-}$ P14 are disadvantaged metabolically prior to arrival in the TME, which may compromise durable anti-tumor immune responses.

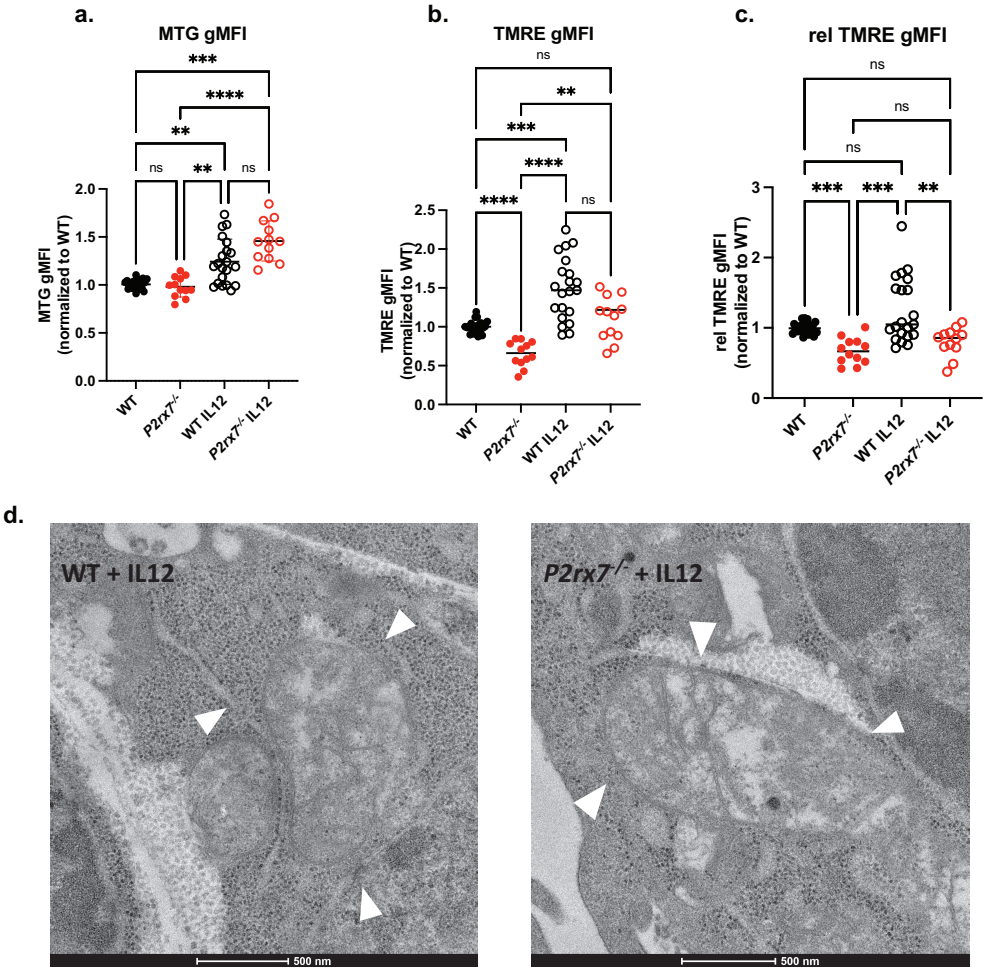

Figure 2.9: *P2rx7*$^{-/-}$ exhibit defects in mitochondrial function but not mass during activation.

WT and *P2rx7*$^{-/-}$ P14 cells were activated for 72 hours in vitro with anti-CD3, -CD28, IL2, and +/- IL12. **(a-c)** Mitochondrial mass and membrane potential was measured in WT and P2rx7-/- P14 cells after in vitro activation by evaluating levels of MTG or TMRE, respectively. Fold changes of **a)** MTG gMFI, **b)** TMRE gMFI, and **c)** relative TMRE gMFI (normalized to MTG gMFI). **(a-c)** For each independent experiment, fold change in gMFI of indicated molecular probe was calculated relative to average gMFI of WT (untreated) P14 cells. **d)** Representative electron micrographs showing mitochondrial structure and size of *in vitro* activated WT and *P2rx7*$^{-/-}$ P14 cells (with IL-12). Data are from 2-5 independent experiments. Graphical data shown as means with error bars indicating SEM. *, $P \leqslant 0.05$; **, $P \leqslant 0.01$; ***, $P \leqslant 0.001$; ****, $P \leqslant 0.0001$. Statistical significance determined by One-way ANOVA..

2.3 Discussion

Previous studies have shown that mice that lack P2RX7 display accelerated tumor growth and have fewer tumor-infiltrating lymphocytes compared to WT mice (*109, 111*). However, P2RX7 is expressed on many cell types, including various immune populations and many tumors (*99*), making the cell intrinsic role for P2RX7 difficult to discern from such studies. Indeed, expression of P2RX7 by tumor cells (including B16 melanoma) can contribute to their growth, as indicated by studies showing that P2RX7 pharmacological blockade limits tumor growth (*109, 111*). The situation is further complicated by the capacity of high levels of eATP to transform P2RX7 signaling from a non-selective cation channel into a lethal macropore. The high eATP concentrations often found in the TME may therefore make P2RX7 expression a liability rather than a benefit for immune cells. Indeed, while we previously showed that P2RX7 expression is beneficial for the establishment and maintenance of $CD8^+$ memory T cells following responses to chronic and acute infections (*87, 88*), recent studies suggested that P2RX7 was detrimental for $CD8^+$ T cell-mediated tumor immunotherapy (*119*). Nevertheless, it was not clear what role P2RX7 would play in adoptive immunotherapy by $CD8^+$ T cells that were optimally stimulated for efficient tumor control.

Our studies built on the observation that IL-12 treatment of tumor-specific $CD8^+$ T cells during *in vitro* activation dramatically improves their persistence and ability to eradicate tumors (*120, 121*). Indeed, while our data indicate that P2RX7 expression offers no benefit for sub-optimally stimulated $CD8^+$ T cells, the enhanced tumor control induced by IL-12 cultured $CD8^+$ T cells was severely blunted by P2RX7-deficiency. *P2rx7*$^{-/-}$ $CD8^+$ T cells are responsive to IL-12, as indicated by increased expression of IFNγ post-activation and reduced expression of transcription factors associated with T cell exhaustion (e.g. TOX) (*120, 121*). However, IL-12 reprogramming was still not sufficient to promote

effective anti-tumor responses in P2RX7-deficient T cells. P2RX7 deficiency correlated with reduced production of functional mitochondria in tumor infiltrating $CD8^+$ T cells, an effect that was also observed following in vitro activation prior to adoptive transfer.

As tumors expand, their increased metabolic demand creates an environment that is extremely hypoxic and depleted of nutrients. This poses an obstacle that infiltrating immune cells must adapt to in order to meet their own metabolic needs. Mitochondrial health and homeostasis is dependent on controlled biosynthesis and autophagic degradation of mitochondria (*131*). These processes are often impaired in tumor infiltrating $CD8^+$ T cells, resulting in poor mitochondrial quality and the accumulation of damaged mitochondria compared to splenic $CD8^+$ T cells (*54, 56*). Consistent with those studies, we also find that mitochondria in tumor infiltrating $CD8^+$ T cells have a lower mitochondrial membrane potential and an increased frequency of depolarized mitochondria. These characteristics were significantly worsened in *P2rx7*$^{-/-}$ $CD8^+$ T cells within the tumor. P2RX7 deficient $CD8^+$ T cells also showed mitochondrial impairments and reduced baseline and maximum levels of oxidative phosphorylation (OXPHOS) after in vitro activation. The glycolytic capacity of in vitro activated *P2rx7*$^{-/-}$ $CD8^+$ T cells was not impaired compared to WT $CD8^+$ T cells. T cells shift their metabolism to predominately utilize aerobic glycolysis upon activation (*14*). P2RX7 deficient $CD8^+$ T cells may be able to compensate for mitochondrial defects initially by relying on glycolysis, but likely lack the plasticity necessary to adapt to changes in nutrient and oxygen availability in the TME.

Metabolic alternations in tumor infiltrating $CD8^+$ T cells have been identified as early events that ultimately lead to T cell exhaustion (*56, 57, 132*). Furthermore, manipulation of $CD8^+$ T cells to optimize mitochondrial function and structure has been shown to correlate with reduced expression of inhibitory receptors (*133*-

135), and can even restore functionality of exhausted T cells (*55, 136*). Consistent with this, intratumoral *P2rx7*$^{-/-}$ CD8^{+} T cells exhibit increased expression of some exhaustion markers and reduced production of IFN-γ as the anti-tumor response progresses. These changes occur alongside continued mitochondrial dysfunction and correlate with selective loss of *P2rx7*$^{-/-}$ CD8^{+} T cells within the tumor and dLN. These data reinforce the strong link between mitochondrial fitness and T cell function and survival. Our data also indicate that mitochondrial function may in some cases be an early indicator of an effective T cell anti-tumor response before the onset of exhaustion.

While our data suggest that the role of P2RX7 in promoting CD8^{+} T cell responses and metabolic fitness is similar in the context of acute/chronic infections and tumors, the numeric defect among tumor-infiltrating *P2rx7*$^{-/-}$ CD8^{+} T cells was more subtle than our observations in infection models (*87, 88*). While this may relate to the early time points of analysis required for studies involving the rapidly growing B16 model, it is also possible that this finding relates to the dual functions of P2RX7: While P2RX7-deficiency may compromise mitochondrial maintenance, overstimulation of P2RX7, due to high expression levels or elevated concentrations of eATP in the TME may induce P2RX7 to form a macropore resulting in WT T cell death (*64, 79, 137*). In normal tissues, eATP concentrations are in the nM range, but in the TME, eATP concentrations can reach hundreds of μM (*62*). P2RX7 macropore formation can also be induced by NAD^{+}-mediated ribosylation of P2RX7 by the ectoenzyme ARTC2.2 (*66*). For this reason, we use nanobody-mediated ARTC2.2 antagonism at the time of harvest, which we have shown improves recovery of P2RX7-expressing CD8^{+} T cells during tissue processing where NAD^{+} might be released from necrotic cells (*84, 85*). However, this will not protect P2RX7-expressing T cells from high concentrations of eATP within the tumor in vivo. For these reasons, it is likely that the TME may be especially hostile to P2RX7-expressing WT CD8+ T cells, yet

our data indicate that this is outweighed by their improved ability to control tumor growth. Still, given the complicated nature of P2RX7 signaling, particularly in high eATP/NAD^+ environments where the receptor could be a liability, it is not suprising that there is some discrepancy on the cell intrinsic role of P2RX7 in the context of $CD8^+$ T cell-mediated ACT. Furthermore, P2RX7 may have a distinct role on $CD4^+$ T cells, where its expression may promote survival of T_{reg} cells (*64*). Indeed, Romagnani *et al*. observed that P2RX7-deficiency was advantageous for $CD4^+$ T cell survival and tumor control (*119*). Nevertheless, our findings suggest a need for careful evaluation of how tumor-specific T cells are activated in order to address whether P2RX7 plays a beneficial versus a detrimental role.

In summary, we report that P2RX7-deficient $CD8^+$ T cells exhibit increased mitochondrial dysfunction, reduced proliferation, increased levels of apoptosis and elevated expression of exhaustion markers as tumor burden increases, leading to loss of *P2rx7*$^{-/-}$ $CD8^+$ donor cells within the tumor and in secondary lymphoid organs. We conclude that these combined defects account for impaired tumor control when *P2rx7*$^{-/-}$ $CD8^+$ T cells are used for ACT. Strategies to boost mitochondrial health $CD8^+$ TILs have shown to improve T cell survival and function under metabolic stressors imposed by the TME (*134, 138*). These data demonstrate that stimulation of the P2RX7 signaling pathway may be a promising therapeutic option to boost metabolic function of $CD8^+$ T cells in ACT. Furthermore, the requirement for P2RX7 in order to generate an effective anti-tumor response has clinical relevance as P2RX7 loss-of-function variants are relatively common in the human population (*126*) and patients with those mutations may require ACT protocols that boost mitochondrial health of transferred T cells.

2.4 Materials and Methods

2.4.1 Mice

Female 6- to 8-week-old adult C57BL/6 and B6.SJL mice were purchased from Charles River (via the National Cancer Institute). *P2rx7*$^{-/-}$ mice were purchased from Jackson Laboratories and backcrossed to the P14 (LCMV-gp33/D^{b} specific) and OT-I (OVA/K^{b} specific) TCR transgenic backgrounds, with introduction of Thy-1 and CD45 congenic markers to distinguish wild type (WT) and *P2rx7*$^{-/-}$ cells. Animals were maintained under specific-pathogen-free conditions at the University of Minnesota. All experimental procedures were approved by the Institutional Animal Care and Use Committee at the University of Minnesota. Animals were randomly assigned to experimental groups.

2.4.2 In vitro activation and adoptive transfer of CD8^{+} T cells

Naïve CD8^{+} T cells were isolated from the spleens of WT or *P2rx7*$^{-/-}$ P14 or OT-I transgenic mice with the mouse naïve CD8^{+} T cell isolation kit (Miltenyi Biotech). A total of 2.5 x 10^{5} isolated T cells were stimulated in flat bottom 24-well plates with anti-CD3 (10 μg/mL), anti-CD28 (20 μg/mL), human IL-2 (2.5 IU/mL), and with or without murine IL-12 (5 ng/mL) for 72 hours in RPMI medium (RPMI 1640 supplemented with 10% FBS, 100 U/mL penicillin/streptomycin, 2mM L-glutamine) at 37^{o}C/5% CO_2. After 72 hours, 2.5 x 10^{5}- 5.0 x 10^{5} activated T cells were transferred intravenously (i.v.) into recipient mice.

2.4.3 In vivo tumor experiments

Mice were injected subcutaneously with 1.5 x 10^{5} - 3.0 x 10^{5} B16.gp33 cells (provided by Dr. Ananda Goldrath, UCSD) or B16.OVA cells (provided by Dr. Matt Mescher, UMN) in the right flank. After thawing cell lines, B16 cells were expanded and passaged once prior to transfer. After tumors became palpable (~7 days), tumor-bearing mice received 5.0 x 10^{5} activated P14 or OT-I T cells (or

2.5 x 10^5 for co-transfer experiments). Tumor growth and survival was monitored until mice reached an end-point criteria of 120 mm^2 or ulceration.

2.4.4 Flow cytometry

Mice were sacrificed at indicated times and spleens, tumor draining inguinal lymph nodes and tumors were harvested and homogenized. In all experiments involving isolation of lymphocytes from tumors, 50 μg of Treg-Protector (anti-ARTC2.2) nanobody (BioLegend) was injected i.v. 30 minutes prior to mouse sacrifice as previously described [8, 9]. Tumors were removed, cut into small pieces, and digested with 3mg/mL Collagenase type I solution for 1 hour at 37°C and then dissociated via gentleMACS Dissociator (Miltenyi Biotec) twice. Isolated mouse cells were stained with antibodies to CD8α (clone 53-6.7, BD Biosciences), CD44 (clone IM7, Tonbo Biosciences), CD69 (clone H1.2F3, BioLegend), CD103 (clone M290, BD Biosciences), P2RX7 (clone 1F11, BD Biosciences), CD279 (PD-1) (clone 29F.1A12, Biolegend), CD366 (Tim3) (clone RMT3-23, BioLegend), CD223 (Lag3) (clone C9B7W, BioLegend), CD39 (clone Duha59, Biolegend), TCF1 (clone C63D9, Cell Signaling Technologies), TOX (clone TXRX10, Thermo), Ki67 (clone SolA15, Thermo), IFN-γ (clone XMG1.2, Tonbo Biosciences), granzyme B (clone GB11, Thermo Fisher Scientific). All cells were stained at antibody dilutions of 1:200, except for granzyme B (1:100), IFN-γ (1:100), TCF1 (1:100), TOX (1:50), and P2RX7 (1:50). Cells stained intracellularly for granzyme B, IFN-γ, Ki67, TCF1, and Tox were permeabilized using eBioscience transcription factor fixation/permeabilization kits. Cell viability was determined with Ghost Dye 780 (Tonbo Biosciences). Enumeration of lymphocytes was achieved using CountBright Absolute Counting Beads (Invitrogen).

For mitochondrial mass and membrane potential measurements, 1-2 x 10^6 cells were incubated with 100nM MTG (Thermofisher Scientific) and 80nM TMRE (BD

Biosciences) simultaneously for 20 minutes in RPMI 1640 supplemented with 2% FBS at 37°C prior to ex vivo staining. In order to account for experiment-to-experiment variability, gMFIs of either MTG or TMRE in donor WT CD8 P14 cells within the spleen of each experiment were averaged and fold change of donor WT or *P2rx7*$^{-/-}$ CD8^{+} T cells within the tumor or dLN for each experiment was calculated relative to splenic WT donor cells. Mitochondrial reactive oxygen species (ROS) were evaluated by incubating 1-2 x 10^6 cells with 5uM MitoSOX reagent (ThermoFisher) in RPMI 1640 supplemented with 2% FBS at 37°C prior to *ex vivo* staining.

Apoptosis was analyzed using an Annexin V Apoptosis Detection Kit I (BD) according to manufacturer instructions. Briefly, after extracellular staining, cells were washed 2x in PBS (without serum) and resuspended in Annexin V binding buffer. Approximately 15-30 minutes prior to reading the samples, Annexin V-APC and Propidium Iodide (PI) staining solution was added directly to the sample in Annexin V binding buffer. Apoptotic cells were discriminated from dead/necrotic cells by PI and viability ghost dye staining (e.g. Annexin V^{+} LD/PI^{-}).

Flow cytometric analysis was performed on a LSR II or LSR Fortessa (BD Biosciences) and data was analyzed using FlowJo software (Treestar).

2.4.5 Metabolic assays

OCR and ECAR were assessed in in vitro activated WT and *P2rx7*$^{-/-}$ T cells (activated with or without IL-12 or BzATP for 72 hours) using a 96-well XF Extracellular flux analyzer, according to the manufacturer's instructions (Seahorse Bioscience), similar to earlier studies [8, 9]. Briefly, 2 x 10^5 activated cells were plated onto Seahorse XFe96 (Agilent) plates (coated with CellTak solution the night before) in warm Seahorse base media (Agilent) supplemented with 2mM L-glutamine, 1mM sodium pyruvate, and 10mM glucose (pH 7.4) the

day of assay. Seahorse XF Mito Stress kit components (1.5 μM Oligomycin, 1 μM FCCP, 0.5 μM Rotenone/AntimycinA) were added to hydrated 96-well sensor cartridge (incubated overnight at 37°C with Agilent calibrant solution) before performing assay. Spare respiratory capacity (SRC) and OCR and ECAR values were defined as previously described (*17, 58*).

2.4.6 Tumor-Killing Assay

B16 melanoma cell killing was evaluated in real-time using the IncuCyte platform. Activated WT or *P2rx7*$^{-/-}$ P14 CD8^{+} T cells were plated into 96-well flat clear-bottom tissue culture-treated microplates, previously coated with Poly-L-ornithine (Sigma Aldrich), along with CellTrace Far Red (Invitrogen) stained B16.gp33 or B16.OVA cells at 1:1 and 3:1 effector:target ratios. Caspase-3/7 green dye (Sartorius) was added to identify dying cells. The plate was then placed in an IncuCyte ZOOM platform housed inside a cell incubator at 37°C/5% CO_2. Images from 5 technical replicates were taken every 30 minutes for 48 hours using a 4X objective lens and then analyzed using IncuCyte Basic Software v2018A (Sartorius). Graphed readouts represent percentage of live B16 melanoma targets (CellTrace Far Red^{+}Caspase-3/7^{-}), normalized to live targets alone at the starting (0 hour) time point.

2.4.7 Transmission electron microscopy

Activated WT and *P2rx7*$^{-/-}$ CD8^{+} T cells (with IL-12) were fixed in 2.5% Glutaraldehyde in 100mM sodium cacodylate, followed by post-fixation in 1% Osmium tetroxide. After washing, samples were stained in 1% Uranyl Acetate for 30 minutes in the dark and washed again. Samples were then dehydrated in Ethanol and embedded in Eponate Resin. Cells were imaged using a JEOL 1200 EXII transmission electron microscope equipped with a SIS MegaView III high resolution CCD camera (1376 x 1032-pixel format, 12 bit).

2.4.8 Human CD8+ T cell cultures

Resting $CD8^+$ T cells were isolated from Ficoll-purified PBMC isolates from leukapheresis products (Memorial Blood Center, St. Paul, MN) using a naïve human CD8+ negative selection kit (Stem Cell). Purified cells were stimulated for 72 hours with αCD3/αCD28 beads (Biolegend) with 4ng/mL IL-2 (Peprotech), and with or without 50ng/mL IL-12. After 72 hours, activated $CD8^+$ T cells continued to be cultured with indicated concentrations IL-2 +/- IL-12 until analysis.

2.4.9 RNA expression analysis

Human $CD8^+$ T cells activated with IL-2 +/- IL-12 were first homogenized using QIAshredder columns (QIAGEN) and RNA was extracted using RNeasy kit (QIAGEN) following manufacturer instructions. From isolated RNA samples, cDNA was prepared with the SuperScript III First-Strand Synthesis SuperMix (ThermoFisher Scientific) following manufacturers' instructions. Gene expression was assessed (in triplicate) with an ABI 7700 sequence-detection system, and amplification was detected with SYBR Green PCR Master Mix (Applied Biosystems) as previously described (*139*). The sequences of primer pairs used to measure hP2rx7 RNA were: forward, 5'- TGT GTC CCG AGT ATC CCA CC -3', reverse, 5'- GGC ACT GTT CAA GAG AGC AG -3', while the primers for GUSB (used as a control housekeeping gene) (*140*) were: forward, 5'- GTC TGC GGC ATT TTG TCG -3', reverse, 5'- CAC ACG ATG GCA TAG GAA TGG -3'.

2.4.10 Statistical analysis

Data were subject to Kolmogorov-Smirnov test to assess normality of samples. Statistical differences were calculated by using paired or unpaired two-tailed Student's t-test or one-way ANOVA with Tukey post-test. In cases where one group in the comparisons was normalized, statistical analysis employed ANOVA with Brown-Forsythe and Welch corrections. Statistical differences for survival

data were assessed using a log-rank Mantel-Cox test. All statistical analysis was performed using Prism 9 (GraphPad Software). Graphical data shown with error bars indicating the SD or SEM. P values of <0.05 (*), <0.01 (**), <0.001 (***), or <0.0001 (****) indicate significant differences between groups.

2.5 Supplemental Figures

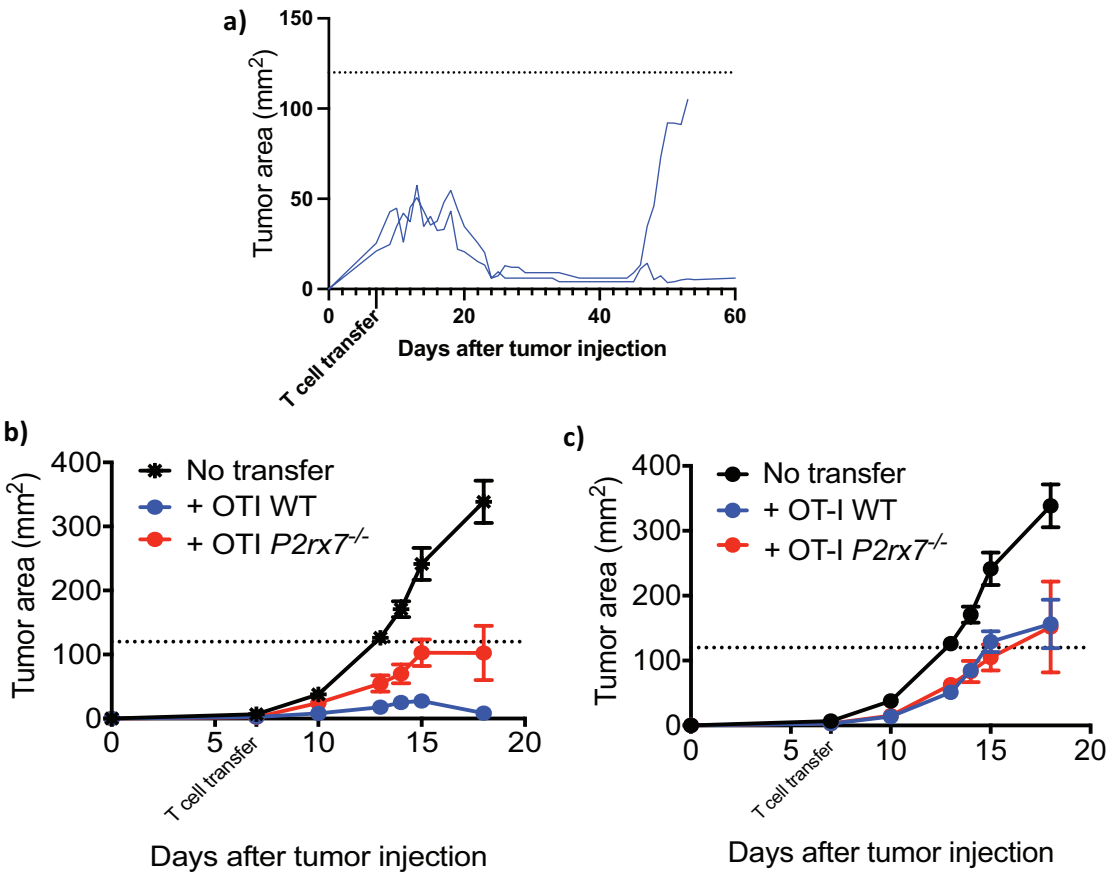

Figure S2.1 OT-I model reveals similar defects in P2rx7$^{-/-}$ CD8^{+} T cell tumor control.

a) Tumor growth kinetics in two individual mice (indicated by # in Fig. 1b-c) that received WT P14 + IL12 and achieved tumor control >40 days. **b-c)** Activated WT and P2rx7-/- OT-I cells **b)** with IL12 or **c)** without IL12 for 72 hours were transferred into mice with palpable B16.OVA tumors. Tumor growth was measured for mice that received **b)** no cell transfer (n=8), WT + IL12 (n=8), or *P2rx7*$^{-/-}$ + IL12 (n=10) OT-I cells or **c)** no cell transfer (n=8) , WT (n=5), or *P2rx7*$^{-/-}$(n=8) OT-I cells. Data from 2-3 independent experiments. Graphical data shown as mean with error bars indicating SEM.

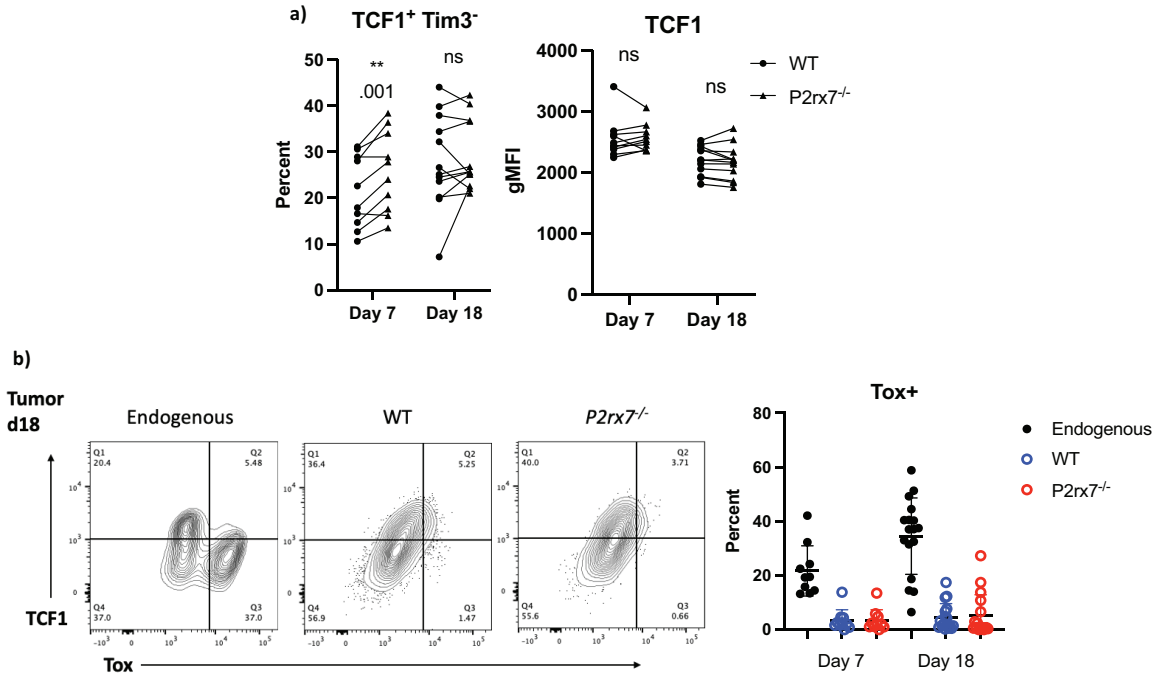

Figure S2.2 No difference in expression of 'stem-like' markers between WT and P2rx7$^{-/-}$ donor cells.

WT and *P2rx7*$^{-/-}$ OT-I cells were activated and cultured with IL-12 in vitro, then equal numbers co-transferred into mice with palpable B16.OVA tumors. Tumors, tumor dLNs, and spleens were harvested from recipient mice 7- or 18-days post-T cell transfer. **a)** Frequency (left) of stem-like population of donor cells (as evaluated by TCF1+ Tim3-) and (right) TCF1 expression within tumor of mice at indicated time points. **b)** TCF-1 and TOX expression by endogenous CD8^{+} T cell and both donor OT-I populations. Representative staining is shown on the left, and aggregated data shown on right. Data are from 2-3 independent experiments. *, P ≤ 0.05; **, P ≤ 0.01; ***, P ≤ 0.001; ****, P ≤ 0.0001. Statistical significance determined by a two-tailed, paired t-test.

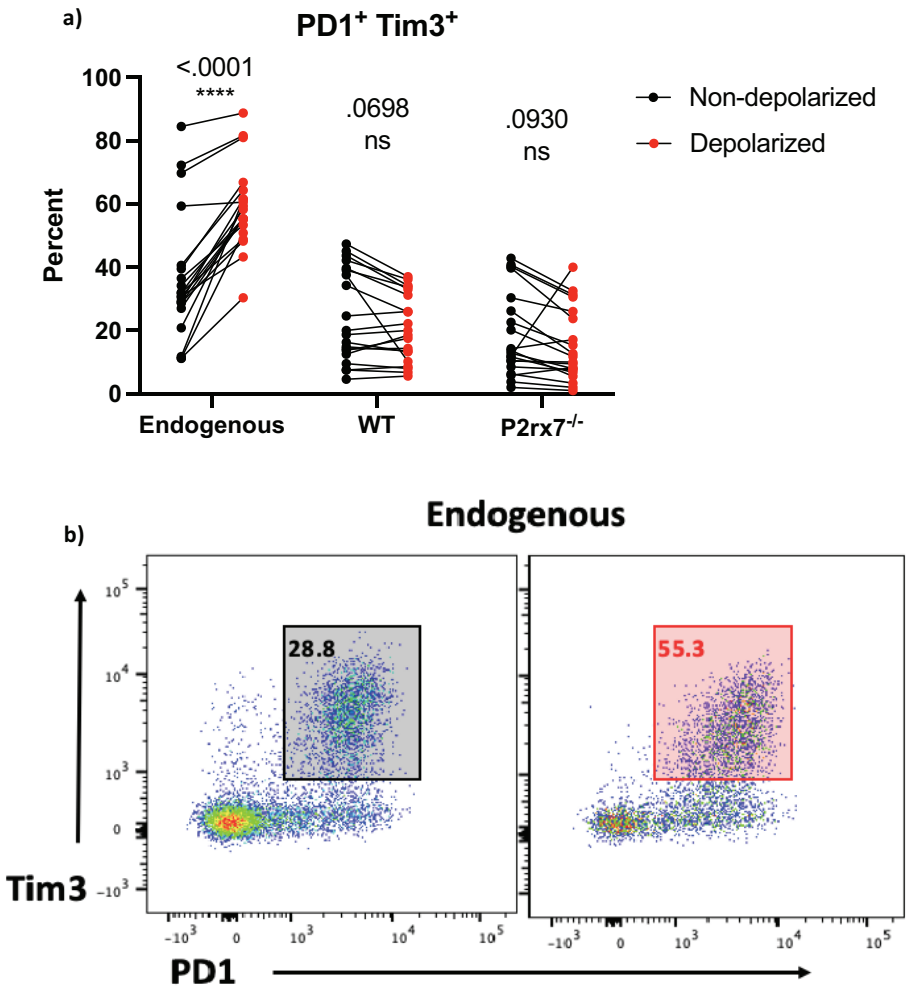

Figure S2.3: IL-12 conditioning of donor cells prevents exhaustion phenotype within populations with depolarized mitochondria.

WT and *P2rx7*$^{-/-}$ OT-I cells were activated and cultured with IL-12 in vitro, then equal numbers co-transferred into mice with palpable B16.OVA. 18 days post T cell transfer, CD8^{+} TIL were analyzed to determine the frequency of PD1^{+}, Tim3^{+} cells within populations that displayed depolarized (or non-depolarized) mitochondria between endogenous polyclonal CD8^{+} TILs versus WT or *P2rx7*$^{-/-}$ donor P14 TILs. **a)** Frequency of PD1^{+} Tim3^{+} cells within depolarized versus non-depolarized populations. **b)** Representative staining of PD1 and Tim3 among depolarized versus non-depolarized populations among endogenous TILs. Data representative of 3 independent experiments. *, P ≤ 0.05; **, P ≤ 0.01; ***, P ≤ 0.001; ****, P ≤ 0.0001. Statistical significance determined by a two-tailed, paired t-test.

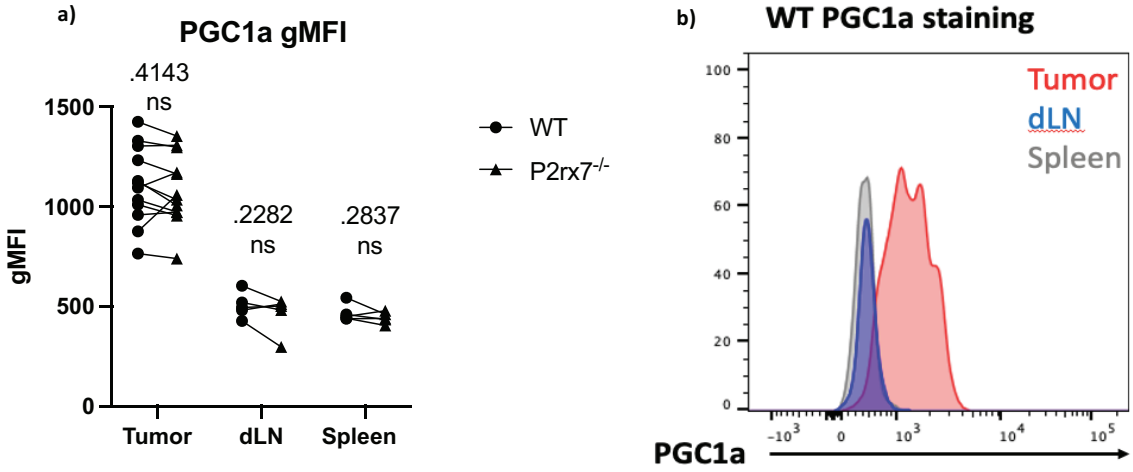

Figure S2.4: PGC1α expression does not differ between WT and P2rx7$^{-/-}$ donor cells.

WT and *P2rx7*$^{-/-}$ OT-I cells were activated and cultured with IL-12 in vitro, then equal numbers co-transferred into mice with palpable B16.OVA. 18 days post T cell transfer, CD8^{+} TILs were analyzed for mitochondrial biogenesis promotor PGC1α expression. **a)** PGC1α gMFI among donor CD8^{+} T cells in tumor, dLN and spleen. **b)** Representative PGC1α staining among WT donor cells in indicated tissues. Data representative of one experiment. Statistical significance determined by a two-tailed, paired t-test.

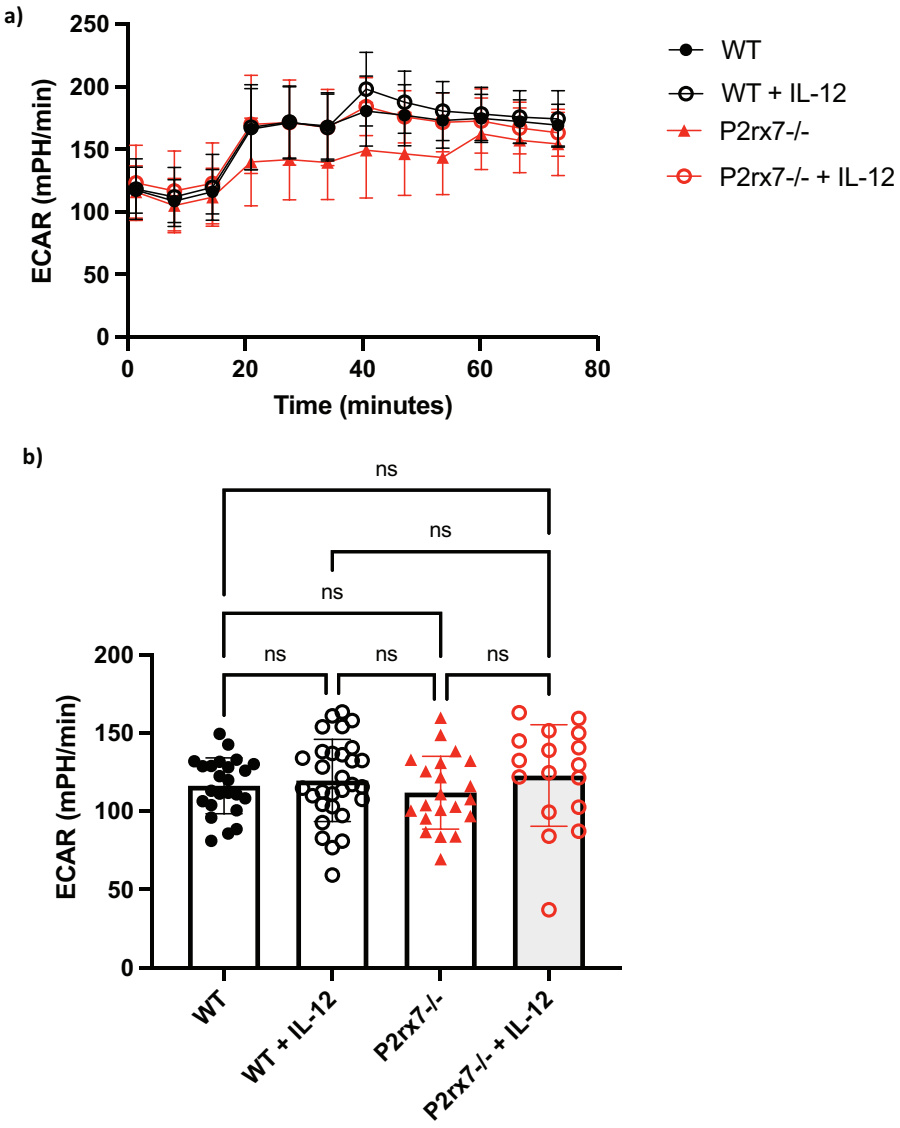

Figure S2.5: Similar aerobic glycolysis by WT and P2rx7$^{-/-}$ CD8^{+} T cells following in vitro activation.

WT and *P2rx7*$^{-/-}$ P14 cells were activated for 72 hours in vitro with anti-CD3, -CD28, IL2, and +/- IL12. Aerobic glycolytic capacity was evaluated by measuring excellular acidification rate (ECAR), via Seahorse extracellular flux assay. **a)** ECAR following sequential addition of listed inhibitors. **b)** Baseline ECAR prior to addition of inhibitors. Data are from 3 independent experiments. Graphical data shown as mean with error bars indicating SEM. Statistical significance determined by a One-way ANOVA.

2.6 Publications and Contributions

Chapter modified with permission from the following published article:

Wanhainen, K.M. *et al.* P2RX7 enhances tumor control by $CD8^+$ T cell in adoptive cell therapy. *Cancer Immunol Res.* 2022; 10(7): 871-884. PMID: 35588154

KMW, HBdS, and SCJ designed the experiments. KMW, CP, MHZ, BdGM, SO, TY, and HDbS performed experiments. KMW and SCJ wrote the manuscript with input from all authors.

Chapter 3

Pharmacologic modulation of P2RX7 to enhance ACT

3.1 Introduction

Given the high levels of eATP within the TME, there is considerable interest in exploiting purinergic signaling pathways to directly inhibit tumor growth and enhance immunotherapy responses. Indeed, P2RX7 expression is elevated (relative to healthy tissue) on many different types of tumors, and high P2RX7 expression is associated with advanced stage and reduced survival in melanoma (*141*). Inhibitors of P2RX7 have shown efficacy in preclinical models by reducing tumor cell proliferation and metastatic potential (*101, 109, 111, 141*). However, P2RX7 antagonists do not exclusively act on tumor cells and are also likely modulating P2RX7 signaling on immune cells within the tumor. Consistent with this, treating tumor-bearing mice with P2RX7 antagonists alters immune cell populations and cytokine milieu within the TME (*109*). Our data demonstrates that P2RX7 is required for $CD8^+$ T cells to sustain an effective anti-tumor response by promoting metabolic function and longevity of tumor-specific T cells. These results indicate the therapeutic potential of P2RX7 stimulation, but there is still uncertainty about whether P2RX7 may become a liability due to its capacity to induce cell-death with overstimulation. Tumors have uniquely evolved ways to benefit from P2RX7 signaling while preventing induction of cell death (*105, 106, 108*). For P2RX7 to be utilized therapeutically, it is essential to understand whether $CD8^+$ T cells can similarly benefit from augmented P2RX7 signaling and determine if we can protect $CD8^+$ T cells from P2RX7-induction of cell death within the TME.

Increasing eATP levels within the TME by inhibiting CD39 ATPase activity has been shown to improve tumor immunotherapy in a $CD8^+$ T cell dependent manner by increasing IFNγ production and proliferative potential (*142*). While this effect is likely in part mediated by reduced production of immunosuppressive adenosine, it is also likely that increased eATP stimulates P2XRs on $CD8^+$ T cells

and enhances their function. We have previously shown that stimulation of $CD8^+$ T cells with non-hydrolysable ATP analog, 2'(3')-O-(4-Benzoylbenzoyl) adenosine-5'-triphosphate (BzATP), leads to increased proliferation and Ca^{2+} influx, without compromising viability, in a P2RX7 dependent manner (*87*). BzATP stimulation of P2RX7 also increases mitochondrial function in memory $CD8^+$ T cells (*87*), suggesting it may similarly benefit $CD8^+$ T cell metabolic function in an anti-tumor response.

While elevated concentrations of eATP within the TME has the potential to induce P2RX7-mediated cell death, eATP is also rapidly turned over by tumor cells to produce adenosine (*143*). Furthermore, P2RX7 has a low affinity for eATP, so induction of P2RX7-macropore occurs more readily via ADP-ribosylation using extracellular NAD^+ ($eNAD^+$). Similar to eATP, NAD^+ is passively released from cells during inflammation and tissue damage where it accumulates in the extracellular space. ADP-ribosyltransferases (ARTs) use $eNAD^+$ to covalently modify P2RX7 resulting in pore formation (*66*). ARTC2.2 is expressed by murine T cells and has been shown to promote cell death in P2RX7-expressing cells during tissue processing protocols where $eNAD^+$ is released (*84, 85*). Blockade of ARTC2.2 with an antagonizing nanobody improves recovery $CD8^+$ T cells from NLT in a P2RX7 dependent manner (*84*). While we use the ARTC2.2 blocking nanobody during all NLT and tumor harvests, this does not protect P2RX7-expressing $CD8^+$ T cells *in vivo* within the TME where $eNAD^+$ is also highly abundant.

In addition to ARTC2.2 expression on $CD8^+$ T cells, many tumors also express ART1 and it is associated with poor prognosis and a more aggressive tumor (*106, 144-146*). Notably, ART1 expression in human non-small cell lung cancer (NSCLC) tumors was associated with a reduction in infiltrating P2RX7-expressing $CD8^+$ (*106*). Additionally, ART1 blockade or deletion in murine

NSCLC or melanoma tumors increased infiltration of polyclonal P2RX7-expressing $CD8^+$ T cells and resulted in reduced tumor burden (*106*). These results suggest that ART1 interacts with P2RX7 on tumor infiltrating $CD8^+$ T cells and likely contributes to P2RX7-mediated cell death. Consistent with this, strategies to reduce NAD^+ synthesis improved $CD8^+$ T cell responses in gastric cancer (*147*). Together, these results suggest that targeting $eNAD^+$ or ART enzymes may help to protect P2RX7 expressing $CD8^+$ T cells from pore formation and cell death, while still allowing for eATP signaling to modulate $CD8^+$ T cell function.

Here, we demonstrate that transient in vitro stimulation of $CD8^+$ T cells with a P2RX7 agonist BzATP in place of IL-12 also improved ACT and enhanced mitochondrial function while reducing expression of some exhaustion markers. While $CD8^+$ T cells were only exposed to BzATP during *in vitro* activation, continued P2RX7 signaling *in vivo* was required to elicit enhanced tumor control. While eATP signaling through P2RX7 enhances ACT, we also found that P2RX7-expressing cells are vulnerable to ART1-mediated cell death in B16 melanoma models. These results indicate that P2RX7 stimulation can be leveraged to promote $CD8^+$ T cell anti-tumor immunity, but simultaneously reinforce to complex nature of P2RX7 particularly highly inflammatory environments.

3.2 Results

3.2.1 P2RX7 agonism increases mitochondrial function in activated CD8$^+$ T cells.
Our group has previously shown that P2RX7 agonism with a titrated dose of BzATP was able to induce CD8$^+$ T cell proliferation and Ca^{2+} influx without inducing cell death. BzATP also promoted CD8$^+$ T cell differentiation into a memory-like state by promoting AMPK activation and enhanced OXPHOS (*87*). We hypothesized that BzATP might similar boost CD8$^+$ TIL metabolic function and longevity.

We have previously shown that BzATP can boost mitochondrial function in CD8$^+$ T cells cultured *in vitro* with IL-15 (*87*), a cytokine that independently promotes mitochondrial fusion and enhanced function (*17*). It is unknown whether BzATP would have a similar effect in effector CD8$^+$ T cells. In order to investigate this, we activated P14 CD8$^+$ T cells *in vitro* for 72 hours (without IL-12) with 100μM BzATP added every 24 hours of activation. Notably, this dose of BzATP is sufficient to activate P2RX7 but does not drive P2RX7-pore formation (*87*). Indeed, P2RX7 agonism during *in vitro* activation significantly increased baseline and maximum OCR and SRC of WT CD8$^+$ T cells in a P2RX7-dependent manner (Fig. 3.1a-d). Furthermore, P2RX7 agonism also increased mitochondrial mass and function of *in vitro* activated cells, indicated by MTG and TMRE staining, respectively (Fig 3.1e-g). These results are consistent with P2RX7 signaling promoting mitochondrial function, whether it is induced directly via an agonist or indirectly by IL-12 inducing P2RX7 expression (Fig 2.3c-d).

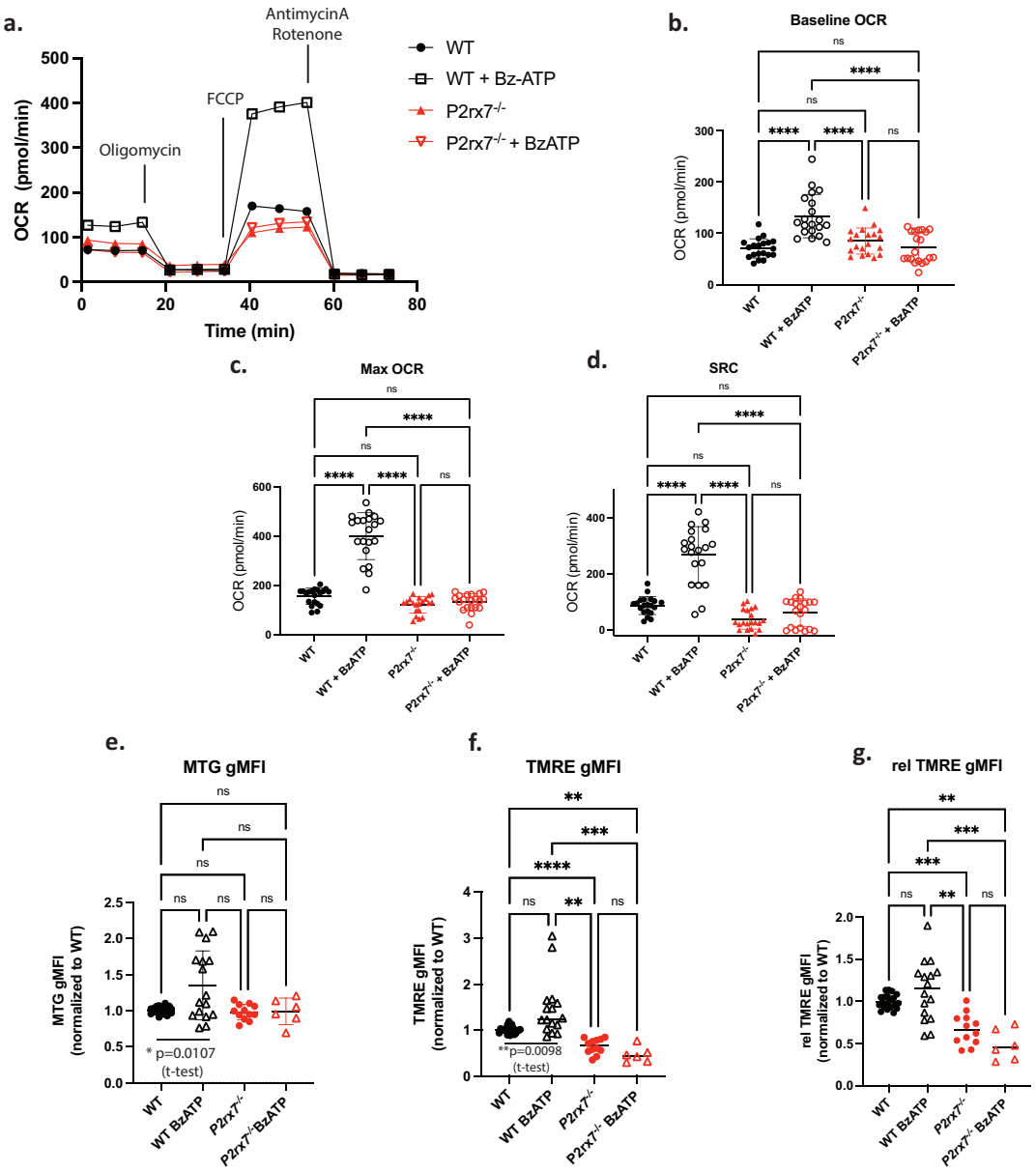

Figure 3.1: P2RX7 agonism increases mitochondrial function in WT CD8+ T cells

WT and *P2rx7*$^{-/-}$ P14 cells were activated for 72 hours in vitro with anti-CD3, -CD28, IL2, and 100uM of BzATP or vehicle (dH_2O) treatment, replenished every 24 hours of activation. **(a-d)** Oxygen consumption rate (OCR) of indicated groups after 72 hour activation was evaluated using Seahorse Extracellular Flux assay. **a)** Oxygen consumption rates (OCRs) were determined for the indicated groups after sequential addition of the listed inhibitors. **b)** Baseline OCR of indicated groups prior to Oligomycin addition. **c)** Max OCR of indicated groups after FCCP addition. **d)** Spare respiratory capacity of indicated groups (calculated based on difference between Max OCR and baseline OCR). **(e-g)** Mitochondrial mass and membrane potential was measured in WT and *P2rx7*$^{-/-}$ P14 cells after in vitro activation by evaluating levels of MTG or TMRE, respectively. Fold changes of **e)** MTG gMFI, **f)** TMRE gMFI, and **g)** relative TMRE gMFI (normalized to MTG gMFI). **(e-g)** For each independent experiment, fold change in gMFI of indicated molecular probe was calculated relative to average gMFI of WT (untreated) P14 cells. Data are from 3 independent experiments. Graphical data shown as means with error bars indicating SEM. *, $P \leqslant 0.05$; **, $P \leqslant 0.01$; ***, $P \leqslant 0.001$; ****, $P \leqslant 0.0001$. Statistical significance determined by One-way ANOVA (except when indicated).

3.2.2 P2RX7 agonism augments ACT

To test whether P2RX7 agonism could be used to enhance immunotherapy by CD8+ T cells cultured in the absence of IL-12, we activated P14 $CD8^+$ T cells in vitro for 72 hours with 3 doses of 100uM BzATP (added every 24 hours), or vehicle (H_2O) treatment, and then transferred these cells into mice bearing B16.gp33 tumors, without further BzATP treatment (Fig 3.2a). While $CD8^+$ T cells activated without IL-12 do not elicit effective anti-tumor responses, we found that addition of BzATP during in vitro activation significantly improved survival and reduced tumor area in comparison to vehicle treated P14 cells (Fig 3.2b-c), albeit less effective than IL-12 cultured cells (Fig 2.1b-c). Importantly, in parallel studies, we found that BzATP treatment had no effect on tumor control mediated by *P2rx7*$^{-/-}$ P14 cells, indicating the effect requires BzATP stimulation of P2RX7 (Fig. 3.2d). Preliminary studies also demonstrated that BzATP stimulation did not further enhance the efficacy of IL-12 cultured WT P14 cells for tumor control (Fig S3.1a), which may indicate that these treatments operate in similar functional pathways.

To determine the effects of transient BzATP treatment on the phenotype and mitochondrial homeostasis of TILs, tumors from mice were harvested 7 days post-T cell transfer. Interestingly, BzATP treatment during in vitro activation led to reduced numbers of P14 cells per gram of tumor at the time of harvest (Fig 3.3a), but increased proliferation of those cells (Fig 3.3b) and reduced the frequency of P14 cells expressing the inhibitory receptors Tim3 and CD39 (Fig 3.3c-d), but not Lag3 or PD1 (Fig. 3.3e-f). Consistent with transient P2RX7 stimulation in vitro promoting mitochondrial function of TILs, BzATP treated P14 cells in the tumor exhibited higher mitochondrial membrane potential and function per mitochondrion (Fig 3.4b-c), despite no significant change in mitochondrial mass or frequency of P14 cells with depolarized mitochondria (Fig 3.4a,d). Unexpectedly, BzATP treated P14 cells in lymphoid tissues showed reduced

mitochondrial mass and membrane potential (Fig. 7a-c), suggesting *in vitro* BzATP treatment may preferentially benefit mitochondrial function in tumor-infiltrating cells. These results reinforce the connection between mitochondrial fitness and enhanced tumor control by CD8⁺ T cells. These results also highlight the potential for P2RX7 stimulation of cultures CD8⁺ T cells to promote tumor control. However, WT CD8⁺ cells are vulnerable to cell death through P2RX7 overstimulation, so it is important to consider that the beneficial effects of P2RX7 may be simultaneously counteracted by increased CD8⁺ T cell death.

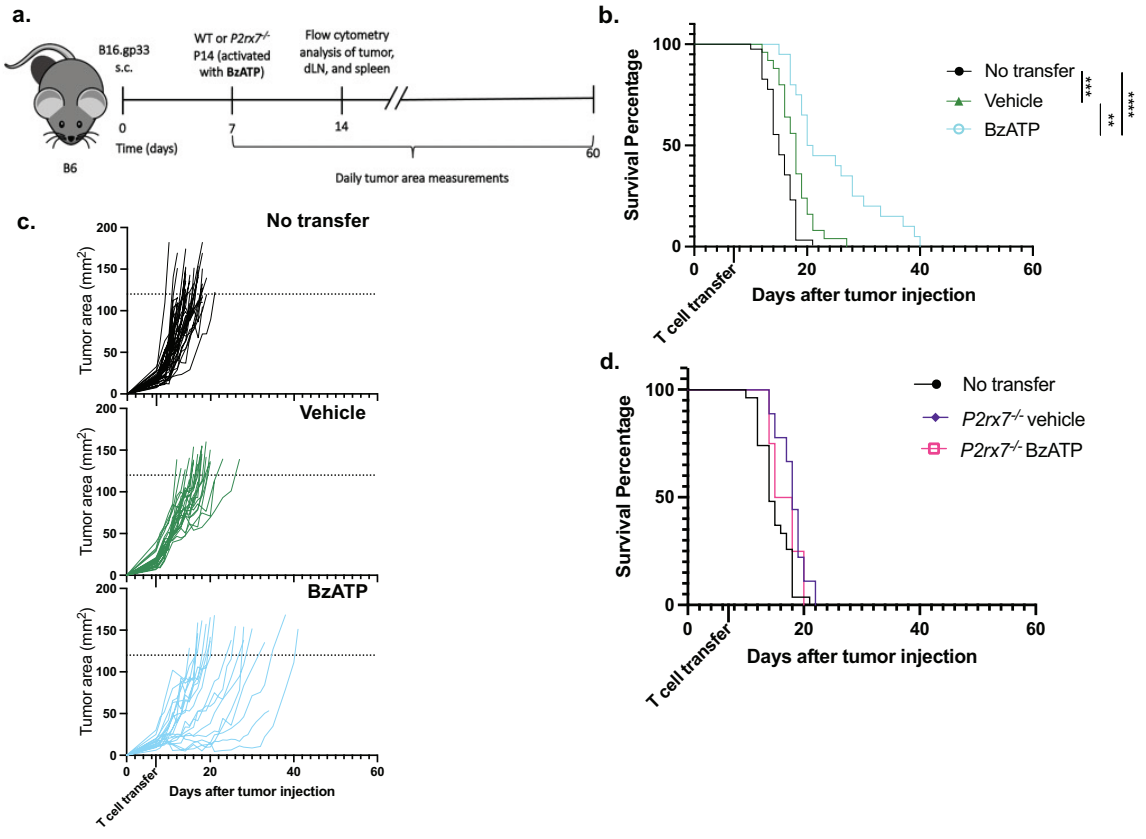

Figure 3.2 P2RX7 agonism during in vitro activation improves survival and tumor control of WT CD8+ T cells

a) B6 mice were injected with 3 x 10^5 B16.gp33 melanoma s.c. and once tumors became palpable (~7 days post-injection) 5 x 10^5 P14 cells were transferred i.v. after 72 hours activation with anti-CD3/-CD28, 2.5 IU/mL IL-2, and +/- 100uM of BzATP (or vehicle dH_2O treatment) every 24 hours of activation. b) Survival curves and c) tumor growth curves for tumor-bearing mice that received vehicle treated WT P14 cells (n=25), BzATP treated WT P14 (n=20), or no T cell transfer (n=40). **d)** Survival curve for tumor-bearing mice that received vehicle (n=9) or BzATP (n=4) treated *P2rx7*$^{-/-}$ P14 cells or no cell transfer (n=27). **(b-d)** Endpoint criteria for survival experiments were tumor ulceration or an area of 120mm^2 (indicated by dashed line). Data are from 3 independent experiments. *, $P \leqslant 0.05$; **, $P \leqslant 0.01$; ***, $P \leqslant 0.001$; ****, $P \leqslant 0.0001$. Statistical significance for **b** and **d** determined by a log-rank Mantel-Cox test.

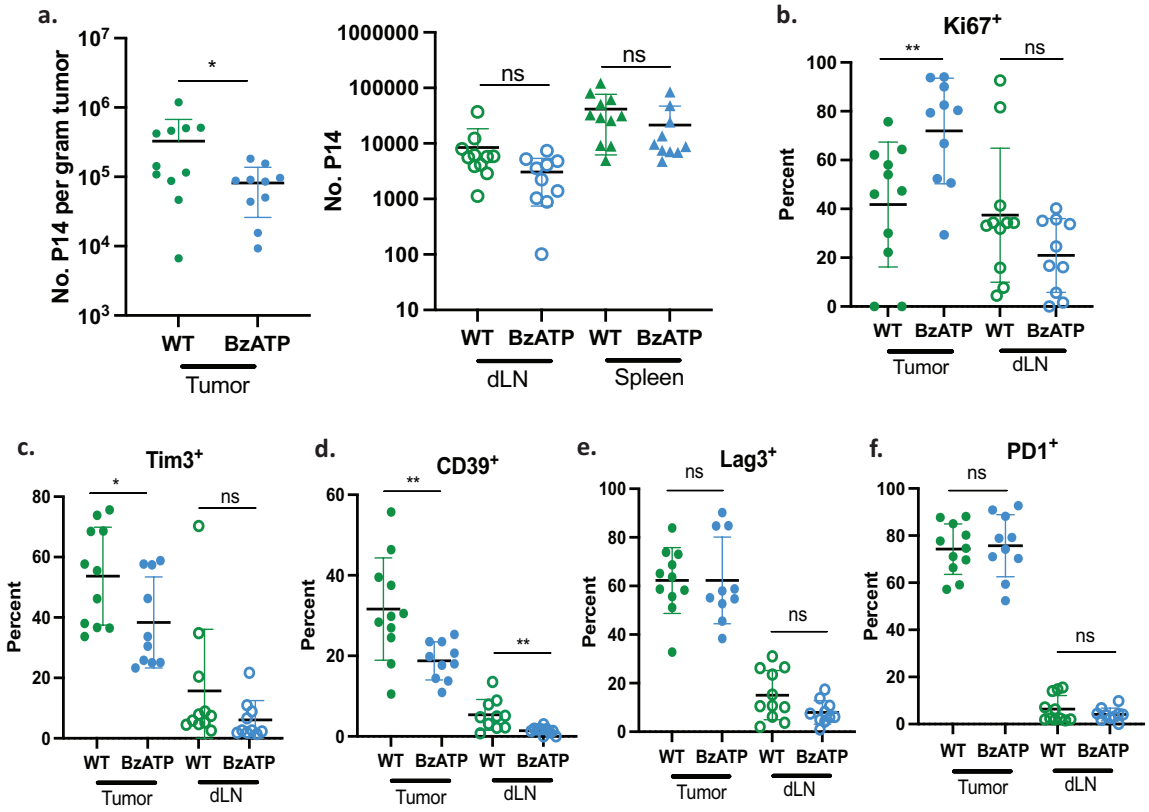

Figure 3.3 P2RX7 agonism increases proliferative potential of WT CD8⁺ and reduces expression of some exhaustion markers.

B6 mice were injected with 3 x 10^5 B16.gp33 melanoma s.c. and once tumors became palpable (~7 days post-injection) 5 x 10^5 P14 cells were transferred i.v. after 72 hours activation with anti-CD3/-CD28, 2.5 IU/mL IL-2, and +/- 100uM of BzATP (or vehicle dH2O treatment) every 24 hours of activation. Tumors, dLN and spleens from mice with B16.gp33 tumors that received either vehicle or BzATP treated WT P14 donor cells were harvested at day 7 post T cell and assessed for **a)** number of P14 within indicated tissues, **b)** frequency of Ki67⁺, **c)** frequency of Tim3⁺, **d)** frequency of CD39⁺, **e)** frequency of Lag3⁺, and **f)** frequency of PD1⁺ P14 cells.). Data are from 2 independent experiments. Graphical data shown as means with error bars indicating SEM. *, P ⩽ 0.05; **, P ⩽ 0.01; ***, P ⩽ 0.001; ****, P ⩽ 0.0001. Statistical significance evaluated by a two-tailed, unpaired t-test.

3.2.3 P2RX7 signaling in vivo is required to sustain anti-tumor responses

Since P2RX7 has the capacity of being overstimulated within the TME given the high levels of eATP and eNAD⁺, we next wanted to determine whether P2RX7 stimulation during T cell activation/priming was sufficient to program enhanced mitochondrial function and longevity in CD8⁺ T cells. In order to address this, we systemically injected P2RX7 pharmacologic antagonists into tumor-bearing mice to block P2RX7 activity *in vivo.* The pharmacologic antagonist A740003 (A740)

has been shown to reduce tumor burden in B16 melanoma burden in WT mice when administered i.p. every other day (starting on day 5 post-tumor inoculation) (*109, 111*). Consistent with these findings, we also observe that A740 treatment results in a mild but significant improvement in survival (Fig S3.2a-b). However, the a dose of A740 used in these studies is considerably lower than what we have used previously to inhibit P2RX7 on CD8⁺ T cells (50 μg/kg versus 80 mg/kg) (*87*). Concerns that the low dose inhibitor may not be potent enough to act on CD8⁺ T cells led us to use the inhibitor A438074 (A438) at the higher dose in our experiments.

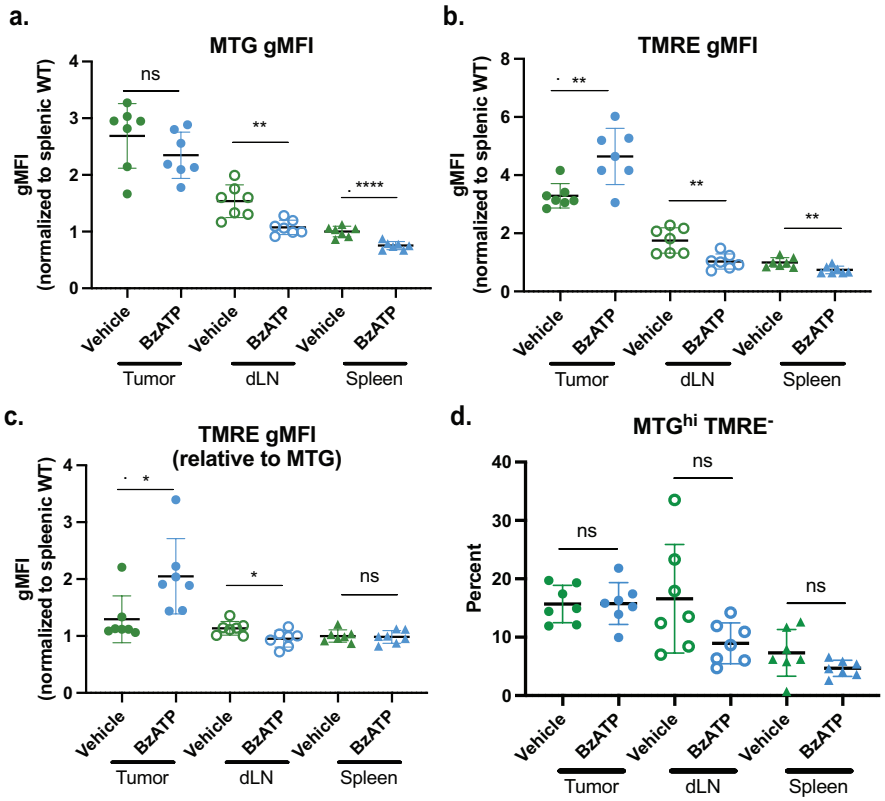

Figure 3.4: P2RX7 agonism enhances TIL mitochondrial function

B6 mice were injected with 3x105 B16.gp33 melanoma s.c. and once tumors became palpable (~7 days post-injection) 5x105 P14 cells were transferred i.v. after 72 hours activation with anti-CD3/-CD28, 2.5 IU/mL IL-2, and +/- 100uM of BzATP (or vehicle dH2O treatment) every 24 hours of activation. Tumors, dLN and spleens from mice with B16.gp33 tumors that received either vehicle or BzATP treated WT P14 donor cells were harvested at day 7 post T cell transfer and assessed for **a)** mitochondrial mass (MTG staining gMFI); **b)** mitochondrial membrane potential (TMRE gMFI), **c)** relative TMRE gMFI, and **d)** frequency of cells with depolarized mitochondria ($MTG^{hi}TMRE^{-}$). **(a-c)** For each independent experiment, fold change in gMFI of indicated molecular probe was calculated relative to average gMFI of vehicle-treated WT P14 cells within the spleen. Graphical data shown as means with error bars indicating SEM. *, $P \leqslant 0.05$; **, $P \leqslant 0.01$; ***, $P \leqslant 0.001$; ****, $P \leqslant 0.0001$. Statistical significance evaluated by a two-tailed, unpaired t-test.

In order to determine whether sustained P2RX7 signaling was required to elicit a strong anti-tumor response, we transferred P14 cells activated for 72 hours with BzATP treatment (as described in *3.2*) into mice with B16.gp33 tumors. On the day of T cell transfer, we began treating tumor-bearing mice i.p. with 80 mg/kg A438 or vehicle (PBS) and continued treatment every other day until mice reached end point criteria (Fig 3.5a). A438 treatment alone reduced tumor burden and improved survival (Fig 3.5b-c), as previously reported (*109, 111*). Interestingly, A438 treatment significantly compromised the ability of BzATP treated donor P14 cells to enhance survival, indicating that $CD8^+$ T cells require continuous P2RX7 signaling *in vivo.* However, when $CD8^+$ T cells were activated with IL-12 rather than BzATP, preliminary data demonstrates that A438 does not negatively (or positively) impact $CD8^+$ T cell tumor control (Fig 3.5d-e). These data suggest that while P2RX7 stimulation can boost mitochondrial fitness of $CD8^+$ T cells prior to transfer into tumor bearing mice, it likely does not lead to the immense transcriptional and epigenetic changes that IL-12 is known to induce in $CD8^+$ T cells (*148*). Additionally, while P2RX7 stimulation can therapeutically enhance ACT, this strategy is dependent on sustained P2RX7 signaling *in vivo*.

3.2.4 ART1 induces cell death of P2RX7-expressing $CD8^+$ T cells.

Our results have shown that $CD8^+$ T cells benefit from P2RX7 sensing of eATP *in vivo.* Therefore, while blocking P2RX7 would protect $CD8^+$ TILs from cell death, it may also have detrimental effects on $CD8^+$ TIL function. We next wanted to investigate whether inhibiting ART1-mediated ADP-ribosylation of P2RX7 could enhance $CD8^+$ T cell anti-tumor responses and protect P2RX7-expressing cells within the tumor. A recently published study by Wennerberg, *et al.,* demonstrated knocking out or blocking ART1 on KP1 lung cancer impaired tumor growth and increased polyclonal $CD8^+$ T cell infiltration and P2RX7 expression (*106*). This

group also generated a B16.F10 cell line in which ART1 was CRISPR'd out (B16.ART1^{KO}), which they generously shared with us.

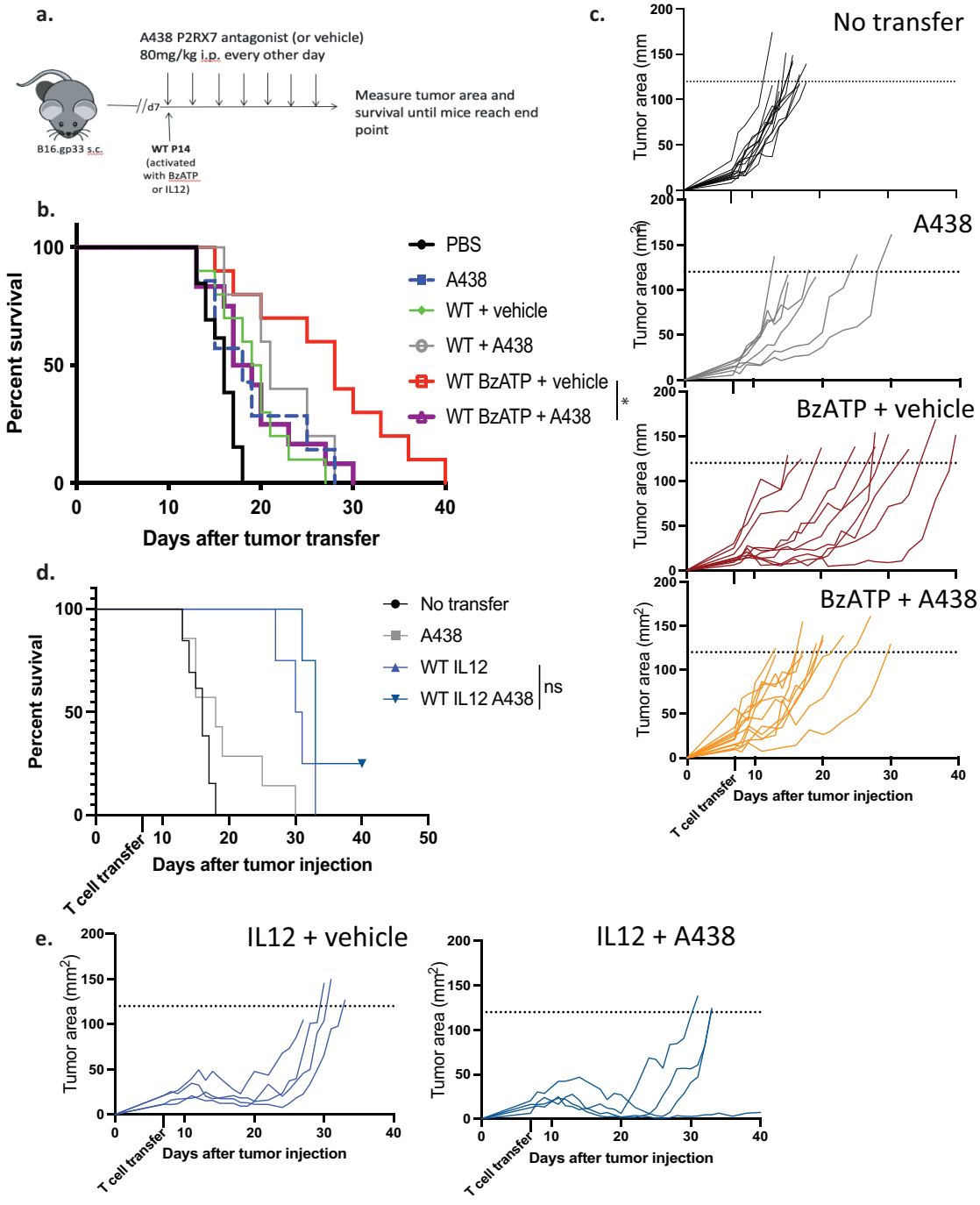

Figure 3.5 P2RX7 antagonism in vivo lessens the beneficial effect of BzATP treatment

a) B6 mice were injected with 3 x 10^5 B16.gp33 melanoma s.c. and once tumors became palpable (~7 days post-injection) 5 x 10^5 WT were transferred i.v. after 72 hours activation with anti-CD3/-CD28, 2.5 IU/mL IL-2, +/- IL-12, and +/- 100uM of BzATP (or vehicle dH_2O treatment) every 24 hours of activation. After T cell transfer, mice were treated with 80mg/kg of P2RX7 antagonist A438 (or vehicle PBS treatment) i.p. every other day until mice reach endpoint criteria. **b)** Mice were that received indicated treatments (No transfer, n=13; A438, n=7; WT vehicle, n=10; WT A438, n=5; BzATP vehicle, n=10; BzATP A438, n=12) were monitored for survival and **c)** tumor burden. **d)** Mice that received IL-12 activated cells and treated with vehicle (n=4) or A438 (n=4) were monitored for survival and **e)** tumor burden. Data are from 2-3 independent experiments. *, $P \leqslant 0.05$; **, $P \leqslant 0.01$; ***, $P \leqslant 0.001$. Statistical significance was determined by a log-rank Mantel-Cox test.

Wennerberg, *et al.* showed that B16.ART1^{KO} does not grow as efficiently in immunocompetent hosts despite equivalent growth to the parent B16.F10 cell line *in vitro* (*106*). This suggests that ART1 deficiency may unleash a response from P2RX7-expressing immune cells. We confirmed that B16.ART1^{KO} does not (data not shown). However, we found that we could overcome this by transferring more tumor cells (3 x 10^5 versus 1 x 10^5), and B16.F10 and B16.ART1^{KO} grew equivalently (Fig 3.6a-b).

In order to investigate the impact of ART1 deficiency on WT tumor-specific CD8$^+$ T cell ACT, we transferred activated (with or without IL-12) tyrosine-related protein 2 (Trp2) specific TCR transgenic CD8$^+$ T cells into mice with palpable B16.F10 and B16.ART1^{KO} tumors. As expected, Trp2 CD8$^+$ T cells that were activated without IL-12 did not significantly reduce tumor burden or increase survival in mice with B16.F10 tumors. Notably, when transferred into mice with B16.ART1^{KO} tumors Trp2 CD8$^+$ T cells were able to effectively reduce tumor burden and improve survival like IL-12 primed CD8$^+$ T cells (Fig 3.6a-b). However, in these preliminary experiments there was no difference between IL-12 primed Trp2 CD8$^+$ T cell responses to B16.F10 or B16.ART1^{KO}. These results do suggest that P2RX7-expressing CD8$^+$ T cells are disadvantaged in ART1-expressing tumors which limits overall efficacy.

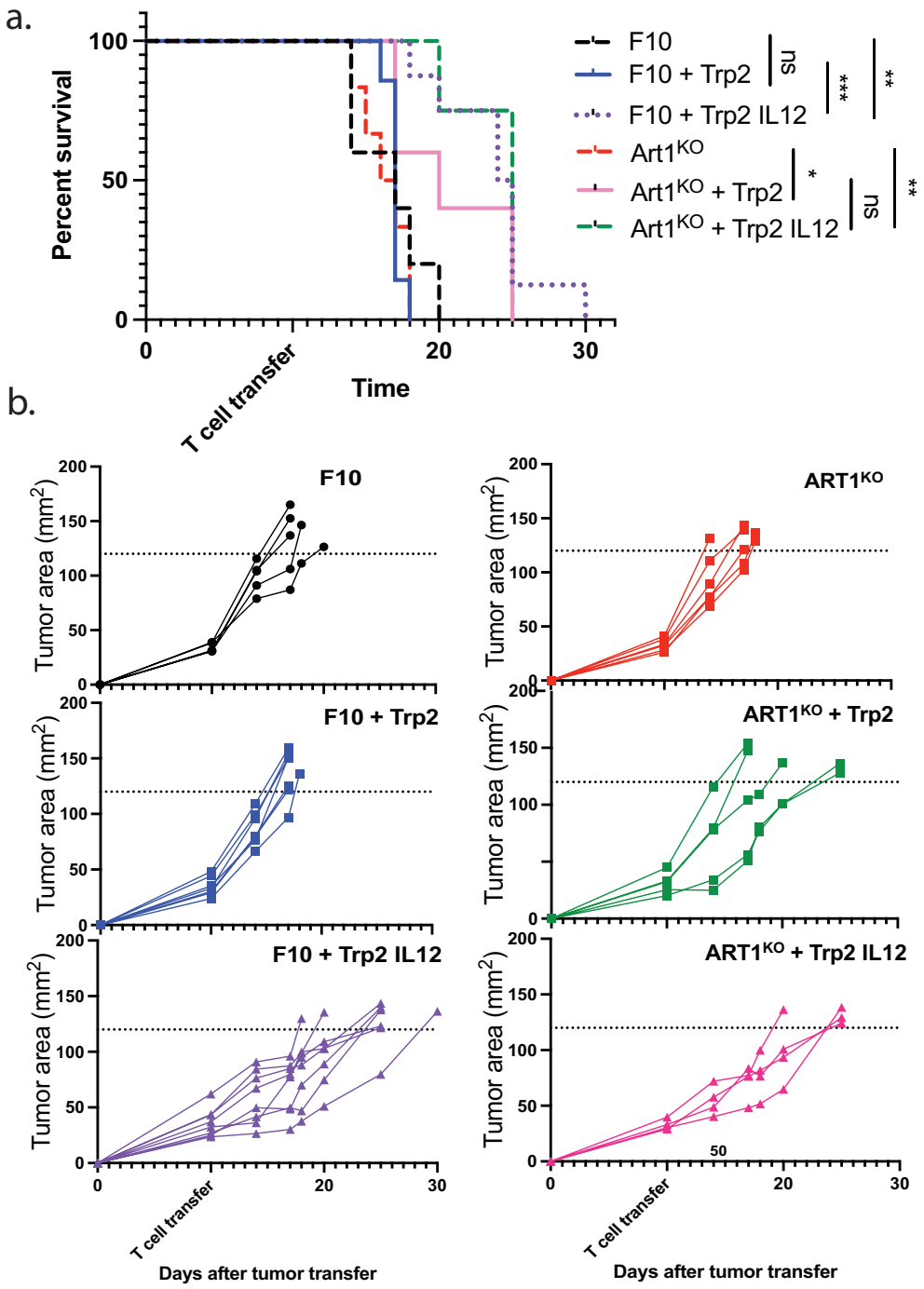

Figure 3.6: ART1 deficiency improves tumor control of Trp2 CD8+ T cells

B6 mice were injected with $3x10^5$ B16.F10 or B16.ART1^{KO} melanoma cells s.c. and once tumors became palpable (~7 days post-injection) $5x10^5$ Trp2 CD8+ T cells were transferred i.v. after 72 hours activation with anti-CD3/-CD28 and 2.5 IU/mL IL-2 +/- 5 ng/mL IL-12. **a)** Survival curve and **b)** tumor growth curves for individual tumor-bearing mice with B16.F10 tumors that received no cell transfer (n=5), WT Trp2 cells (n=6), or WT Trp2 cells + IL12 (n=7), or mice with B16.ART1^{KO} tumors that received no cell transfer (n=6), WT Trp2 cells (n=5) or WT Trp2 cells + IL12 (n=4). Endpoint criteria for survival experiments were tumor ulceration or an area of 120mm^2 (indicated by dashed line).

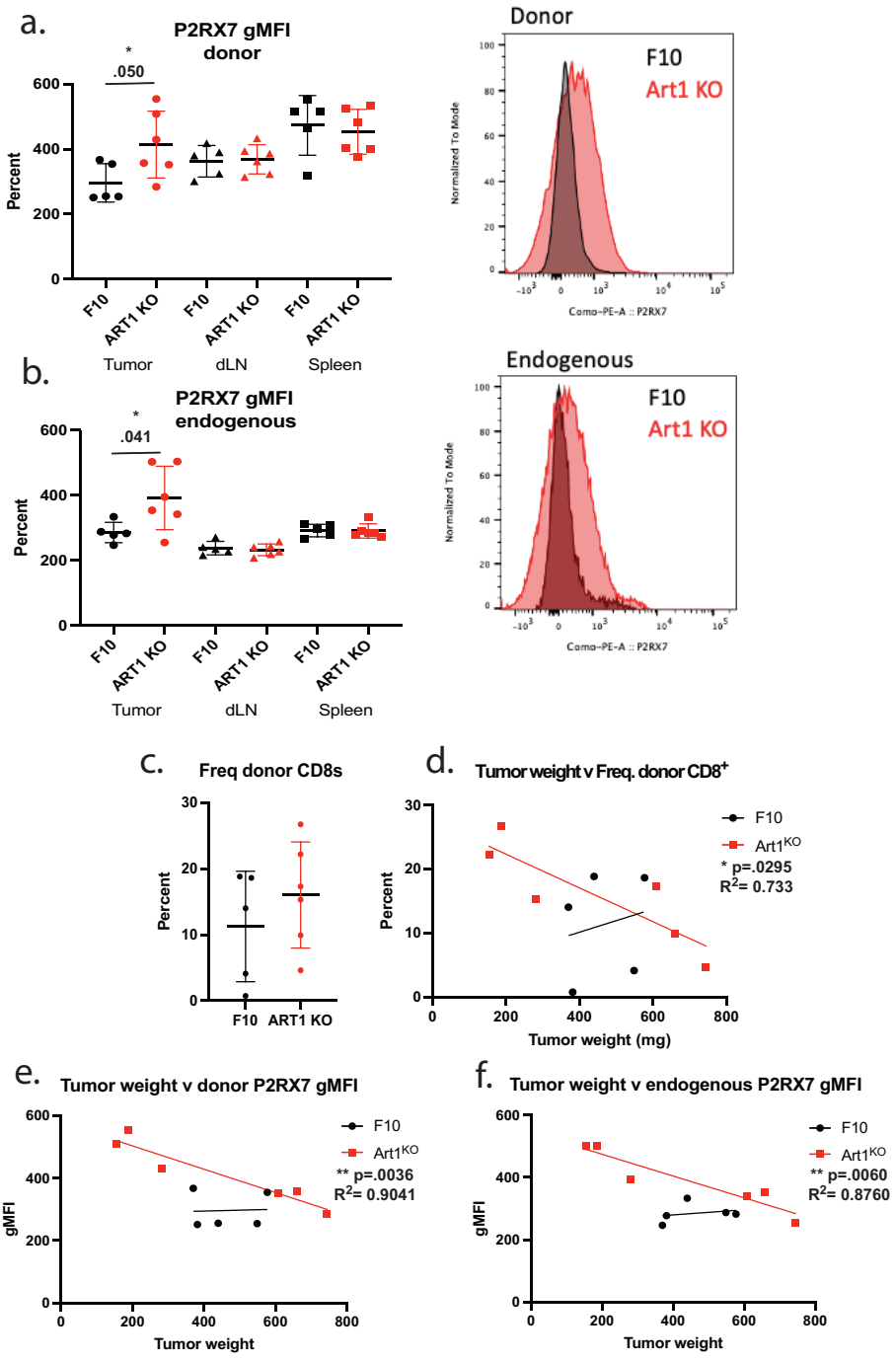

Figure 3.7: ART1 impairs accumulation of P2RX7-expressing CD8+ T cells within the TME

B6 mice were injected with 3 x 10^5 B16.F10 or B16.ART1^{KO} melanoma cells s.c. and once tumors became palpable (~7 days post-injection) 5 x 10^5 Trp2 CD8+ T cells were transferred i.v. after 72 hours activation with anti-CD3/-CD28 and 2.5 IU/mL IL-2 + 5 ng/mL IL-12**.** Tumor, dLN and spleen were harvested from mice at d10 post T cell transfer. Donor Trp2 and endogenous CD8+ T cells were assessed for **a-b)** P2RX7 gMFI, **c)** frequency of donor CD8+ T cells, and correlation between tumor size and **d)** frequency donor CD8+ T cells and **e-f)** P2RX7 gMFI. Results representative of one experiment. Graphical data shown as means with error bars indicating SEM. *, P ⩽ 0.05; **, P ⩽ 0.01. Statistical significance for **a** and **b** evaluated by a two-tailed, unpaired t-test and simple linear regression for **d-f.**

In order to determine whether P2RX7-expressing $CD8^+$ T cells succumb to P2RX7-induced cell death in ART1-expressing B16 tumors, we harvested mice with B16.F10 or B16.$ART1^{KO}$ tumors that received Trp2 $CD8^+$ T cells activated with IL-12. Consistent with our hypothesis, donor Trp2 and polyclonal $CD8^+$ T cells within B16.$ART1^{KO}$ tumors had higher expression of P2RX7 than those in B16.F10 tumors, and this difference was not evident within lymphoid tissues (Fig 3.7a-b). There was also a trend for increased recovery of donor $CD8^+$ T cells within mice with B16.$ART1^{KO}$ tumors (Fig 3.7c). Interestingly, among mice with $ART1^{KO}$ tumors, P2RX7 expression and frequency of Trp2 $CD8^+$ TILs negatively correlated with tumor burden (Fig 3.7d-f). This suggests that while P2RX7-expressing cells are not susceptible to ART1-induced cell death, increased tumor burden (and increased levels of eATP and $eNAD^+$) renders P2RX7-expressing $CD8^+$ T cells vulnerable to cell death via ARTC2.2/NAD^+ or eATP overstimulation.

Together, these results demonstrate that P2RX7 expression on $CD8^+$ T cells can have both a positive and negative role within the TME. Stimulation of P2RX7 during $CD8^+$ T cell activation can enhance anti-tumor immunity in ACT. However, P2RX7 expressing cells are still vulnerable to P2RX7-induced cell death. Therefore, mechanisms to prevent P2RX7-pore formation *in vivo* are of therapeutic interest and may further augment $CD8^+$ T cell immunotherapy.

3.3 Discussion

We have demonstrated that P2RX7 deficiency impairs $CD8^+$ T cell responses to B16 melanoma. *P2rx7*$^{-/-}$ $CD8^+$ T cells exhibit impaired mitochondrial function, which was evident prior to transfer into tumor-bearing mice. These defects were likely exacerbated by the hypoxic and nutrient depleted TME. Indeed, we did observe impaired survival and phenotypic changes consistent with $CD8^+$ T cell exhaustion among donor *P2rx7*$^{-/-}$ $CD8^+$ T cells. Given the essential role for P2RX7 in $CD8^+$ T cell anti-tumor responses, we hypothesized that P2RX7 agonism could further augment $CD8^+$ T cell ACT. Consistent with our hypothesis, we report that transient P2RX7 agonism (with BzATP) increased mitochondrial mass and function in tumor-infiltrating WT CD8+ T cells enhanced tumor control and improved TIL survival, in the absence of IL-12 culture as a tertiary signal during *in vitro* T cell activation. Despite enhanced tumor control in BzATP-treated group, there were fewer $CD8^+$ T cells within tumors at the time of harvest, suggesting that transient P2RX7 stimulation may increase susceptibility to P2RX7-pore formation and cell death. Increased proliferation and mitochondrial function of BzATP-treated $CD8^+$ T cells may compensate for reduced numbers within the tumor. However, $CD8^+$ T cell ACT could be further enhanced if P2RX7-pore formation and cell death could be blocked once $CD8^+$ T cells priming, and tumor infiltration has occurred.

Many different types of tumors utilize P2RX7 signaling to enhance proliferative and metastatic capacity (*99*), thus systemic administration of P2RX7 inhibitors have been shown to reduce tumor burden and progression in murine melanoma models (*109, 111, 141*). However, P2RX7 antagonists used in these experiments can also block P2RX7 signaling on circulating and intratumoral immune cell populations. Indeed, we have shown that the P2RX7 blockade *in vivo* using the pharmacologic antagonist A438 compromises $CD8^+$ T cell memory generation

(*87*). Additionally, our group has previously shown that loss of P2RX7 signaling impairs maintenance of $CD8^+$ memory T cell populations, both using an inducible knock-out of P2RX7 and administration of A438 antagonist (*87*). Consistent with our findings in infection models, blockade of P2RX7 *in vivo* compromises the efficacy of BzATP-treated $CD8^+$ T cells to control B16 melanoma.

The importance of sustained P2RX7 signaling is further supported by preliminary findings that *Panx1*$^{-/-}$ $CD8^+$ T cells exhibit poor tumor control relative to WT $CD8^+$ T cell (data not shown). $CD8^+$ T cells actively export eATP through Panx1 channels, which allows for autocrine P2RX7 signaling in scenarios where inflammation has receded and eATP concentrations are reduced to physiologic levels (*149*). Despite high eATP concentrations within the TME (*62*), it seems that Panx1 still has a role in sustaining P2RX7 signaling in $CD8^+$ TILs, although it is possible that this is related to other functions of Panx1, since it can export other metabolites in addition to eATP (*150*). Tumor and immunosuppressive cells within the TME (e.g. T_{regs}) express high levels of ectonucleotidases CD39 and CD73 that rapidly metabolize eATP into adenosine to impair $CD8^+$ T cell responses to the tumor (*113, 151, 152*). It is possible that rapid turnover of eATP prevents sufficient P2RX7 activation, thus Panx1 maintains pericellular eATP concentrations to sustain P2RX7 signaling.

Since P2RX7 ion-channel function is required for effective anti-tumor immunity, blocking P2RX7 *in vivo* is not an ideal therapeutic option for preventing induction of P2RX7-pore formation within the TME. However, $eNAD^+$ concentrations within the TME are sufficient for either ARTC2.2 on $CD8^+$ T cells or ART1 on tumor cells to ADP-ribosylate P2RX7, inducing cell death. ART1 is highly expressed on B16.F10 tumor cell lines (*106*) and impairs $CD8^+$ T cell responses preventing $P2RX7^+$ $CD8^+$ T cell populations from accumulating within tumors. ART1 also can promote tumor growth and invasiveness (*144-146*), thus ART1 blockade

would both directly prevent tumor progression while also indirectly augmenting $CD8^+$ T cell responses.

However, ART1 knockdown or blockade also can promote survival of immunosuppressive immune cells that express high levels of P2RX7, such as CD4 T_{regs} (*153*). Therefore, strategies that specifically prevent ADP-ribosylation of P2RX7 on $CD8^+$ T cells are of therapeutic interest. ADP-ribosyl cyclase CD38 is expressed on both activated T cells and cancer cells (*154, 155*), and catalyzes degradation of $eNAD^+$ into ADP-ribose (*156*). CD38 tightly regulates $eNAD^+$ concentrations and is thought to have an important role in maintaining T cell homeostasis (*157*), but passive release of $eNAD^+$ from damaged/dying tissue may overwhelm the enzymatic activity of CD38, allowing $eNAD^+$ to accumulate. Overexpression of CD38 on donor $CD8^+$ in ACT may help reduce local concentrations of $eNAD^+$ and reduce ADP-ribosylation of P2RX7. Consistent with this, dual $CD38^+$ $P2RX7^+$ $CD8^+$ T cells were enriched in ART1-expressing human tumors (*106*), suggesting that CD38 expression enables $CD8^+$ T cell survival. Additionally, the amino acid residues on P2RX7 that are targets for ADP-ribosylation by ARTC2.2 have been identified: an arginine to lysine mutation at site 125 of P2RX7 (R125K) prevents P2RX7-pore formation through ADP-ribosylation but does not compromise receptor sensitivity to eATP (*158*). Hence overexpression of CD38 and/or P2RX7 R125K point mutant on $CD8^+$ T cells could theoretically prevent ADP-ribosylation of P2RX7 by both ARTC2.2 and ART1. We have generated both CD38 and P2RX7 R125K retrovirus and plan to test both strategies in future experiments.

3.4 Materials and Methods

3.4.1 Mice

Female 6- to 8-week-old adult C57BL/6 and B6.SJL mice were purchased from Charles River (via the National Cancer Institute). *P2rx7*$^{-/-}$ mice were purchased from Jackson Laboratories and backcrossed to the P14 (LCMV-gp33/D^{b} specific) and OT-I (OVA/K^{b} specific) TCR transgenic backgrounds, with introduction of Thy-1 and CD45 congenic markers to distinguish wild type (WT) and *P2rx7*$^{-/-}$ cells. C57BL/6 Trp2 TCR transgenic mice were generated by Dr. A. Andy Hurwitz. Animals were maintained under specific-pathogen-free conditions at the University of Minnesota. All experimental procedures were approved by the Institutional Animal Care and Use Committee at the University of Minnesota. Animals were randomly assigned to experimental groups.

3.4.2 In vitro activation and adoptive transfer of CD8^{+} T cells

Naïve CD8^{+} T cells were isolated from the spleens of WT or *P2rx7*$^{-/-}$ P14 or OT-I transgenic mice with the mouse naïve CD8^{+} T cell isolation kit (Miltenyi Biotech). A total of 2.5 x 10^{5} isolated T cells were stimulated in flat bottom 24-well plates with anti-CD3 (10 ug/mL), anti-CD28 (20 ug/mL), human IL-2 (2.5 IU/mL), and with or without murine IL-12 (5 ng/mL) for 72 hours in RPMI medium (RPMI 1640 supplemented with 10% FBS, 100 U/mL penicillin/streptomycin, 2mM L-glutamine) at 37^{o}C/5% CO_2. For P2RX7 agonism experiments, isolated CD8^{+} T cells were similarly activated with anti-CD3/-CD28 and IL2, then 100uM of BzATP (or dH_2O as a vehicle treatment) was added every 24 hours to the cultures for the 72-hour activation. After 72 hours, 2.5 x 10^{5}- 5.0 x 10^{5} activated T cells were transferred intravenously (i.v.) into recipient mice.

3.4.3 In vivo tumor experiments

Mice were injected subcutaneously with 1.5 x 10^5 - 3.0 x 10^5 B16.gp33 cells (provided by Dr. Ananda Goldrath, UCSD), B16.OVA cells (provided by Dr. Matt Mescher, UMN), B16.F10 or B16.ART1^{KO} (provided by Dr. Brendon Stiles, Weill Cornell Medicine and Albert Einstein College of Medicine) in the right flank. After thawing cell lines, B16 cells were expanded and passaged once prior to transfer. Cell lines did not undergo Mycoplasma testing. After tumors became palpable (~7 days), tumor-bearing mice received 5.0 x 10^5 activated P14, OT-I, or Trp2 $CD8^+$ T cells T cells Tumor growth and survival was monitored until mice reached an end-point criteria of 120mm^2 or ulceration. Where indicated, mice were treated with a P2RX7 antagonist A-438079 (80mg/kg) or A740003 (50μg/kg) (or PBS as a vehicle treatment) intraperitoneally (i.p.) every other day beginning when tumors became palpable (~7 days post tumor injection).

3.4.4 Flow cytometry

Mice were sacrificed at indicated times and spleens, tumor draining inguinal lymph nodes and tumors were harvested and homogenized. In all experiments involving isolation of lymphocytes from tumors, 50μg of Treg-Protector (anti-ARTC2.2) nanobody (BioLegend) was injected i.v. 30 minutes prior to mouse sacrifice as previously described [8, 9]. Tumors were removed, cut into small pieces, and digested with 3mg/mL Collagenase type I solution for 1 hour at 37oC and then dissociated via gentleMACS Dissociator (Miltenyi Biotec) twice. Isolated mouse cells were stained with antibodies to CD8α (clone 53-6.7, BD Biosciences), CD44 (clone IM7, Tonbo Biosciences), CD69 (clone H1.2F3, BioLegend), CD103 (clone M290, BD Biosciences), P2RX7 (clone 1F11, BD Biosciences), CD279 (PD-1) (clone 29F.1A12, Biolegend), CD366 (Tim3) (clone RMT3-23, BioLegend), CD223 (Lag3) (clone C9B7W, BioLegend), CD39 (clone Duha59, Biolegend), Ki67 (clone SolA15, Thermo). All cells were stained at

antibody dilutions of 1:200 except for P2RX7 (1:50). Cells stained intracellularly for Ki67 were permeabilized using eBioscience transcription factor fixation/permeabilization kits. Cell viability was determined with Ghost Dye 780 (Tonbo Biosciences). Enumeration of lymphocytes was achieved using CountBright Absolute Counting Beads (Invitrogen).

For mitochondrial mass and membrane potential measurements, 1-2 x 10^6 cells were incubated with 100nM MTG (Thermofisher Scientific) and 80nM TMRE (BD Biosciences) simultaneously for 20 minutes in RPMI 1640 supplemented with 2% FBS at 37^{o}C prior to ex vivo staining. In order to account for experiment-to-experiment variability, gMFIs of either MTG or TMRE in donor WT CD8 P14 cells within the spleen of each experiment were averaged and fold change of donor WT or *P2rx7*$^{-/-}$ CD8$^+$ T cells within the tumor or dLN for each experiment was calculated relative to splenic WT donor cells. Mitochondrial reactive oxygen species (ROS) were evaluated by incubating 1-2 x 10^6 cells with 5μM MitoSOX reagent (ThermoFisher) in RPMI 1640 supplemented with 2% FBS at 37^{o}C prior to ex vivo staining.

Flow cytometric analysis was performed on a LSR II or LSR Fortessa (BD Biosciences) and data was analyzed using FlowJo software (Treestar).

3.4.5 Metabolic assays

OCR and ECAR were assessed in in vitro activated WT and *P2rx7*$^{-/-}$ T cells (activated with or without IL-12 or BzATP for 72 hours) using a 96-well XF Extracellular flux analyzer, according to the manufacturer's instructions (Seahorse Bioscience), similar to earlier studies (*87, 88*). Briefly, 2 x 10^5 activated cells were plated onto Seahorse XFe96 (Agilent) plates (coated with CellTak solution the night before) in warm Seahorse base media (Agilent) supplemented with 2mM L-glutamine, 1mM sodium pyruvate, and 10mM glucose

(pH 7.4) the day of assay. Seahorse XF Mito Stress kit components (1.5μM Oligomycin, 1μM FCCP, 0.5μM Rotenone/AntimycinA) were added to hydrated 96-well sensor cartridge (incubated overnight at 37°C with Agilent calibrant solution) before performing assay. Spare respiratory capacity (SRC) and OCR and ECAR values were defined as previously described (*17, 58*).

3.4.6 Statistical analysis

Data were subject to Kolmogorov-Smirnov test to assess normality of samples. Statistical differences were calculated by using paired or unpaired two-tailed Student's t-test or one-way ANOVA with Tukey post-test. In cases where one group in the comparisons was normalized, statistical analysis employed ANOVA with Brown-Forsythe and Welch corrections. Statistical differences for survival data were assessed using a log-rank Mantel-Cox test. Statistical differences for correlation analyses were evaluated using simple linear regression. All statistical analysis was performed using Prism 9 (GraphPad Software). Graphical data shown with error bars indicating the SD or SEM. P values of <0.05 (*), <0.01 (**), <0.001 (***), or <0.0001 (****) indicate significant differences between groups.

3.5 Supplemental Figures

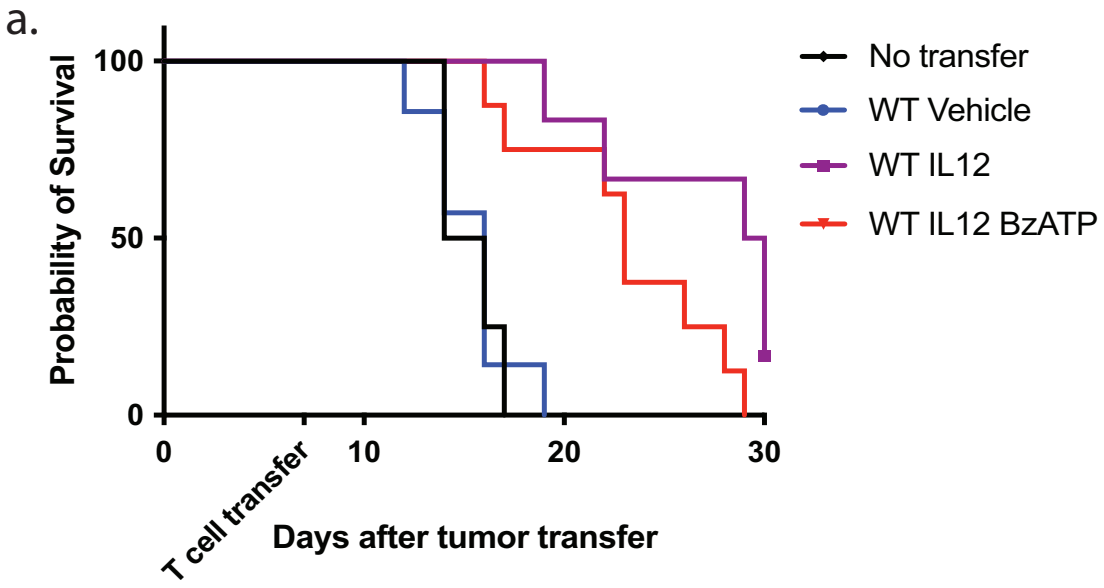

Figure S3.1: BzATP stimulation does not augment tumor control by IL-12-cultured CD8⁺ T cells.

B6 mice were injected with 3 x 10^5 B16.gp33 melanoma s.c. and once tumors became palpable (~7 days post-injection) 5 x 10^5 WT or *P2rx7*$^{-/-}$ P14 cells were transferred i.v. after 72 hours activation with anti-CD3/-CD28, 2.5 IU/mL IL-2, +/- IL-12, and +/- 100μM of BzATP (or vehicle dH2O treatment) every 24 hours of activation. **a)** Survival curve for tumor-bearing mice that received vehicle (n=7), IL-12 (n=7) or BzATP + IL-12 (n=8) treated WT P14 cells or no cell transfer (n=4). Endpoint criteria for survival experiments were tumor ulceration or an area of 120mm^2. Data representative of two independent experiments.

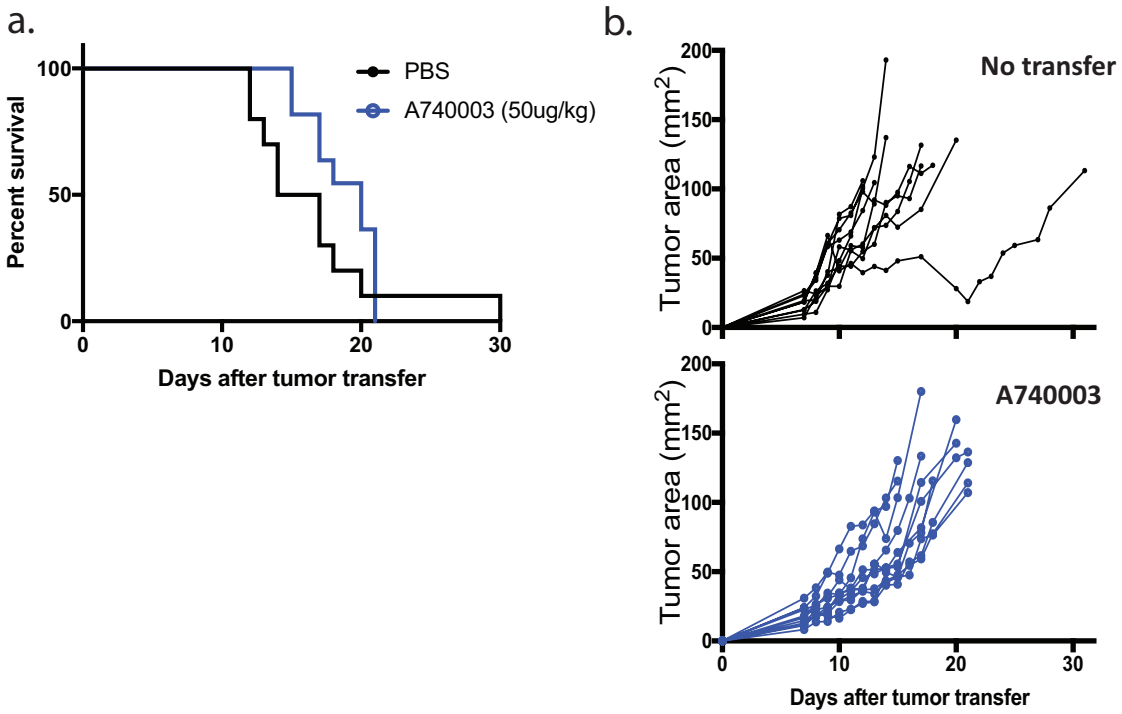

Figure S3.2: P2RX7 antagonism moderately reduces tumor burden.

B6 mice were injected with 3 x 10^5 B16.gp33 melanoma s.c. and once tumors became palpable (~7 days post-injection), mice were treated i.p. with A740003 P2RX7 antagonist (50μg/kg) every other day until mice reach endpoint criteria. **a)** Mice were that received indicated treatments (No transfer, n=8; A740003, n=10) were monitored for survival and **b)** tumor burden. Data are from 2 independent experiments. *, $P \leqslant 0.05$; **, $P \leqslant 0.01$; ***, $P \leqslant 0.001$. Statistical significance was determined by a log-rank Mantel-Cox test.

3.6 Publications and Contributions

Chapter modified with permission from the following published article:

Wanhainen, K.M. *et al.* P2RX7 enhances tumor control by $CD8^+$ T cell in adoptive cell therapy. *Cancer Immunol Res.* 2022; 10(7): 871-884. PMID: 35588154

KMW, HBdS, and SCJ designed the experiments. KMW, CP, MHZ, BdGM, SO, TY, and HDbS performed experiments. KMW and SCJ wrote the manuscript with input from all authors.

Chapter 4

Conclusions and Clinical Application

4.1 P2RX7 is important for CD8$^+$ T cell antitumor immunity

The role of P2RX7 in anti-tumor immunity is complex given the capacity of the receptor to act as a 'double edged sword.' Low-level, tonic stimulation of P2RX7 promotes metabolic fitness and longevity, while overstimulation induces irreversible macropore formation and cell death (*64*). Extensive tissue damage and death as tumors progress results in passive release of DAMPs, such as eATP and eNAD$^+$, which activate P2RX7 ion channel function but can also induce pore formation (*62, 99*). Thus, whether P2RX7 is beneficial or a liability to immune cells within the tumor is unclear.

P2RX7 plays an important role in the host immune responses against tumors as demonstrated by observations that tumors grow more rapidly in P2RX7 deficient hosts (*109, 111, 112*). Tumors in P2RX7 deficient hosts are characterized with reduced CD8$^+$ T cell infiltration and immunosuppressive cytokine profiles (*109*). Indeed, P2RX7 has an essential role in activating the NLRP3 inflammasome and inflammatory cytokine production which facilitates NK and T cell activation within the tumor (*115, 116*). However, a recent study by Romagnani, *et al.* showed that P2RX7 expression impairs CD4$^+$ and CD8$^+$ T cell accumulation within tumors and limits suppression of B16 melanoma (*119*). These results contrasted our previous findings that P2RX7 promotes metabolic fitness of CD8$^+$ T cells and is essential for responses to both acute and chronic infections (*87, 88*). Furthermore, *P2rx7*$^{-/-}$ CD8$^+$ T cells were particularly impaired in generating the TCF1$^+$ 'stem-like' population in response to LCMV Clone 13 infection (*87*), which has been shown to sustain CD8$^+$ T cell responses to both chronic infections and tumors (*117, 118*). Given parallels between CD8$^+$ T cell responses to chronic infections and tumors (*159*), it seemed likely that P2RX7 deficiency would similarly impair CD8$^+$ T cell anti-tumor responses.

The study by Romagnani *et al.* utilized CD8$^+$ T cells that were activated *in vitro* using TCR stimulation and IL-2 only. However, many studies have demonstrated the importance of including IL-12 as a tertiary signal for CD8$^+$ T cell activation in order to generate effective responses to B16 melanoma and other tumors (*120, 160-162*). IL-12 programs transcriptional and epigenetic changes in CD8$^+$ T cells that enhance cytotoxicity and survival (*148*). We also found that IL-12 conditioning during T cell activation promoted increases in mitochondrial mass and function. While P2RX7 deficient CD8$^+$ T cells similarly developed enhanced cytotoxicity following activation with IL-12, long-term survival of *P2rx7*$^{-/-}$ CD8$^+$ T cells was impaired relative to WT CD8$^+$ T cells in tumor-bearing mice. IL-12 priming also did not increase mitochondrial function in *P2rx7*$^{-/-}$ CD8$^+$ T cells. Given the importance of mitochondrial metabolism and CD8$^+$ T cell long-term survival (*14*), it is probable that defects in mitochondrial function prior to transfer into tumor-bearing mice were exacerbated within the TME, resulting in poor survival of *P2rx7*$^{-/-}$ CD8$^+$ T cells and impaired anti-tumor immunity.

Our results also expand on findings from many other groups linking impaired mitochondrial homeostasis and CD8$^+$T cell dysfunction. Metabolic stressors within the TME are known impairs mitochondria biogenesis and removal of damaged mitochondria. These changes drive epigenetic and transcriptional changes within the CD8$^+$ T cell that drives expression of inhibitory receptors (*54-57, 163*). IL-12 conditioning is known to reduce induction of factors that promote CD8$^+$ T cell exhaustion (*120, 121*). Consistent with these studies, neither WT nor *P2rx7*$^{-/-}$ CD8$^+$ T cells exhibit a TOX$^+$ population in contrast to endogenous non-IL-12 conditioned CD8$^+$ T cells within the same tumor. However, *P2rx7*$^{-/-}$ CD8$^+$ still exhibited increased expression of some inhibitory receptors and reduced proliferative capacity as tumor burden increased. These defects occurred alongside continued mitochondrial dysfunction among *P2rx7*$^{-/-}$ CD8$^+$ T cells, reinforcing the importance of metabolic homeostasis for effective T cell function.

Our findings that P2RX7 deficient CD8$^+$ T cells exhibit impaired tumor control is relevant for human health as P2RX7 is a highly polymorphic receptor. In humans there are at least 9 splice variants of P2RX7 and at least 16 SNPs within the coding region of P2RX7 have been identified and are known to impact receptor activity (*164*). In some studies, loss of function mutations in P2RX7 increase susceptibility of individuals to intracellular bacterial infections such as tuberculosis (*126*). Less is known about the impact of P2RX7 loss of function variants and cancer development, but several small case-studies do suggest that P2RX7 deficiency correlates with tumor development. The well-characterized loss of function variant Glu496Ala is associated with increased tumor grade in a cohort of breast cancer patients (*115*). Similarly, this loss of function variant was also associated with development of hepatocellular carcinoma and chronic lymphocytic leukemia, and a separate partial loss of function variant is associated with development of cervical cancer (*165-167*). These studies suggest that loss of P2RX7 may be associated with impaired immune surveillance of tumors. Consistent with that hypothesis, we have shown that P2RX7 is essential for generation and maintenance of CD8$^+$ T_{RM} in NLT(*88*), which have an essential role in preventing tumor progression (*41*). Loss of function mutations in P2RX7 may also predict patients that will have poor responses to immunotherapy.

4.2 Therapeutic exploitation of purinergic signaling in the TME

We also demonstrated that transient P2RX7 stimulation can enhance mitochondrial function in CD8$^+$ T cells and lead to improved ACT responses. The positive impact of P2RX7 agonism was dependent on sustained P2RX7 signaling within the TME. Strategies that increase eATP levels, such as Panx1 over expression, may complement transient P2RX7 agonism and further enhance

ACT. Furthermore, a small molecule activator of P2RX7 administered *in vivo* has been shown to enhance anti-tumor responses in lung carcinoma and B16 melanoma models by stimulating P2RX7-DCs, inducing IL-18 production and subsequent NK and T cell activation (*116*). Importantly, P2RX7 activation using the small molecule affected immune cell function and without inducing tumor cell proliferation and progression in either B16 melanoma or lung carcinoma models (*116*), suggesting this compound may be a feasible therapeutic option to boost immunotherapy in other tumors models as well.

Furthermore, the requirement for sustained P2RX7 signaling *in vivo* indicates that use of P2RX7 antagonists to block pro-metastatic and -proliferative function of P2RX7 on tumors may have detrimental off-target effects on $CD8^+$ T cells. However, tumors commonly express variants of P2RX7 that retain ion channel ability but are unable to induce cell death through formation of the P2RX7-pore (*105, 106*). A P2RX7 variant that is unable to form a functional macropore (nfP2X7) has been described on many human cancers and can be discriminated from WT P2RX7 with an antibody targeting a distinct sequence (*105*). While this antibody has not been reported to have blocking activity, it is likely possible to develop an antagonist that specifically blocks this variant.

In addition to utilizing elevated concentrations of eATP to promote growth and metastasis, tumors also convert eATP to immunosuppressive adenosine through high expression of ectonucleotidases CD39 and CD73 (*152*). CD39 is the rate-limiting enzyme in adenosine synthesis, and blockade of CD39 not only reduces extracellular adenosine (eADO) concentrations but also allows for eATP concentrations to persist and promote inflammatory responses. Indeed, antibodies targeting CD39 showed preclinical efficacy and are currently being investigated in clinical trials, often in combination with chemotherapy or immunotherapy agents (*100*). Many commonly used chemotherapy drugs have

an immunostimulatory effect through release of eATP from dying cells (*94*). To counteract this, tumors increase expression of CD39 in response to certain chemotherapy drugs, resulting in resistance to therapy (*168, 169*). Together, these studies further support the importance of eATP signaling within the TME and suggest that CD39 blockade can have a dual therapeutic effect of reducing immunosuppression while also augmenting P2RX7 signaling within the TME.

4.3 Mechanisms to protect CD8$^+$ T cells from P2RX7-induced cell death

Despite the requirement for P2RX7-eATP signaling within the TME, P2RX7 can still induce pore formation and cell death from eATP overstimulation or NAD$^+$-ADP-ribosylation by ARTs on CD8$^+$ T cells or tumor cells. NAD$^+$ induced cell death (NICD) is of particular interest as much lower concentrations of NAD$^+$ can induce P2RX7-macropore formation relative to eATP (*64, 66*). We and others show that ART1 expression on B16 and lung tumors selectively targets P2RX7$^+$ CD8$^+$ T cells within the tumor (*106*). Consistent with P2RX7 being required for establishing CD8$^+$ T_{RM} populations (*88*), ART1 blockade increased P2RX7$^+$ CD103$^+$ CD8$^+$ T_{RM} cell populations in tumor-bearing lungs (*106*). CD8$^+$ T_{RM} express very high levels of P2RX7 relative to circulating CD8$^+$ T cell populations and have been shown to be particularly susceptible to NICD (*84-86, 88*). Given the positive correlation between tumor infiltrating CD8$^+$ T_{RM} and improved patient outcome in many different types of cancer (*37-39, 170*), strategies to enhance persistence of these populations is of therapeutic relevance. Our data demonstrated that deletion of ART1 on B16 melanoma enables tumor control of CD8$^+$ T cells that are activated with TCR stimulation and IL-2 alone, which typically does not promote effective anti-tumor immunity (*120, 121*). This provides further evidence that inhibition of NICD can enhance immunotherapy, even in CD8$^+$ T cells that would typically induce suboptimal responses.

The ART1 blocking antibody described in Wennerberg, *et al.* exhibited preclinical efficacy in the KP1 lung carcinoma model (*106*). However, use of this antibody also protected immunosuppressive T_{regs} that also express high levels of P2RX7 (*106*). A point mutation in P2RX7 (R125K) prevents auto-ADP-ribosylation by ARTC2.2 on murine $CD8^+$ T cells (*158*). Whether mutation of this site also prevents ADP-ribosylation through ART1 remains to be investigated. However, this could present a therapeutic opportunity in which NICD is specifically inhibited on $CD8^+$ T cells.

Overexpression of CD38 on $CD8^+$ to reduce local $eNAD^+$ concentrations is also an appealing option to reduce NICD. Indeed, CD38 is upregulated on human and mouse $CD8^+$ T cells upon activation (*154*) and may protect effector T cells from NICD as they traffic into inflamed tissues where $eNAD^+$ is abundant (*157*). Consistent with this, blockade of CD38 increases ADP-ribosylation of $P2RX7^+$ $CD8^+$ T cells *in vitro* (*106*). However, augmenting CD38 function in tumor settings may indirectly cause immunosuppression. CD38 metabolizes $eNAD^+$ into ADP-ribose, which can be further broken down into adenosine (*143*). Indeed, CD38 has been linked to ICB resistance in preclinical lung adenocarcinoma models (*155*). However, CD38 blockade in combination with ICB was recently tested in a clinical trial in NSCLC patients and resulted in tumor progression (*171*). As ART1 is expressed in NSCLC, it is possible that reduced $eNAD^+$ metabolism led to increased NICD in $CD8^+$ TILs which outweighed potential immunosuppressive effects of CD38. Thus, further investigation into the role of CD38 and prevention of NICD *in vivo* is needed.

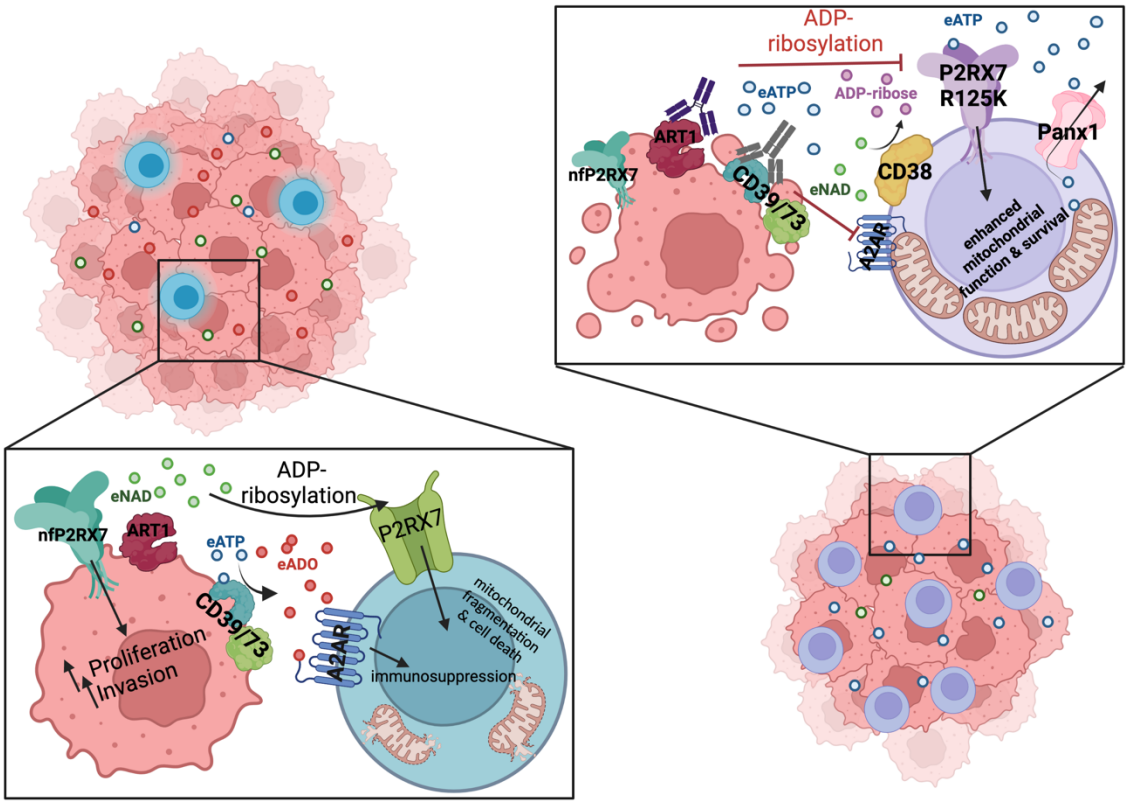

Figure 4.1: Model for enhancing P2RX7 signaling to optimize ACT

(Left) P2RX7 can be a liability to tumor immunotherapy in some contexts. Tumors express variants of P2RX7 that retain ion channel activity but do not form the lethal macropore (e.g., nfP2RX7), which allows tumors to utilize P2RX7 signaling to enhance proliferation and metastasis. Tumors also express ADP-ribosyltransferase 1 (ART1), which utilizes $eNAD^+$ to catalyze ADP-ribosylation of P2RX7 resulting in pore formation, mitochondrial damage and cell death. Furthermore, tumor expression of CD39 and CD73 transform inflammatory eATP into immunosuppressive adenosine (eADO), which acts on adenosine receptors (e.g., A2AR) on T cells to induce immunosuppression.
(Right) Strategies that enhance P2RX7-eATP signaling while also preventing P2RX7-mediated cell death have potential to improve $CD8^+$ T cell anti-tumor responses. NICD of $CD8^+$ T cells can be prevented directly, by blocking ART1 on tumor cells or by mutating the ADP-ribosylation site on P2RX7, or indirectly, reducing $eNAD^+$ levels with CD38 overexpression. Furthermore, blockade of CD39 on tumor cells reduces eADO concentrations within the TME, which has s dual beneficial effect of reducing immunosuppression and increasing eATP-P2RX7 signaling on $CD8^+$ T cells. Lastly, overexpression of the Pannexin I (Panx1) on $CD8^+$ T cells can similarly maintain P2RX7 signaling via autocrine export of ATP. Together, these modifications could enhance $CD8^+$ T cell infiltration, survival and function within the tumor.

4.4 Concluding remarks

ACT has emerged as a promising treatment for many different types of tumors. Expansion of patient $CD8^+$ T cells *in vitro* prior reinfusion provides many opportunities to manipulate $CD8^+$ T cells in ways that enhance anti-tumor

responses. Here we show that P2RX7 is required for $CD8^+$ T cell immunotherapy by promoting mitochondrial fitness. As P2RX7 loss-of-function mutations are relatively common in the population (*126*), P2RX7 overexpression or other strategies that boost mitochondrial function may be required in patients with these mutations undergoing ACT. Furthermore, we demonstrate that transient P2RX7 stimulation can used to boost metabolic function of $CD8^+$ TIL. Since efficacy was dependent on sustained P2RX7 stimulation, strategies that enhance P2RX7- eATP signaling within the TME may provide further therapeutic benefit (Fig 4.1). Lastly, we identify that tumors use NICD to promote cell death in infiltrating $CD8^+$ T cells in a P2RX7 dependent manner. Inhibition of NICD either directly (blocking ART1 on tumors) or indirectly (by modulating $eNAD^+$ concentrations or mutating ADP-ribosylation site on P2RX7) will protect $CD8^+$ T cells that express high levels of P2RX7 (e.g. $CD8^+$ T_{RM}) and allow for P2RX7 to promote effective anti-tumor responses.

References

1. K. Buchmann, Evolution of Innate Immunity: Clues from Invertebrates via Fish to Mammals. *Front Immunol* **5**, 459 (2014).
2. L. M. Zimmerman, L. A. Vogel, R. M. Bowden, Understanding the vertebrate immune system: insights from the reptilian perspective. *J Exp Biol* **213**, 661-671 (2010).
3. M. F. Flajnik, M. Kasahara, Origin and evolution of the adaptive immune system: genetic events and selective pressures. *Nat Rev Genet* **11**, 47-59 (2010).
4. D. Nemazee, Mechanisms of central tolerance for B cells. *Nat Rev Immunol* **17**, 281-294 (2017).
5. M. S. Krangel, Mechanics of T cell receptor gene rearrangement. *Curr Opin Immunol* **21**, 133-139 (2009).
6. L. Klein, B. Kyewski, P. M. Allen, K. A. Hogquist, Positive and negative selection of the T cell repertoire: what thymocytes see (and don't see). *Nat Rev Immunol* **14**, 377-391 (2014).
7. M. H. Andersen, D. Schrama, P. Thor Straten, J. C. Becker, Cytotoxic T cells. *J Invest Dermatol* **126**, 32-41 (2006).
8. J. Reimann, S. H. Kaufmann, Alternative antigen processing pathways in anti-infective immunity. *Curr Opin Immunol* **9**, 462-469 (1997).
9. P. Guermonprez, J. Valladeau, L. Zitvogel, C. Théry, S. Amigorena, Antigen presentation and T cell stimulation by dendritic cells. *Annu Rev Immunol* **20**, 621-667 (2002).
10. J. M. Curtsinger, D. C. Lins, M. F. Mescher, Signal 3 determines tolerance versus full activation of naive CD8 T cells: dissociating proliferation and development of effector function. *J Exp Med* **197**, 1141-1151 (2003).
11. E. A. Butz, M. J. Bevan, Massive expansion of antigen-specific CD8+ T cells during an acute virus infection. *Immunity* **8**, 167-175 (1998).
12. C. Stemberger *et al.*, A single naive CD8+ T cell precursor can develop into diverse effector and memory subsets. *Immunity* **27**, 985-997 (2007).
13. S. C. Jameson, D. Masopust, Understanding Subset Diversity in T Cell Memory. *Immunity* **48**, 214-226 (2018).
14. E. L. Pearce, M. C. Poffenberger, C. H. Chang, R. G. Jones, Fueling immunity: insights into metabolism and lymphocyte function. *Science* **342**, 1242454 (2013).
15. M. G. Vander Heiden, L. C. Cantley, C. B. Thompson, Understanding the Warburg effect: the metabolic requirements of cell proliferation. *Science* **324**, 1029-1033 (2009).
16. D. O'Sullivan *et al.*, Memory CD8(+) T cells use cell-intrinsic lipolysis to support the metabolic programming necessary for development. *Immunity* **41**, 75-88 (2014).

17. G. J. van der Windt *et al.*, Mitochondrial respiratory capacity is a critical regulator of CD8+ T cell memory development. *Immunity* **36**, 68-78 (2012).
18. K. Araki *et al.*, mTOR regulates memory CD8 T-cell differentiation. *Nature* **460**, 108-112 (2009).
19. E. L. Pearce *et al.*, Enhancing CD8 T-cell memory by modulating fatty acid metabolism. *Nature* **460**, 103-107 (2009).
20. Y. Pan *et al.*, Survival of tissue-resident memory T cells requires exogenous lipid uptake and metabolism. *Nature* **543**, 252-256 (2017).
21. R. D. Schreiber, L. J. Old, M. J. Smyth, Cancer immunoediting: integrating immunity's roles in cancer suppression and promotion. *Science* **331**, 1565-1570 (2011).
22. A. Van Pel, T. Boon, Protection against a nonimmunogenic mouse leukemia by an immunogenic variant obtained by mutagenesis. *Proc Natl Acad Sci U S A* **79**, 4718-4722 (1982).
23. C. Castelli *et al.*, T-cell recognition of melanoma-associated antigens. *J Cell Physiol* **182**, 323-331 (2000).
24. D. H. Kaplan *et al.*, Demonstration of an interferon gamma-dependent tumor surveillance system in immunocompetent mice. *Proc Natl Acad Sci U S A* **95**, 7556-7561 (1998).
25. V. Shankaran *et al.*, IFNgamma and lymphocytes prevent primary tumour development and shape tumour immunogenicity. *Nature* **410**, 1107-1111 (2001).
26. F. Alfei, P. C. Ho, W. L. Lo, DCision-making in tumors governs T cell anti-tumor immunity. *Oncogene* **40**, 5253-5261 (2021).
27. J. P. Böttcher *et al.*, NK Cells Stimulate Recruitment of cDC1 into the Tumor Microenvironment Promoting Cancer Immune Control. *Cell* **172**, 1022-1037.e1014 (2018).
28. E. W. Roberts *et al.*, Critical Role for CD103(+)/CD141(+) Dendritic Cells Bearing CCR7 for Tumor Antigen Trafficking and Priming of T Cell Immunity in Melanoma. *Cancer Cell* **30**, 324-336 (2016).
29. S. Lorenzi *et al.*, Type I IFNs control antigen retention and survival of CD8α(+) dendritic cells after uptake of tumor apoptotic cells leading to cross-priming. *J Immunol* **186**, 5142-5150 (2011).
30. K. Hildner *et al.*, Batf3 deficiency reveals a critical role for CD8alpha+ dendritic cells in cytotoxic T cell immunity. *Science* **322**, 1097-1100 (2008).
31. S. Spranger, D. Dai, B. Horton, T. F. Gajewski, Tumor-Residing Batf3 Dendritic Cells Are Required for Effector T Cell Trafficking and Adoptive T Cell Therapy. *Cancer Cell* **31**, 711-723.e714 (2017).
32. M. L. Broz *et al.*, Dissecting the Tumor Myeloid Compartment Reveals Rare Activating Antigen-Presenting Cells Critical for T Cell Immunity. *Cancer Cell* **26**, 938 (2014).

33. A. R. Sánchez-Paulete *et al.*, Cancer Immunotherapy with Immunomodulatory Anti-CD137 and Anti-PD-1 Monoclonal Antibodies Requires BATF3-Dependent Dendritic Cells. *Cancer Discov* **6**, 71-79 (2016).
34. M. E. Mikucki *et al.*, Non-redundant requirement for CXCR3 signalling during tumoricidal T-cell trafficking across tumour vascular checkpoints. *Nat Commun* **6**, 7458 (2015).
35. A. M. Cornel, I. L. Mimpen, S. Nierkens, MHC Class I Downregulation in Cancer: Underlying Mechanisms and Potential Targets for Cancer Immunotherapy. *Cancers (Basel)* **12**, (2020).
36. D. Amsen, K. P. J. M. van Gisbergen, P. Hombrink, R. A. W. van Lier, Tissue-resident memory T cells at the center of immunity to solid tumors. *Nat Immunol* **19**, 538-546 (2018).
37. Z. Q. Wang *et al.*, CD103 and Intratumoral Immune Response in Breast Cancer. *Clin Cancer Res* **22**, 6290-6297 (2016).
38. J. Koh *et al.*, Prognostic implications of intratumoral CD103+ tumor-infiltrating lymphocytes in pulmonary squamous cell carcinoma. *Oncotarget* **8**, 13762-13769 (2017).
39. F. L. Komdeur *et al.*, CD103+ tumor-infiltrating lymphocytes are tumor-reactive intraepithelial CD8+ T cells associated with prognostic benefit and therapy response in cervical cancer. *Oncoimmunology* **6**, e1338230 (2017).
40. H. H. Workel *et al.*, CD103 defines intraepithelial CD8+ PD1+ tumour-infiltrating lymphocytes of prognostic significance in endometrial adenocarcinoma. *Eur J Cancer* **60**, 1-11 (2016).
41. S. L. Park *et al.*, Tissue-resident memory $CD8^+$ T cells promote melanoma-immune equilibrium in skin. *Nature* **565**, 366-371 (2019).
42. B. T. Malik *et al.*, Resident memory T cells in the skin mediate durable immunity to melanoma. *Sci Immunol* **2**, (2017).
43. P. C. Rosato *et al.*, Virus-specific memory T cells populate tumors and can be repurposed for tumor immunotherapy. *Nat Commun* **10**, 567 (2019).
44. J. J. Milner *et al.*, Runx3 programs CD8+ T cell residency in non-lymphoid tissues and tumours. *Nature* **552**, 253-257 (2017).
45. A. P. Ganesan *et al.*, Tissue-resident memory features are linked to the magnitude of cytotoxic T cell responses in human lung cancer. *Nat Immunol* **18**, 940-950 (2017).
46. J. Edwards *et al.*, CD103+ Tumor-Resident CD8+ T cells are Associated with Improved Survival in Immunotherapy-Naive Melanoma Patients and Expand Significantly During Anti-PD-1 Treatment. *Clin Cancer Res* **24**, 3036-3045 (2018).
47. G. H. Attrill *et al.*, Higher proportions of CD39+ tumor-resident cytotoxic T cells predict recurrence-free survival in patients with stage III melanoma treated with adjuvant immunotherapy. *J Immunother Cancer* **10**, (2022).

48. Y. Q. Xie *et al.*, Redox-responsive interleukin-2 nanogel specifically and safely promotes the proliferation and memory precursor differentiation of tumor-reactive T-cells. *Biomater Sci* **7**, 1345-1357 (2019).
49. C. Li *et al.*, The Transcription Factor Bhlhe40 Programs Mitochondrial Regulation of Resident CD8. *Immunity* **52**, 201-202 (2020).
50. P. C. Ho *et al.*, Phosphoenolpyruvate Is a Metabolic Checkpoint of Anti-tumor T Cell Responses. *Cell* **162**, 1217-1228 (2015).
51. A. K. Neumann *et al.*, Hypoxia inducible factor 1 alpha regulates T cell receptor signal transduction. *Proc Natl Acad Sci U S A* **102**, 17071-17076 (2005).
52. I. B. Barsoum, C. A. Smallwood, D. R. Siemens, C. H. Graham, A mechanism of hypoxia-mediated escape from adaptive immunity in cancer cells. *Cancer Res* **74**, 665-674 (2014).
53. W. C. Adams *et al.*, Anabolism-Associated Mitochondrial Stasis Driving Lymphocyte Differentiation over Self-Renewal. *Cell Rep* **17**, 3142-3152 (2016).
54. N. E. Scharping *et al.*, The Tumor Microenvironment Represses T Cell Mitochondrial Biogenesis to Drive Intratumoral T Cell Metabolic Insufficiency and Dysfunction. *Immunity* **45**, 701-703 (2016).
55. N. E. Scharping *et al.*, Mitochondrial stress induced by continuous stimulation under hypoxia rapidly drives T cell exhaustion. *Nat Immunol* **22**, 205-215 (2021).
56. Y. R. Yu *et al.*, Disturbed mitochondrial dynamics in CD8$^+$ TILs reinforce T cell exhaustion. *Nat Immunol* **21**, 1540-1551 (2020).
57. B. Bengsch *et al.*, Bioenergetic Insufficiencies Due to Metabolic Alterations Regulated by the Inhibitory Receptor PD-1 Are an Early Driver of CD8(+) T Cell Exhaustion. *Immunity* **45**, 358-373 (2016).
58. M. D. Buck *et al.*, Mitochondrial Dynamics Controls T Cell Fate through Metabolic Programming. *Cell* **166**, 63-76 (2016).
59. F. I. Ataullakhanov, V. M. Vitvitsky, What determines the intracellular ATP concentration. *Biosci Rep* **22**, 501-511 (2002).
60. M. L. Cotrina *et al.*, Connexins regulate calcium signaling by controlling ATP release. *Proc Natl Acad Sci U S A* **95**, 15735-15740 (1998).
61. R. Corriden, P. A. Insel, Basal release of ATP: an autocrine-paracrine mechanism for cell regulation. *Sci Signal* **3**, re1 (2010).
62. P. Pellegatti *et al.*, Increased level of extracellular ATP at tumor sites: in vivo imaging with plasma membrane luciferase. *PLoS One* **3**, e2599 (2008).
63. J. Linden, F. Koch-Nolte, G. Dahl, Purine Release, Metabolism, and Signaling in the Inflammatory Response. *Annu Rev Immunol* **37**, 325-347 (2019).
64. F. Di Virgilio, D. Dal Ben, A. C. Sarti, A. L. Giuliani, S. Falzoni, The P2X7 Receptor in Infection and Inflammation. *Immunity* **47**, 15-31 (2017).

65. Z. Yan *et al.*, Experimental characterization and mathematical modeling of P2X7 receptor channel gating. *J Neurosci* **30**, 14213-14224 (2010).
66. B. Rissiek, F. Haag, O. Boyer, F. Koch-Nolte, S. Adriouch, P2X7 on Mouse T Cells: One Channel, Many Functions. *Front Immunol* **6**, 204 (2015).
67. M. Kim, L. H. Jiang, H. L. Wilson, R. A. North, A. Surprenant, Proteomic and functional evidence for a P2X7 receptor signalling complex. *EMBO J* **20**, 6347-6358 (2001).
68. E. Adinolfi *et al.*, Trophic activity of a naturally occurring truncated isoform of the P2X7 receptor. *FASEB J* **24**, 3393-3404 (2010).
69. M. Er-Lukowiak *et al.*, A *P2rx7* passenger mutation affects the vitality and function of T cells in congenic mice. *iScience* **23**, 101870 (2020).
70. C. Guo, M. Masin, O. S. Qureshi, R. D. Murrell-Lagnado, Evidence for functional P2X4/P2X7 heteromeric receptors. *Mol Pharmacol* **72**, 1447-1456 (2007).
71. R. Kopp, A. Krautloher, A. Ramírez-Fernández, A. Nicke, P2X7 Interactions and Signaling - Making Head or Tail of It. *Front Mol Neurosci* **12**, 183 (2019).
72. V. J. Brock *et al.*, P2X4 and P2X7 are essential players in basal T cell activity and Ca. *Sci Adv* **8**, eabl9770 (2022).
73. D. Yang, Y. He, R. Muñoz-Planillo, Q. Liu, G. Núñez, Caspase-11 Requires the Pannexin-1 Channel and the Purinergic P2X7 Pore to Mediate Pyroptosis and Endotoxic Shock. *Immunity* **43**, 923-932 (2015).
74. B. Gu, L. J. Bendall, J. S. Wiley, Adenosine triphosphate-induced shedding of CD23 and L-selectin (CD62L) from lymphocytes is mediated by the same receptor but different metalloproteases. *Blood* **92**, 946-951 (1998).
75. H. Moon, H. Y. Na, K. H. Chong, T. J. Kim, P2X7 receptor-dependent ATP-induced shedding of CD27 in mouse lymphocytes. *Immunol Lett* **102**, 98-105 (2006).
76. H. P. Langston, Y. Ke, A. T. Gewirtz, K. E. Dombrowski, J. A. Kapp, Secretion of IL-2 and IFN-gamma, but not IL-4, by antigen-specific T cells requires extracellular ATP. *J Immunol* **170**, 2962-2970 (2003).
77. O. R. Baricordi *et al.*, An ATP-activated channel is involved in mitogenic stimulation of human T lymphocytes. *Blood* **87**, 682-690 (1996).
78. O. R. Baricordi *et al.*, Increased proliferation rate of lymphoid cells transfected with the P2X(7) ATP receptor. *J Biol Chem* **274**, 33206-33208 (1999).
79. M. Proietti *et al.*, ATP-gated ionotropic P2X7 receptor controls follicular T helper cell numbers in Peyer's patches to promote host-microbiota mutualism. *Immunity* **41**, 789-801 (2014).

80. U. Schenk *et al.*, ATP inhibits the generation and function of regulatory T cells through the activation of purinergic P2X receptors. *Sci Signal* **4**, ra12 (2011).
81. É. Salles *et al.*, P2X7 receptor drives Th1 cell differentiation and controls the follicular helper T cell population to protect against Plasmodium chabaudi malaria. *PLoS Pathog* **13**, e1006595 (2017).
82. Z. D. Fan *et al.*, Involvement of P2X7 receptor signaling on regulating the differentiation of Th17 cells and type II collagen-induced arthritis in mice. *Sci Rep* **6**, 35804 (2016).
83. K. Atarashi *et al.*, ATP drives lamina propria T(H)17 cell differentiation. *Nature* **455**, 808-812 (2008).
84. H. Borges da Silva, H. Wang, L. J. Qian, K. A. Hogquist, S. C. Jameson, ARTC2.2/P2RX7 Signaling during Cell Isolation Distorts Function and Quantification of Tissue-Resident CD8. *J Immunol* **202**, 2153-2163 (2019).
85. B. Rissiek *et al.*, Blockade of Murine ARTC2.2 During Cell Preparation Preserves the Vitality and Function of Liver Tissue-Resident Memory T Cells. *Front Immunol* **9**, 1580 (2018).
86. R. Stark *et al.*, T_{RM} maintenance is regulated by tissue damage via P2RX7. *Sci Immunol* **3**, (2018).
87. H. Borges da Silva *et al.*, The purinergic receptor P2RX7 directs metabolic fitness of long-lived memory CD8. *Nature* **559**, 264-268 (2018).
88. H. Borges da Silva *et al.*, Sensing of ATP via the Purinergic Receptor P2RX7 Promotes CD8. *Immunity* **53**, 158-171.e156 (2020).
89. T. Vardam-Kaur *et al.*, The Extracellular ATP Receptor P2RX7 Imprints a Promemory Transcriptional Signature in Effector CD8. *J Immunol* **208**, 1686-1699 (2022).
90. E. Adinolfi *et al.*, Basal activation of the P2X7 ATP receptor elevates mitochondrial calcium and potential, increases cellular ATP levels, and promotes serum-independent growth. *Mol Biol Cell* **16**, 3260-3272 (2005).
91. P. Chiozzi *et al.*, Amyloid β-dependent mitochondrial toxicity in mouse microglia requires P2X7 receptor expression and is prevented by nimodipine. *Sci Rep* **9**, 6475 (2019).
92. A. B. Mackenzie, M. T. Young, E. Adinolfi, A. Surprenant, Pseudoapoptosis induced by brief activation of ATP-gated P2X7 receptors. *J Biol Chem* **280**, 33968-33976 (2005).
93. S. Penuela, R. Gehi, D. W. Laird, The biochemistry and function of pannexin channels. *Biochim Biophys Acta* **1828**, 15-22 (2013).
94. A. Boyd-Tressler, S. Penuela, D. W. Laird, G. R. Dubyak, Chemotherapeutic drugs induce ATP release via caspase-gated pannexin-1 channels and a caspase/pannexin-1-independent mechanism. *J Biol Chem* **289**, 27246-27263 (2014).
95. Y. H. Chiu *et al.*, A quantized mechanism for activation of pannexin channels. *Nat Commun* **8**, 14324 (2017).

96. U. Schenk *et al.*, Purinergic control of T cell activation by ATP released through pannexin-1 hemichannels. *Sci Signal* **1**, ra6 (2008).
97. C. Ledderose *et al.*, Purinergic P2X4 receptors and mitochondrial ATP production regulate T cell migration. *J Clin Invest* **128**, 3583-3594 (2018).
98. L. Yip *et al.*, Autocrine regulation of T-cell activation by ATP release and P2X7 receptors. *FASEB J* **23**, 1685-1693 (2009).
99. F. Di Virgilio, A. C. Sarti, S. Falzoni, E. De Marchi, E. Adinolfi, Extracellular ATP and P2 purinergic signalling in the tumour microenvironment. *Nat Rev Cancer*, (2018).
100. S. Guo, F. Han, W. Zhu, CD39 - A bright target for cancer immunotherapy. *Biomed Pharmacother* **151**, 113066 (2022).
101. E. Adinolfi *et al.*, Expression of P2X7 receptor increases in vivo tumor growth. *Cancer Res* **72**, 2957-2969 (2012).
102. F. Hattori *et al.*, Feasibility study of B16 melanoma therapy using oxidized ATP to target purinergic receptor P2X7. *Eur J Pharmacol* **695**, 20-26 (2012).
103. G. Schneider *et al.*, Extracellular nucleotides as novel, underappreciated pro-metastatic factors that stimulate purinergic signaling in human lung cancer cells. *Mol Cancer* **14**, 201 (2015).
104. E. Takai, M. Tsukimoto, H. Harada, S. Kojima, Autocrine signaling via release of ATP and activation of P2X7 receptor influences motile activity of human lung cancer cells. *Purinergic Signal* **10**, 487-497 (2014).
105. S. M. Gilbert *et al.*, ATP in the tumour microenvironment drives expression of nfP2X. *Oncogene* **38**, 194-208 (2019).
106. E. Wennerberg *et al.*, Expression of the mono-ADP-ribosyltransferase ART1 by tumor cells mediates immune resistance in non-small cell lung cancer. *Sci Transl Med* **14**, eabe8195 (2022).
107. N. Schwarz *et al.*, Alternative splicing of the N-terminal cytosolic and transmembrane domains of P2X7 controls gating of the ion channel by ADP-ribosylation. *PLoS One* **7**, e41269 (2012).
108. C. N. J. Young *et al.*, Sustained activation of P2X7 induces MMP-2-evoked cleavage and functional purinoceptor inhibition. *J Mol Cell Biol* **10**, 229-242 (2018).
109. E. De Marchi *et al.*, The P2X7 receptor modulates immune cells infiltration, ectonucleotidases expression and extracellular ATP levels in the tumor microenvironment. *Oncogene*, (2019).
110. A. Giannuzzo *et al.*, Targeting of the P2X7 receptor in pancreatic cancer and stellate cells. *Int J Cancer* **139**, 2540-2552 (2016).
111. E. Adinolfi *et al.*, Accelerated tumor progression in mice lacking the ATP receptor P2X7. *Cancer Res* **75**, 635-644 (2015).
112. P. Hofman *et al.*, Genetic and pharmacological inactivation of the purinergic P2RX7 receptor dampens inflammation but increases tumor

incidence in a mouse model of colitis-associated cancer. *Cancer Res* **75**, 835-845 (2015).
113. X. Y. Li *et al.*, Targeting CD39 in Cancer Reveals an Extracellular ATP- and Inflammasome-Driven Tumor Immunity. *Cancer Discov* **9**, 1754-1773 (2019).
114. S. S. Faria *et al.*, NLRP3 inflammasome-mediated cytokine production and pyroptosis cell death in breast cancer. *J Biomed Sci* **28**, 26 (2021).
115. F. Ghiringhelli *et al.*, Activation of the NLRP3 inflammasome in dendritic cells induces IL-1beta-dependent adaptive immunity against tumors. *Nat Med* **15**, 1170-1178 (2009).
116. L. Douguet *et al.*, A small-molecule P2RX7 activator promotes anti-tumor immune responses and sensitizes lung tumor to immunotherapy. *Nat Commun* **12**, 653 (2021).
117. S. J. Im *et al.*, Defining CD8+ T cells that provide the proliferative burst after PD-1 therapy. *Nature* **537**, 417-421 (2016).
118. D. T. Utzschneider *et al.*, T Cell Factor 1-Expressing Memory-like CD8(+) T Cells Sustain the Immune Response to Chronic Viral Infections. *Immunity* **45**, 415-427 (2016).
119. A. Romagnani *et al.*, P2X7 Receptor Activity Limits Accumulation of T Cells within Tumors. *Cancer Res* **80**, 3906-3919 (2020).
120. M. Y. Gerner, L. M. Heltemes-Harris, B. T. Fife, M. F. Mescher, Cutting edge: IL-12 and type I IFN differentially program CD8 T cells for programmed death 1 re-expression levels and tumor control. *J Immunol* **191**, 1011-1015 (2013).
121. C. G. Tucker *et al.*, Adoptive T Cell Therapy with IL-12-Preconditioned Low-Avidity T Cells Prevents Exhaustion and Results in Enhanced T Cell Activation, Enhanced Tumor Clearance, and Decreased Risk for Autoimmunity. *J Immunol* **205**, 1449-1460 (2020).
122. S. A. Rosenberg, N. P. Restifo, Adoptive cell transfer as personalized immunotherapy for human cancer. *Science* **348**, 62-68 (2015).
123. C. H. June, R. S. O'Connor, O. U. Kawalekar, S. Ghassemi, M. C. Milone, CAR T cell immunotherapy for human cancer. *Science* **359**, 1361-1365 (2018).
124. S. L. Topalian, C. G. Drake, D. M. Pardoll, Immune checkpoint blockade: a common denominator approach to cancer therapy. *Cancer Cell* **27**, 450-461 (2015).
125. J. J. Martínez-García *et al.*, P2X7 receptor induces mitochondrial failure in monocytes and compromises NLRP3 inflammasome activation during sepsis. *Nat Commun* **10**, 2711 (2019).
126. S. J. Fuller, L. Stokes, K. K. Skarratt, B. J. Gu, J. S. Wiley, Genetics of the P2X7 receptor and human disease. *Purinergic Signal* **5**, 257-262 (2009).

127. J. M. Schenkel *et al.*, Conventional type I dendritic cells maintain a reservoir of proliferative tumor-antigen specific TCF-1. *Immunity* **54**, 2338-2353.e2336 (2021).
128. A. K. Molodtsov *et al.*, Resident memory CD8$^+$ T cells in regional lymph nodes mediate immunity to metastatic melanoma. *Immunity* **54**, 2117-2132.e2117 (2021).
129. K. A. Connolly *et al.*, A reservoir of stem-like CD8$^+$ T cells in the tumor-draining lymph node preserves the ongoing antitumor immune response. *Sci Immunol* **6**, eabg7836 (2021).
130. D. B. Rivadeneira, G. M. Delgoffe, Antitumor T-cell Reconditioning: Improving Metabolic Fitness for Optimal Cancer Immunotherapy. *Clin Cancer Res* **24**, 2473-2481 (2018).
131. K. E. Beckermann, S. O. Dudzinski, J. C. Rathmell, Dysfunctional T cell metabolism in the tumor microenvironment. *Cytokine Growth Factor Rev* **35**, 7-14 (2017).
132. M. Gu *et al.*, NF-κB-inducing kinase maintains T cell metabolic fitness in antitumor immunity. *Nat Immunol* **22**, 193-204 (2021).
133. O. U. Kawalekar *et al.*, Distinct Signaling of Coreceptors Regulates Specific Metabolism Pathways and Impacts Memory Development in CAR T Cells. *Immunity* **44**, 712 (2016).
134. A. V. Menk *et al.*, 4-1BB costimulation induces T cell mitochondrial function and biogenesis enabling cancer immunotherapeutic responses. *J Exp Med* **215**, 1091-1100 (2018).
135. A. H. Long *et al.*, 4-1BB costimulation ameliorates T cell exhaustion induced by tonic signaling of chimeric antigen receptors. *Nat Med* **21**, 581-590 (2015).
136. K. Chamoto *et al.*, Mitochondrial activation chemicals synergize with surface receptor PD-1 blockade for T cell-dependent antitumor activity. *Proc Natl Acad Sci U S A* **114**, E761-E770 (2017).
137. F. Aswad, H. Kawamura, G. Dennert, High sensitivity of CD4+CD25+ regulatory T cells to extracellular metabolites nicotinamide adenine dinucleotide and ATP: a role for P2X7 receptors. *J Immunol* **175**, 3075-3083 (2005).
138. A. Teijeira *et al.*, Mitochondrial Morphological and Functional Reprogramming Following CD137 (4-1BB) Costimulation. *Cancer Immunol Res* **6**, 798-811 (2018).
139. J. Y. Lee *et al.*, The transcription factor KLF2 restrains CD4$^+$ T follicular helper cell differentiation. *Immunity* **42**, 252-264 (2015).
140. R. Schmidt *et al.*, CRISPR activation and interference screens decode stimulation responses in primary human T cells. *Science* **375**, eabj4008 (2022).

141. A. Pegoraro *et al.*, P2X7 promotes metastatic spreading and triggers release of miRNA-containing exosomes and microvesicles from melanoma cells. *Cell Death Dis* **12**, 1088 (2021).
142. M. Sade-Feldman *et al.*, Defining T Cell States Associated with Response to Checkpoint Immunotherapy in Melanoma. *Cell* **176**, 404 (2019).
143. G. G. Yegutkin, D. Boison, ATP and Adenosine Metabolism in Cancer: Exploitation for Therapeutic Gain. *Pharmacol Rev* **74**, 797-822 (2022).
144. Y. Tang *et al.*, Inhibition of arginine ADP-ribosyltransferase 1 reduces the expression of poly(ADP-ribose) polymerase-1 in colon carcinoma. *Int J Mol Med* **32**, 130-136 (2013).
145. L. Yang, M. Xiao, X. Li, Y. Tang, Y. L. Wang, Arginine ADP-ribosyltransferase 1 promotes angiogenesis in colorectal cancer via the PI3K/Akt pathway. *Int J Mol Med* **37**, 734-742 (2016).
146. G. L. Song *et al.*, Regulation of the RhoA/ROCK/AKT/β-catenin pathway by arginine-specific ADP-ribosytransferases 1 promotes migration and epithelial-mesenchymal transition in colon carcinoma. *Int J Oncol* **49**, 646-656 (2016).
147. H. Y. Liu *et al.*, Targeting NAD metabolism regulates extracellular adenosine levels to improve the cytotoxicity of CD8+ effector T cells in the tumor microenvironment of gastric cancer. *J Cancer Res Clin Oncol*, (2022).
148. P. Agarwal *et al.*, Gene regulation and chromatin remodeling by IL-12 and type I IFN in programming for CD8 T cell effector function and memory. *J Immunol* **183**, 1695-1704 (2009).
149. P. J. Sáez *et al.*, ATP promotes the fast migration of dendritic cells through the activity of pannexin 1 channels and P2X. *Sci Signal* **10**, (2017).
150. C. B. Medina *et al.*, Metabolites released from apoptotic cells act as tissue messengers. *Nature* **580**, 130-135 (2020).
151. S. F. Häusler *et al.*, Anti-CD39 and anti-CD73 antibodies A1 and 7G2 improve targeted therapy in ovarian cancer by blocking adenosine-dependent immune evasion. *Am J Transl Res* **6**, 129-139 (2014).
152. R. D. Leone, L. A. Emens, Targeting adenosine for cancer immunotherapy. *J Immunother Cancer* **6**, 57 (2018).
153. S. Hubert *et al.*, Extracellular NAD+ shapes the Foxp3+ regulatory T cell compartment through the ART2-P2X7 pathway. *J Exp Med* **207**, 2561-2568 (2010).
154. C. Sandoval-Montes, L. Santos-Argumedo, CD38 is expressed selectively during the activation of a subset of mature T cells with reduced proliferation but improved potential to produce cytokines. *J Leukoc Biol* **77**, 513-521 (2005).

155. L. Chen *et al.*, CD38-Mediated Immunosuppression as a Mechanism of Tumor Cell Escape from PD-1/PD-L1 Blockade. *Cancer Discov* **8**, 1156-1175 (2018).
156. F. Haag *et al.*, Extracellular NAD and ATP: Partners in immune cell modulation. *Purinergic Signal* **3**, 71-81 (2007).
157. S. Adriouch *et al.*, NAD+ released during inflammation participates in T cell homeostasis by inducing ART2-mediated death of naive T cells in vivo. *J Immunol* **179**, 186-194 (2007).
158. S. Adriouch *et al.*, ADP-ribosylation at R125 gates the P2X7 ion channel by presenting a covalent ligand to its nucleotide binding site. *FASEB J* **22**, 861-869 (2008).
159. J. L. Collier, S. A. Weiss, K. E. Pauken, D. R. Sen, A. H. Sharpe, Not-so-opposite ends of the spectrum: CD8. *Nat Immunol* **22**, 809-819 (2021).
160. M. P. Rubinstein *et al.*, Ex vivo interleukin-12-priming during CD8(+) T cell activation dramatically improves adoptive T cell transfer antitumor efficacy in a lymphodepleted host. *J Am Coll Surg* **214**, 700-707; discussion 707-708 (2012).
161. C. Tan *et al.*, Local secretion of IL-12 augments the therapeutic impact of dendritic cell-tumor cell fusion vaccination. *J Surg Res* **185**, 904-911 (2013).
162. L. Zhang *et al.*, Improving adoptive T cell therapy by targeting and controlling IL-12 expression to the tumor environment. *Mol Ther* **19**, 751-759 (2011).
163. P. J. Siska *et al.*, Mitochondrial dysregulation and glycolytic insufficiency functionally impair CD8 T cells infiltrating human renal cell carcinoma. *JCI Insight* **2**, (2017).
164. R. Sluyter, The P2X7 Receptor. *Adv Exp Med Biol* **1051**, 17-53 (2017).
165. Y. C. Yang *et al.*, Functional variant of the P2X7 receptor gene is associated with human papillomavirus-16 positive cervical squamous cell carcinoma. *Oncotarget* **7**, 82798-82803 (2016).
166. S. Duan, J. Yu, Z. Han, Z. Cheng, P. Liang, Association Between P2RX7 Gene and Hepatocellular Carcinoma Susceptibility: A Case-Control Study in a Chinese Han Population. *Med Sci Monit* **22**, 1916-1923 (2016).
167. J. S. Wiley *et al.*, A loss-of-function polymorphic mutation in the cytolytic P2X7 receptor gene and chronic lymphocytic leukaemia: a molecular study. *Lancet* **359**, 1114-1119 (2002).
168. S. Loi *et al.*, CD73 promotes anthracycline resistance and poor prognosis in triple negative breast cancer. *Proc Natl Acad Sci U S A* **110**, 11091-11096 (2013).
169. N. Aroua *et al.*, Extracellular ATP and CD39 Activate cAMP-Mediated Mitochondrial Stress Response to Promote Cytarabine Resistance in Acute Myeloid Leukemia. *Cancer Discov* **10**, 1544-1565 (2020).

170. T. Duhen *et al*., Co-expression of CD39 and CD103 identifies tumor-reactive CD8 T cells in human solid tumors. *Nat Commun* **9**, 2724 (2018).
171. R. N. Pillai *et al*., Daratumumab Plus Atezolizumab in Previously Treated Advanced or Metastatic NSCLC: Brief Report on a Randomized, Open-Label, Phase 1b/2 Study (LUC2001 JNJ-54767414). *JTO Clin Res Rep* **2**, 100104 (2021).